AMERICAN MUSEUM
Novitates

PUBLISHED BY THE AMERICAN MUSEUM OF NATURAL HISTORY
CENTRAL PARK WEST AT 79TH STREET, NEW YORK, NY 10024
Number 3480, 65 pp., 26 figures, 6 tables July 25, 2005

A New Protocetid Whale (Cetacea: Archaeoceti) from the Late Middle Eocene of South Carolina

JONATHAN H. GEISLER,[1] ALBERT E. SANDERS,[2] AND ZHE-XI LUO[3]

ABSTRACT

A new genus and species of protocetid cetacean, *Carolinacetus gingerichi*, is described from a partial skull, the posterior portion of both dentaries, 13 vertebrae, and elements of 15 ribs found in the Cross Member of the late middle Eocene Tupelo Bay Formation in Berkeley County, South Carolina. That formation is also defined and named in this paper. Although the holotype skull of *Carolinacetus* is fragmentary, it includes the best preserved petrosal of any described specimen from the archaeocete families of Pakicetidae, Ambulocetidae, Remingtonocetidae, and Protocetidae. The phylogenetic relationships of *Carolinacetus* were determined by a cladistic analysis of a dataset that includes 16 cetacean taxa and 5 outgroups scored for 107 morphological characters. *Carolinacetus* was found to be the basalmost cetacean known from North America, and the most conspicuous character supporting this position is the external, bony nares being anterior to P1. Other noteworthy findings are that *Georgiacetus* is more basal than *Babiacetus* and that Remingtonocetidae occupies a branch between Pakicetidae and Protocetidae. Based on our phylogenetic analysis, the genus *Gaviacetus* is removed from the Basilosauridae and restored to the Protocetidae. Possible dispersal routes of protocetids from the Old World to the New World are discussed, and a route westward along the southern coast of Greenland is considered to be the most likely avenue of protocetid migration to North America.

[1] Department of Geology and Geography and Georgia Southern Museum, Georgia Southern University, Statesboro, GA30460-5149 (geislerj@georgiasouthern.edu).
[2] Department of Natural Sciences, The Charleston Museum, 360 Meeting Street, Charleston, SC 29403 (asanders@charlestonmuseum.org).
[3] Section of Vertebrate Paleontology, Carnegie Museum of Natural History, Pittsburgh, PA 15213-4080 (LuoZ@CarnegieMNH.org).

 ISSN 0003-0082

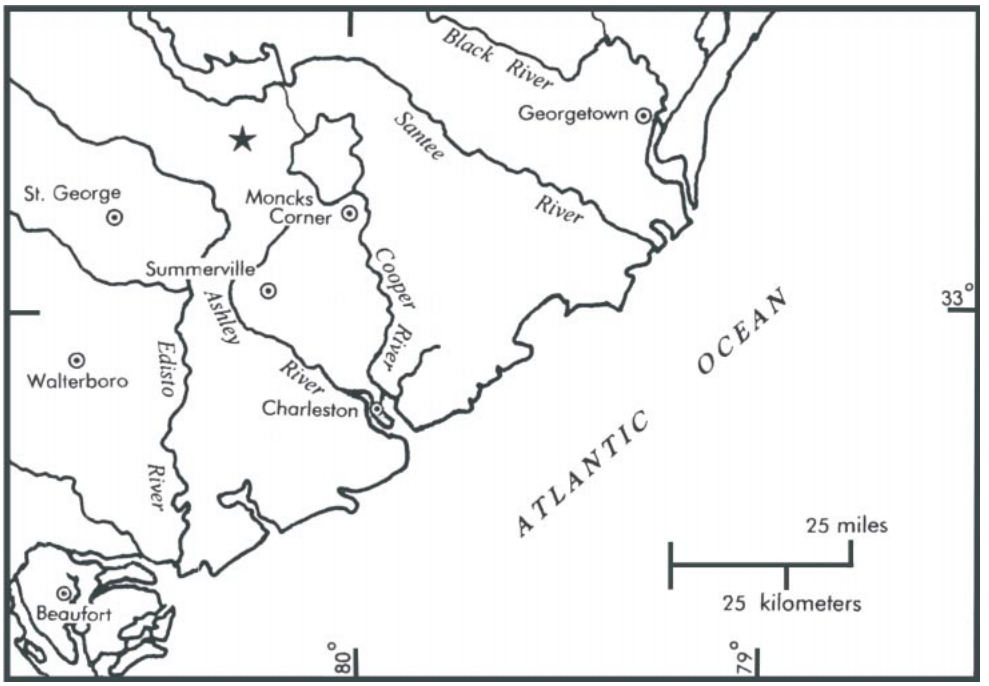

Fig. 1. Type locality (indicated by the star) of *Carolinacetus gingerichi*, new genus and species: South Carolina, Berkeley County; Martin Marietta Berkeley (''Cross'') Quarry. Cross Member, Tupelo Bay Formation, late Middle Eocene (Middle Bartonian).

INTRODUCTION

The family Protocetidae is a paraphyletic group of archaeocete cetaceans that flourished during the middle Eocene (Lutetian and Bartonian). Their immediate descendants, the late Eocene basilosaurids, are more closely related to the extant cetacean suborders Odontoceti (toothed whales) and Mysticeti (baleen-bearing whales). Protocetid remains have provided important insights into the origin of Cetacea (Gingerich et al., 2001a; Geisler and Uhen, 2003), the evolution of underwater hearing (Luo and Gingerich, 1999; Spoor et al., 2002; Nummela et al., 2004), and the evolution of aquatic locomotion (Gingerich et al., 1994, 2001a; Buchholtz, 1998; Fish, 1998). As recently as the 1980s, the published record of North American protocetids consisted of a single vertebra from Texas discussed by Kellogg (1936). During the past 15 years, protocetid remains have been found at several localities in the southeastern United States (Albright, 1996; McLeod and Barnes, 1996), and three new taxa have been described: *Georgiacetus vogtlensis* (Hulbert et al., 1998), *Natchitochia jonesi* (Uhen, 1998b), and *Eocetus wardii* (Uhen, 1999). In the present study, we describe *Carolinacetus gingerichi*, a new genus and species of protocetid whale from the middle Eocene Tupelo Bay Formation of South Carolina. The preserved skeletal elements of this animal indicate that it is the basalmost cetacean known from North America.

The holotype, Charleston Museum PV5401, was discovered in sediments of lower middle Eocene age in April 1994 by Bricky Way, the first author, and other members of the College of Charleston Geology Club during a fieldtrip to the Martin Marietta Berkeley Quarry in Berkeley County, South Carolina (fig. 1). Because of its proximity to the small town of Cross, this quarry is familiarly known as the ''Cross Quarry''. Although isolated teeth of protocetids have

been reported from the Cross Quarry (Albright, 1996; McLeod and Barnes, 1996), this specimen is the first partial skeleton discovered there.

The existence of this new protocetid from South Carolina was first reported at the Sixth North American Paleontological Convention (Geisler et al., 1996). Subsequent studies utilized the undescribed holotype of *Carolinacetus* (referring to it as the ''Cross whale'') to test phylogenetic hypotheses for the sister group to Cetacea (e.g., Geisler and Luo, 1998; O'Leary and Geisler, 1999). Geisler and Luo (1998: fig. 8) also used the partial skull to infer the pattern of cranial vasculature in early cetaceans. The skull figured prominently in their discussion because of the superb preservation of the petrosal and the fact that nonpreservation of the basion of the skull provided a unique endocranial view of the petrosal and surrounding structures. Geisler and Luo (1998) recognized two features not previously reported in cetaceans, a postglenoid foramen at the squamosal/petrosal suture and endocranial space for a large retia mirabile medial to the petrosal.

In the following description of *Carolinacetus gingerichi* we distinguish this new genus and species from previously described protocetids, particularly those from North America, and we present a phylogenetic analysis of archaeocete cetaceans. Although several studies have developed hypotheses for basal cetacean phylogeny (e.g., Uhen, 1998a, 1999), our attempt benefits from the recent publication of pakicetid postcrania (Thewissen et al., 2001), protocetid postcrania (Gingerich et al., 2001a), and description of the protocetids *Artiocetus clavus* (Gingerich et al., 2001a) and *Qaisracetus arifi* (Gingerich et al., 2001b), which together document previously unknown grades in cetacean evolution.

MATERIALS AND METHODS

Measurements of skeletal elements were made with dial calipers. Maxillary teeth are indicated by upper case letters (M1) and mandibular teeth by lower case letters (m1). Measurements of the anteroposterior length of the crown were taken along the base, and the transverse diameter was measured at the base perpendicular to the long axis of the crown. The vertical dimension of the crown was measured from the base to the tip of the apical cusp.

In the descriptions and comparisons of the holotype vertebral elements of *Carolinacetus* we have employed the methods of utilizing length/width ratios of vertebral centra introduced by Sanders and Barnes (2003). Ratios of the dimensions of centra were determined by dividing the width of the anterior face by the anteroposterior length of the centrum. Higher values reflect a relatively short centrum and lower values indicate more elongate ones.

CHARACTER ANALYSIS

The phylogenetic analysis was based 23 taxa scored for 107 morphological characters, 46 multistate and 61 binary (appendix 1). The character/taxon matrix is shown in appendix 2. Thirty-nine of the 46 multistate characters were ordered to incorporate hypotheses of homology among character states (Wilkinson, 1992). Multistate characters were ordered so that anatomical differences between sequential states were minimized. Most of the characters in the matrix were taken directly from or slightly modified from the following references: Thewissen (1994), Geisler and Luo (1998), Uhen (1998a), Luo and Gingerich (1999), Uhen (1999), and Thewissen and Hussain (2000).

The ingroup included 17 taxa: Pakicetidae (*Pakicetus* and *Ichthyolestes*); Ambulocetidae (*Ambulocetus*); the remingtonocetids *Remingtonocetus harudiensis* and *Dalanistes ahmedi*; nine protocetids, including *Artiocetus clavus*, *Babiacetus indicus*, *Carolinacetus gingerichi*, *Eocetus schweinfurthi*, *E. wardii*, *Georgiacetus vogtlensis*, *Protocetus atavus*, *Qaisracetus arifi*, *Rodhocetus* (*R. kasrani*, *R. balochistanensis*); and the basilosaurids *Basilosaurus cetoides*, *B. isis*, and *Dorudon atrox*. The protocetids *Pappocetus lugardi*, *Indocetus ramani*, *Takracetus simus*, and *Natchitochia jonesi* were not included because their types and referred specimens are fragmentary and do not preserve sufficient anatomical features to adequately place them in a phylogenetic hypothesis. Ingroup monophyly was tested by including three outgroup

taxa from Mesonychidae (*Sinonyx*, *Pachyaena*, and *Mesonyx*) and two taxa from Artiodactyla (*Sus*, and *Hippopotamus*). Most parsimonious trees were rooted using the mesonychids because morphological data (Gingerich et al., 2001a; Thewissen et al., 2001; Geisler and Uhen, 2003) and molecular data (e.g., Gatesy et al., 1996; Gatesy, 1997; Shimamura et al., 1997; Gatesy et al., 1999; Nikaido et al., 1999) support a monophyletic Cetartiodactyla, which includes cetaceans and artiodactyls but not mesonychids.

The branch-and-bound algorithm (Hendy and Penny, 1982), as implemented in the computer program PAUP*4.0b10 (Swofford, 2002), was used to find the most parsimonious trees. Bremer Support (Bremer, 1988, 1994) was calculated using command files generated with the program TreeRot (Sorenson, 1996) and executed in PAUP 3.1.1. The command file was altered so that 500 heuristic replicates were performed for each node and only 15 suboptimal trees were held for each replicate. The length of the shortest unconstrained tree was subtracted from the length of the shortest constrained tree to find the branch support for each node. The degree to which the present matrix contradicted alternative phylogenetic hypotheses was determined by creating constraint trees and then enforcing them during 500 heuristic replicates. Only those synapomorphies that are optimized at the same node under ACCTRAN and DELTRAN optimizations are reported.

INSTITUTIONAL ABBREVIATIONS

ChM, The Charleston Museum, Charleston, SC; GSM, Georgia Southern Museum, Georgia Southern University, Statesboro, GA; NCSM, North Carolina Museum of Natural Sciences, Raleigh, NC; SNMS, Staatliches Museum für Naturkunde, Stuttgart; USGS, United States Geological Survey; USNM, U.S. National Museum of Natural History, Washington, DC.

GEOLOGIC SETTING

Carolinacetus gingerichi was found in a semi-indurated Eocene limestone referred to as the Cross Formation (e.g., Baum et al., 1980; Harris et al., 1993; Weems et al., 2004) or the Cross Member of the Santee Limestone (e.g., Ward et al., 1979; Edwards et al., 1997). Although our main objective in this paper is to describe that new species of whale, observations by the second author (Sanders and Katuna, 2000), plus those published in a recent USGS report (i.e., Edwards et al., 1997), indicate that the geology of the Santee Limestone needs to be revisited.

The name ''Santee white limestone'' was informally applied by Charles Lyell (1845) to calcareous marine deposits that he saw at Eutaw Springs near the Santee River in Orangeburg County, South Carolina, in 1842. Invertebrate fossils that he collected there and at other localities led him to recognize those deposits as being of Claiborne (middle Eocene) age (Lyell, 1845). Since then, the name ''Santee Limestone'' has become an accepted term in the stratigraphic nomenclature of the southeastern United States but has been used by various authors in various ways. Sloan (1908: 460) called it the ''Santee marl'' but was clearly referring to the Santee Limestone.

The type locality of *Carolinacetus gingerichi*—the Martin Marietta Berkeley (''Cross'') Quarry—is also the location of the stratotype of the Cross Member of the Santee Limestone, described by Ward et al. (1979: 8) as a ''bryozoan-brachiopod-bivalve biomicrite.'' In the Berkeley Quarry it is typically less than 3 ft thick (Ward et al., 1979) but thickens to approximately 8 ft in a southwestward direction (personal obs.). The Cross Member is underlain by the middle Eocene Moultrie Member, which Edwards et al. (1997) correlated with nannoplankton (NP) zone 16 (late Lutetian/early Bartonian) (fig. 2).

Several aspects of the Cross Member suggest that this stratigraphic unit be elevated to formational rank. The gamma-ray log for a USGS core near Pregnall, SC, shows a peak at the contact between the Cross and the Moultrie Members (Edwards et al., 1997: fig. 2), which is typical of disconformities between formations and unlike the conformable contacts between members of the same depositional sequence. In addition, the top of the Moultrie Member contains numerous borings, indicative of a hiatus in deposition (Ward et al., 1979). Further examination of

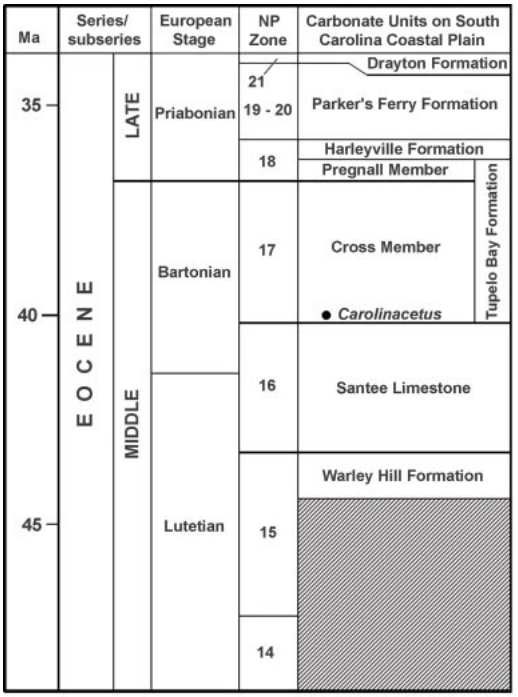

Fig. 2. Chronostratigraphic sequence of upper and middle Eocene carbonate units on the Coastal Plain of South Carolina and correlation with European stages and nannoplankton (NP) zones. Solid circle (●) denotes stratigraphic position of holotype of *Carolinacetus gingerichi*, new genus and species. Time divisions and NP zones follow Berggren et al. (1995).

the Pregnall core reveals that the Cross Member has two lithologic subunits: a lower microfossiliferous limestone that is NP 17 in age and an upper occasionally macrofossiliferous limestone that is NP 18 in age (Edwards et al., 1997).

The Cross Member at both the Berkeley Quarry and the adjacent Martin Marietta Orangeburg Quarry appears to consist entirely of the lower subunit. As in the lower subunit in the Pregnall core (Edwards et al., 1997), the Cross Member at those quarries has abundant quartz and phosphate grains. Nannoplankton in samples of the matrix surrounding the skull of *Carolinacetus* are poorly preserved but suggest an NP 17 date for the Cross Member in the Berkeley Quarry (L. Bybell, personal commun., March 2000). The presence of protocetid whales in the Cross Member at the Berkeley Quarry supports an NP 17 age because protocetids are not known to have survived beyond the Bartonian (Gingerich et al., 1997). Thus, the dating of that subunit as NP 17 by Edwards et al. (1997) is consistent with the fossil cetacean evidence from the Cross Member at the Berkeley Quarry.

Exposures of the upper subunit are best seen in the Giant Cement Quarry near Harleyville, SC, in Dorchester County. It consists of foraminifer-peloid-bivalve grainstones and packstones (L. Edwards, personal commun., February 2004). Only basilosaurid cetaceans (*Basilosaurus*, *Zygorhiza*) have been found in this quarry (Sanders and Katuna, 2000), confirming the NP 18 (Priabonian) date for the upper subunit as reported by Edwards et al. (1997). In North America, species of the Basilosauridae are known only from the Priabonian and are not known to have survived beyond it. In addition, Mr. Billy Palmer, Sr. collected the remains of an undescribed basilosaurid archaeocete (ChM PV6761) from the deepest part of this subunit as exposed in the Blue Circle Quarry, which is a short distance west of the Giant Cement Quarry.

On the strength of the paleontological and stratigraphic evidence, Sanders and Katuna (2000) informally proposed that the Moultrie and the Cross Members be elevated to formational rank, and that the two subunits in the latter be recognized as members of the Cross Formation, that is, a lower Berkeley Member and an upper Pregnall Member, with their stratotypes in the Pregnall core. Sanders and Katuna now think that nomenclatural stability would be better served by preserving the name ''Cross Member'' of Ward et al. (1979: 8) rather than by changing the name to ''Berkeley Member''. Another reason for maintaining use of ''Cross Member'' is that at the type locality in the Berkeley Quarry, the upper subunit is not present and thus is not represented in the type section (Ward et al., 1979: 7; fig. 3). Therefore, we consider it best to restrict the name ''Cross'' to the Cross Member as originally proposed by Ward et al. (1979).

Here, we formally propose the name ''Tupelo Bay Formation'' to incorporate the Cross Member and the previously named Pregnall Member of Sanders and Katuna

(2000) (fig. 2). The type section of the Tupelo Bay Formation is here designated as the ''locally shelly, microfossiliferous limestone'' between the the depths of 189.4 and 90.9 ft in the USGS Pregnall core (Edwards et al., 1997: 15), which was taken from latitude 33°09′08″N and longitude 80°28′14″W (Reid et al., 1986). This core can be examined at the South Carolina Geological Survey in Columbia, South Carolina. The stratotype of the Cross Member in the Berekely Quarry is no longer accessible since quarrying activities ended in 2001 and reclamation efforts began. Thus, under the provisions of article 8, section E, of the North American Stratigraphic Code, we designate the typically microfossiliferous interval between 189.4 and 125 ft of the Pregnall core as the neostratotype of the Cross Member. The Pregnall Member (NP 18) is defined as the occasionally macrofossiliferous limestone between the depths of 125 and 90.9 ft of the Pregnall core, which is also the stratotype of this member.

The namesake of this new formation, Tupelo Bay, is a Carolina bay in Berkeley County that is directly on the boundary of the USGS Pringletown and Sandridge 7.5′ quadrangles. It is bounded triangularly by U.S. Route 178, S.C. Route 311, and County Road 59 and is almost equidistant from the Berkeley Quarry to the northeast and the Giant Cement Quarry to the southwest. The name ''Pregnall Member'' reflects representation of this unit in the USGS core taken near the town of Pregnall.

We also restrict the name Santee Limestone to the formation of NP 16 age underlying the Tupelo Bay Formation (fig. 2) and represented between 258.0 and 189.4 ft within the Pregnall core. This renders the ''Moultrie Member'' of Ward et al. (1979) as equivalent to the Santee Limestone, and thus the name ''Moultrie Member'' should be abandoned. Recent authors (e.g., Baum et al., 1980; Ward et al., 1979) have followed Cooke (1936) in recognizing the stratotype of the Santee Limestone as the outcrop at Eutaw Springs visited by Lyell in 1842. Unfortunately, that locality now lies beneath the waters of Lake Marion and is no longer accessible, although other outcrops of the Santee Limestone can be seen near Eutaw Springs. We continue to recognize Eutaw Springs as the type area for the Santee Limestone, even though the original type section is all but inaccessible.

To summarize, the holotype of *Carolinacetus gingerichi* is from the Cross Member of the Tupelo Bay Formation, which is NP 17 in age. In the timescale of Berggren et al. (1995), NP 17 ranges from 40.2 to 37 Ma. Thus, we estimate the age of the holotype material of *Carolinacetus,* found in the lower 2 ft of the Cross Member, to be approximately 40 Ma.

SYSTEMATIC PALEONTOLOGY

CLASS MAMMALIA LINNAEUS, 1758

ORDER CETACEA BRISSON, 1762

SUBORDER ARCHAEOCETI FLOWER, 1883

FAMILY PROTOCETIDAE STROMER, 1908

Carolinacetus, new genus

DIAGNOSIS: Same as for the species.

ETYMOLOGY: The generic name recognizes South Carolina, USA, as the origin of the holotype.

TYPE SPECIES: *Carolinacetus gingerichi*, new species.

Carolinacetus gingerichi, new species

DIAGNOSIS: Distinguished from other known protocetids by the presence of two autapomorphies: (1) presence of a posterodorsal tongue of the petrosal that is exposed between the exoccipital and the squamosal with the skull in posterior view (fig. 9); (2) mandible with a steep ascending process and a deeply descending ventral margin posteriorly, depth of mandible at the mandibular fossa greater than 2.5 times the depth of the mandible at p4 (fig. 11). It differs from *Georgiacetus vogtlensis* in having the posterior margin of the external nares above the canine; palatal process of the premaxilla terminating between the canine and P1; ascending process of the premaxilla terminating dorsal to P1; and parietal ridge rounded, not acute. *Carolinacetus* differs fron *Natchitochia jonesi* in having anterior thoracic vertebrae that are 10–15% smaller, and no further comparisons can be made because the

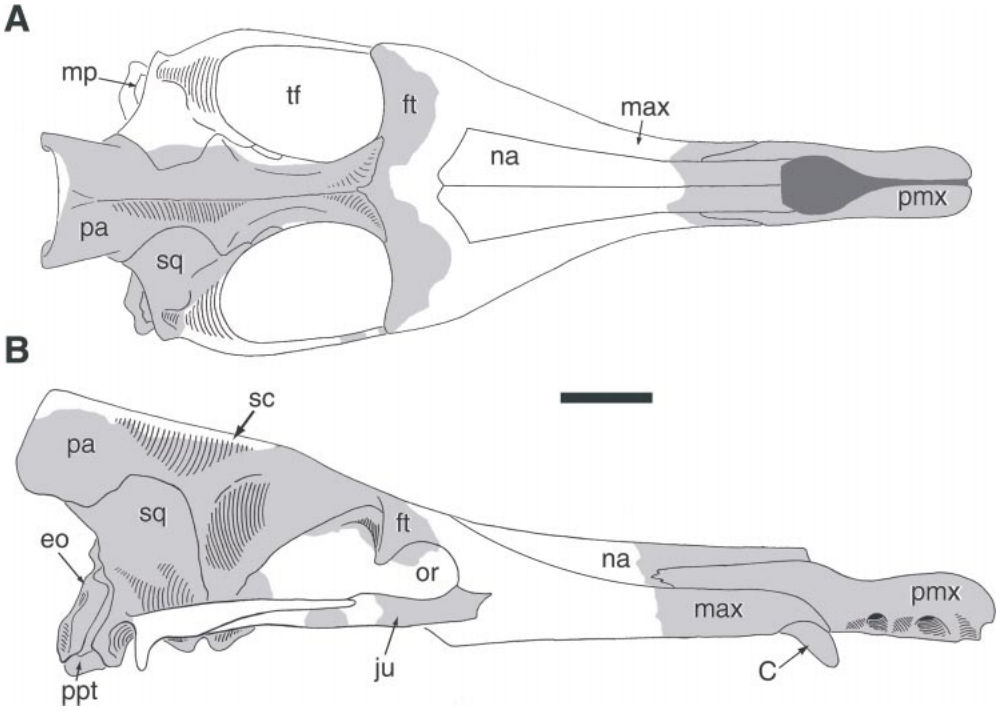

Fig. 3. Reconstructions of the holotype skull of *Carolinacetus gingerichi* (ChM PV5401) in (**A**) dorsal and (**B**) lateral views. Gray areas indicate portions of the skull actually recovered. Scale bar is 10 cm in length. See appendix 3 for anatomical abbreviations.

holotype of the latter taxon includes only vertebrae and fragmentary ribs.

HOLOTYPE: ChM PV5401 (figs. 3–24): incomplete cranium with right petrosal in place, partial tympanic bullae, and detached anterior portion of rostrum; anterior and posterior portions of both mandibles; 11 identifiable teeth; atlas, axis, and 3rd, 4th, 6th, and 7th cervical vertebrae; 1st, 2nd, and 4th–8th thoracic vertebrae; 15 ribs. Collected by A.E. Sanders, J.H. Geisler, C.B. Way, S. Davis, Z.-X. Luo, and J.L. Hanlon, April 1994.

TYPE LOCALITY: South Carolina, Berkeley County; Martin Marietta Berkeley (''Cross'') Quarry, east side of County Road 59, 2.4 km (1.49 mi) south of South Carolina Routes 6 and 45; USGS Chicora 15′ quadrangle, 33°21′ N, 80°13.4′ W.

FORMATION AND AGE: Cross Member, Tupelo Bay Formation, late middle Eocene, middle Bartonian, zone NP 17, ca. 40 Ma.

ETYMOLOGY: The specific name is a patronym honoring Philip D. Gingerich for his many contributions to the present knowledge of the origin of Cetacea and of the diversity of protocetids.

REFERRED SPECIMEN: ChM PV6088, probable sixth thoracic vertebra missing right transverse process, dorsal portion of left transverse process, and tip of spinous process. South Carolina, Berkeley County; Martin Marietta Berkeley Quarry; collected by Billy Palmer, Sr., 9 March 1999. Cross Member, Tupelo Bay Formation, late Middle Eocene.

DESCRIPTION

SKULL

The preserved portions of the holotype skull consist of the anterior end of the rostrum with the right canine in place (figs. 3, 4), detached anterior part of the left nasal, detached portions of the right and left jugals (fig. 3), partial cranium with the right petrosal in place (figs. 5–8), and detached right occipital condyle. Measurements of the cranial elements are given in table 1.

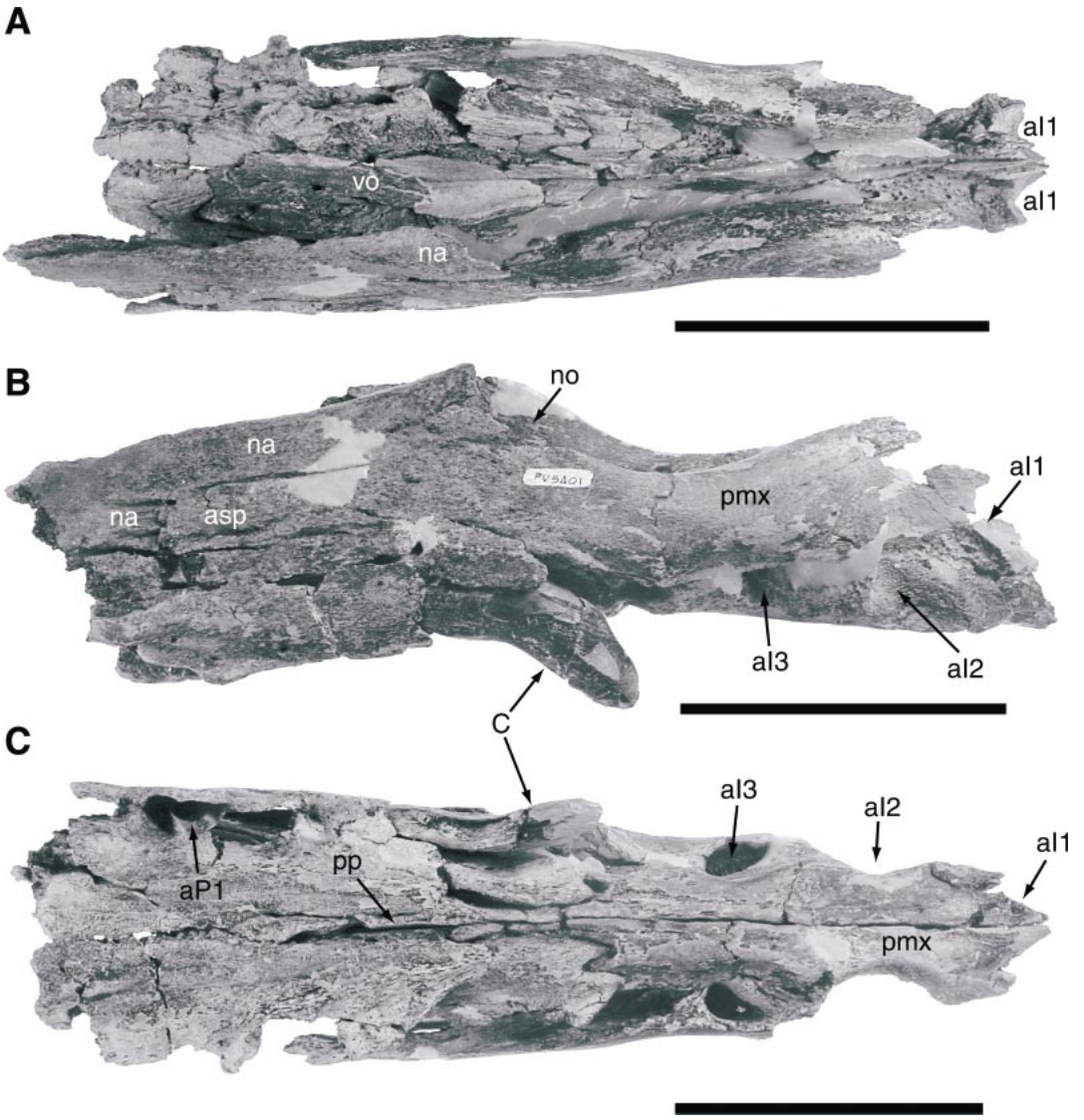

Fig. 4. Anterior end of the rostrum of *Carolinacetus gingerichi* (ChM PV5401) in (**A**) dorsal, (**B**) lateral, and (**C**) ventral views. Note that the external nares (no) are above the canine. Scale bar is 10 cm in length. See appendix 3 for anatomical abbreviations.

The preserved rostral portion extends from the tip of the rostrum to a point just posterior to the alveoli for P1. It is missing the dorsal portions of the premaxillae that enclose the roots of I1, the lateral side of the right maxilla, and the left nasal. In comparison with the maxillae, the premaxillae appear ventrally deflected, probably the result of distortion at the maxillary/premaxillary suture. In addition, there is a gap between the dorsal portions of the right and left premaxillae that can be attributed to distortion. In dorsal view, the rostrum gradually tapers anteriorly, with the external nares being located above the canines, unlike many other described protocetids, in which the nasal opening is situated above P1.

The cranial portion is preserved from the dorsal margin of the foramen magnum to the anterior margins of the orbits but is missing

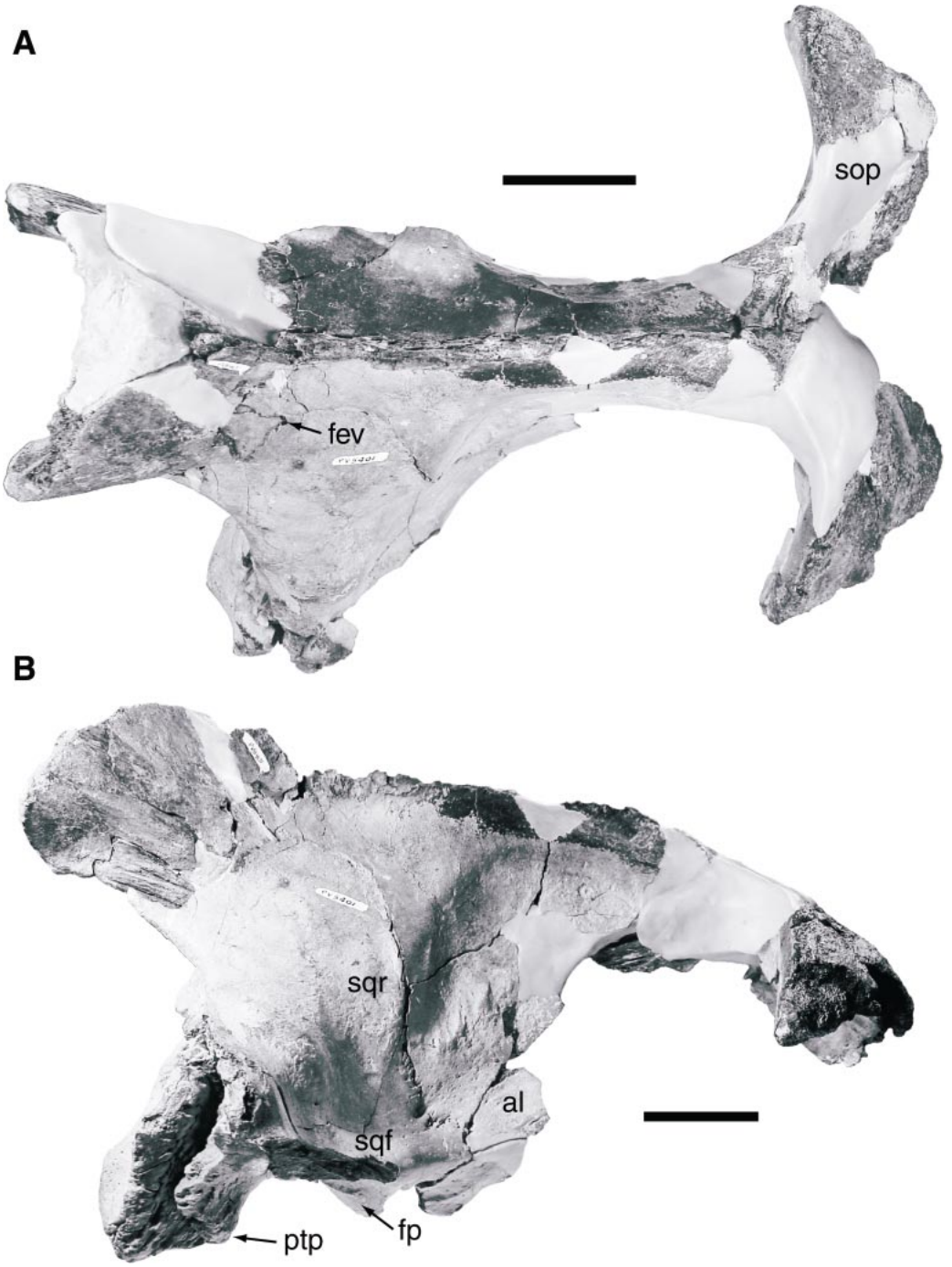

Fig. 5. Partial cranium of *Carolinacetus gingerichi* (ChM PV5401) in (**A**) dorsal and (**B**) lateral views. Scale bar is 5 cm in length. See appendix 3 for anatomical abbreviations.

TABLE 1
Measurements (in mm) of Holotype Skull and Auditory Bones of *Carolinacetus gingerichi*, new genus, new species (ChM PV5401)

Condylobasal length, as preserved	(235)[a]
Greatest length, plane of margins of nuchal crest to tip of rostrum	(290)
Anteroposterior length of parietals along sagittal crest	235
Transverse diameter of supraorbital processes at posterior processes	256
Shortest transverse diameter at parietal ridge	33.1
Greatest outside dimensions across nuchal crest	116
Greatest inside dimensions across nuchal crest	95.2
Vertical diameter of occiput	(138)
Greatest diameter at outside margins of exoccipitals	(284)
Length of external auditory meatus	68.7
Anteroposterior length, detached partial left jugal, as preserved	199.9
Depth at midpoint of detached partial left jugal, as preserved	21
Anteroposterior length of right premaxilla	(285)
Depth of right premaxilla at posterior margin of 12	66.2
Least depth of premaxilla between I3 and C1	46.5
Width of rostrum at P1	(87)
Width of rostrum at I3	64.7
Width of rostum behind I1	40.5
Width of palate at I3	25.8
Length of alveolus, right I2	35
Length of alveolus, left I3	23.3
Length of alveolus, left C1	(38)
Length of alveolus, right P1	18
Width of alveolus, left I3	12.2
Width of alveolus, right P1	10.4
Length of diastema between left I3 and C1	43.3
Length of diastema between left C1 and P1	62
Anteroposterior length of right bulla	68.2
Greatest length of posterior process of right bulla	71.2
Greatest width of posterior process of right bulla	28.5
Anteroposterior diameter of internal acoustic meatus of petrosal	14.4
Length of promontorium of petrosal	16.8

[a] Measurements in parentheses are estimates.

the vertex, the left occipital condyle, the entire ventral region, all of the left squamosal, and the zygomatic process of the right squamosal. In dorsal aspect the cranium is elongate with a prominent sagittal crest, is broadest at the outermost margins of the exoccipital, and is narrowest at a point approximately 75 mm posterior to the posterior margins of the supraorbital processes of the frontals. The temporal fossa is quite extensive, occupying 65% of the anteroposterior length of the cranial region. The nuchal crests of the supraoccipital are horseshoe-shaped in dorsal view, and the entire occiput is projected posterodorsally.

PREMAXILLA: As in other archaeocetes, the premaxilla is elongate and articulates with the maxilla via ascending and palatal processes (fig. 4). The ascending process rises over the dorsal surface of the maxilla and is sutured to it, terminating ca. 21 mm behind the posterior margin of P1. Ventrally, the premaxilla puts forth a palatal process that extends posteriorly for approximately 75 mm behind the anterior tip of the maxilla and terminates at a point adjacent to the diastema between the alveoli for C and P1. Together, the two palatal processes form a wedge between the maxillae. Each of these processes is sutured to the maxilla laterally and articulates medially with the vomer at its posterior end. Just anterior to the anterior edge of the nasal, the dorsal margin of the premaxilla descends rather sharply into a gentle depres-

sion anterior to C, begins to rise dorsally above I3, and above I2 achieves the same elevation as the ascending process. The upper edges of the premaxillae flare dorsally and laterally to form the nasal opening directly above the canine. The nasal opening is confluent anteriorly with a mesorostral gutter that extends anteriorly as far as the diastema between I1 and I2.

The alveoli for the incisors within the premaxilla are aligned longitudinally in two parallel rows, not in a transverse arc as in mesonychids and archaic ungulates (Prothero, 1988; Thewissen, 1994). The alveoli for the right and left I2 are slightly asymmetrical, with the anterior margin of the alveolus for the left I2 being approximately 4 mm anterior to its counterpart on the right side. The first and third alveoli are roughly equal in size, but the alveolus for I2 is considerably deeper and longer anteroposteriorly. The alveoli for I1 are at the extreme anterior end of the rostrum and were at least partially exposed anteriorly. A diastema of 28 mm separates I1 from I2, and I3 is directly behind I2, separated from it by a diastema of only 12 mm. On the ventral surface immediately posterior to the alveolus for I1 there is a small pit that is vascularized and is divided by a sulcus leading into an anterior and a posterior foramen. On the lateral surface posterior to the alveolus for I3 there is a deep, ovate embrasure pit for the lower canine.

MAXILLA: The maxilla is sutured to the premaxilla anteriorly, anteromedially, and dorsally; to the nasals dorsally posterior to the premaxilla; and to the vomer medially. Ventrally, the preserved palatal portion contains the alveoli for C1 and P1 (fig. 4). Between the alveoli for C1 and I3 there is a diastema of ca. 40 mm that spans the maxillary/premaxillary suture and another of ca. 58 mm between C1 and P1. The alveolus for the canine is large, angled posterodorsally, and seated completely on the maxilla. A long, deep, porous embrasure pit occurs in the diastema between C1 and P1 and probably received p1. The anteroposterior length of the alveolus for P1 (13 mm) is small relative to that of the canine and is strongly bilobed. Ventrally, the maxillae form a central trough that deepens and widens posteriorly. The roof of the trough is ca. 29 mm wide and 9 mm deep immediately posterior to the alveolus for P1. In the preserved portion, the walls of the trough reach their greatest height medial to P1. On each side of the trough medial to P1 there are sulci that lead posteriorly to the major palatine foramina 25 mm posterior to P1. On the right side this foramen is only 11 mm beyond P1. The major palatine foramen is the ventral opening for the palatine canal that houses the greater palatine nerve, a ramification of the maxillary branch of the trigeminal nerve (Sisson, 1921). Three well-defined foramina and evidence of a fourth occur on the lateral side of the maxilla in the region of P1.

VOMER: The anterior end of the vomer articulates with the palatal process of the premaxilla laterally, and the remaining posterior portion is sutured to the maxilla laterally and ventrally. A portion of the vomer is exposed ventrally on the midline of the palate between the alveoli for C and P1 (fig. 4). The total exposure is 40 mm in length beginning immediately posterior to the palatal processes of the premaxillae and terminating posteriorly at the level of the anterior edge of the alveolus for P1. In dorsal view, the vomer is a U-shaped trough on the floor of the mesorostral cavity. The morphology of the vomer is correlated with the presence of the ethmoidal plate or a septal cartilage that separates the left from the right nasal passage. The preserved portion of the vomer in *Carolinacetus* is low and U-shaped, as in extant cetaceans; however, it differs from Recent taxa in that it does not extend laterally and dorsally to completely floor the mesorostral cavity. Although the preserved portion in the holotype is restricted in length to the region between the alveoli for C1 and P1, the vomer undoubtedly extended for a considerable distance anteriorly and posteriorly, but almost certainly not beyond the anterior end of the maxilla.

NASAL: The nasal bone articulates laterally with the premaxilla and is sutured to the posterior point of its ascending process. Posterior to the ascending process of the premaxilla, the nasal is sutured ventrally and laterally to the maxilla. The nasal forms the dorsal quarter of the lateral surface of the rostrum and forms half of the roof of the mesorostral trough posterior to the nasal open-

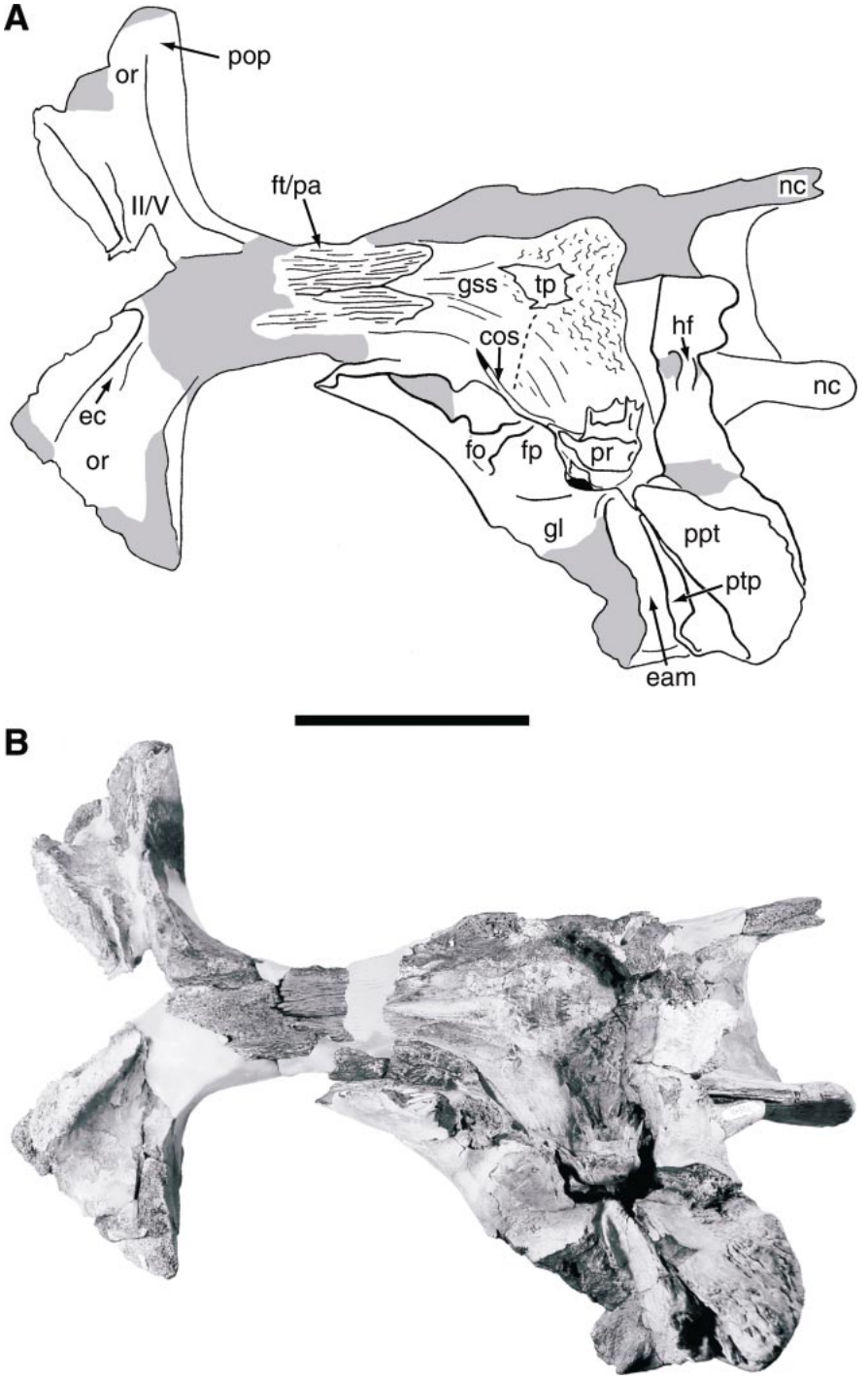

Fig. 6. Line drawing (**A**) and photograph (**B**) of the cranium of *Carolinacetus gingerichi* (ChM PV5401) in ventral view. Dashed line is approximate boundary between middle and posterior cranial fossae. Scale bar is 10 cm in length. See appendix 3 for anatomical abbreviations.

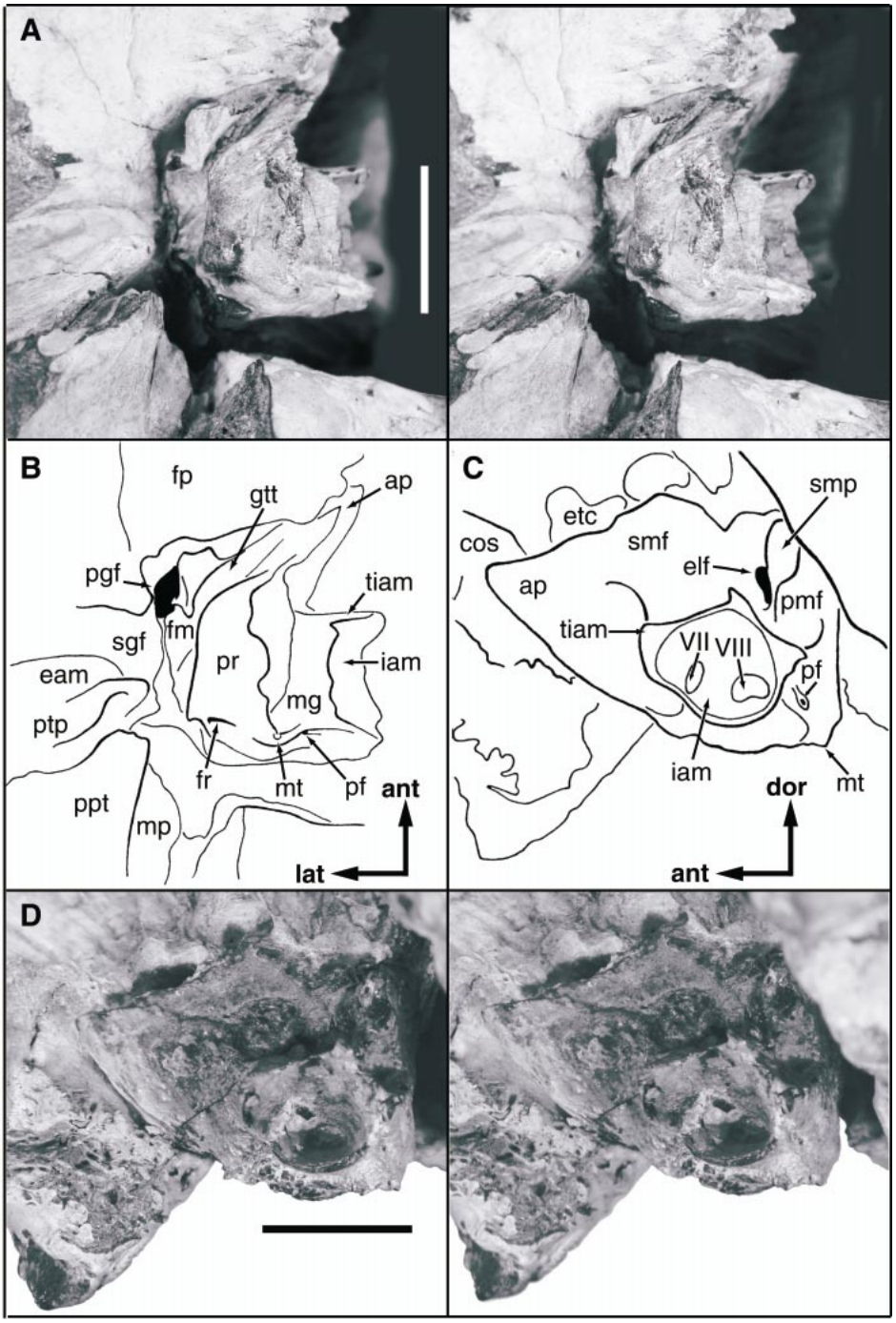

Fig. 7. Stereopairs and line drawings of the right petrosal of *Carolinacetus gingerichi* (ChM PV5401). **A.** Stereopairs of the petrosal in ventral view with (**B**) corresponding line drawing. **C.** Line drawing of the endocranial side of the petrosal with (**D**) corresponding stereopairs. Note the elongate tube (tiam) that houses the internal acoustic meatus and postglenoid foramen (pgf) in the petrosal/squamosal suture. Scale bars are 2 cm in length. See appendix 3 for anatomical abbreviations.

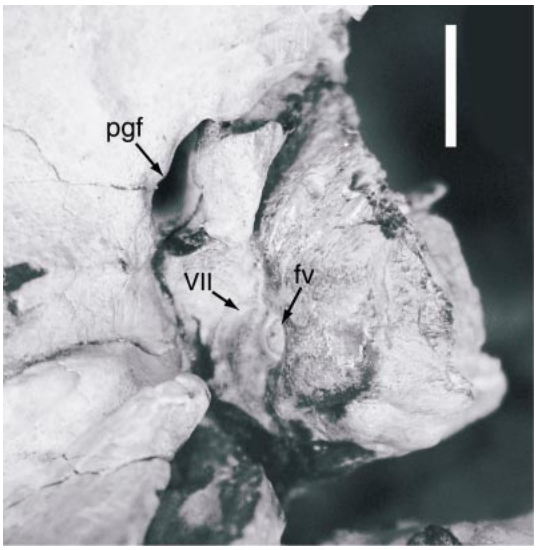

Fig. 8. Ventrolateral view of the right petrosal of *Carolinacetus gingerichi* (ChM PV5401). Anterior is to the top of the page and the scale bar is 1 cm in length. See appendix 3 for anatomical abbreviations.

ing. The anterior tip of the nasal marks the posterior edge of the nasal opening and is level with the posterior edge of the alveolus for C (fig. 4). This position for the nasal opening is comparable to those in *Indocetus ramani* and *Rodhocetus kasrani* (Gingerich et al., 1993, 1994). The ventral internal edge of the nasal is a thin, ventrally expanded lamina. On the inner surface of the nasal, 55 mm posterior to its anterior margin, the turbinate crest begins and broadens vertically and transversely in the posterior direction. Posterior to the level of P1, the turbinate crest thickens to a vertical diameter of 23.7 mm at the broken edge of the specimen. Apparently, the dorsal turbinate (naso-turbinate) was fused to the posterior portions of the turbinate crest as in extant ungulates (Sisson, 1921).

FRONTAL: In dorsal view, the frontals form laterally broad and anteroposteriorly elongate supraorbital processes (fig. 5). The dorsal surface of the supraorbital process is gently convex and slopes ventrally anteriorly and laterally. Approximately half the distance from the midline to the lateral edge of the supraorbital process are two supraorbital foramina that have lost their original roofing and are exposed as open grooves. Curving posteromedially and opening onto the exterior of the cranium laterally, these foramina enclosed supraorbital frontal veins that drained the facial region and connected to the superior sagittal sinus (Sisson, 1921).

The posterior edge of the supraorbital process forms the anterior edge of the temporal fossa and the postorbital process of the frontal. The posterior surface of the postorbital process is oriented vertically and is continuous posteriorly with the laterally facing portion of the temporal fossa. In lateral view, the frontoparietal suture originates along the posterior edge of the postorbital process and is angled posteroventrally. The postorbital process extends laterally beyond the anterior portion of the supraorbital process, but breakage in the skull has obscured the degree of that extension. In parasagittal section, the postorbital process is triangular and is pointed ventrally. The anterior side of the postorbital process is concave and forms the posterior border of the orbit. The ventral edge of this process forms a sharp ridge that curves posteromedially and also forms the posterior edge of a broad trough containing two major orbital foramina missing their original flooring (fig. 6). The central and deepest portion of the trough probably conveyed the ophthalmic branch of the trigeminal nerve and the optic nerve. In the anterolateral corner of the trough there is a small foramen of undetermined utility. The ophthalmic branch of the trigeminal nerve is separated from the ethmoid canal and foramen by a prominent ridge of bone ca. 3–4 mm thick. The ethmoid canal proceeds in a straight line posteromedially and then abruptly turns anteriorly. Lateral to the anterior ridge of bone separating the ophthalmic trough from the ethmoid canal there is an anteroposteriorly oriented row of four minute foramina. In lateral aspect, the supraorbital process is greatly arched dorsally to form the orbit. The frontal of this specimen has been broken anteriorly, revealing numerous laterally elongate frontal sinus cavities.

PARIETAL: The parietal is sutured to the supraoccipital posteriorly, to the squamosal laterally, to the alisphenoid anteroventrally, and to the frontal anteriorly and ventrally. The posterior portion of the parietal is a thin lam-

ina that extends posterodorsally to the edge of the lambdoidal crest. The ventral portion of the parietal anterior to the squamosal/parietal suture is sutured to the alisphenoid anteromedially. The parietal/alisphenoid suture traverses the lateral wall of the braincase steeply and anterodorsally (fig. 5). In dorsal view, the anterior end of the parietal diverges from the midline and curves laterally along the postorbital process to a point ca. 63 mm anterolaterally from the midline. Breakage on the ventral side of the skull reveals a longitudinal frontal/parietal suture on the ventral surface of the parietals anterior to the alisphenoid (fig. 6). This sutural surface is angled posteroventrally and bifurcates at its posterior end ca. 108 mm from the foramen for the optic nerve. The posterior edge of this suture delineates the point at which the frontal forms its part of the roof of the cranial cavity.

The parietals converge along the midline to form a pronounced sagittal crest (fig. 5). The anterior half of the parietals are narrow and form a distinct longitudinal intertemporal constriction. The dorsolateral surface of the parietal is the origin of the anterior half of the temporalis muscle. A low ridge, continuous posteriorly with the squamosal ridge, sweeps anterodorsally to a point ca. 32 mm ventral to the sagittal crest, then anteriorly parallel to the sagittal crest, and terminates on the medial end of the postorbital process. Ventral to this ridge, the parietal is concave and faces laterally; above the ridge, the parietal is flat to concave and faces dorsolaterally. A line of rugosities occurs on the posteroventral corner of the parietal and runs parallel to the parietal/alisphenoid suture. Endocranially, the parietals form the roof and lateral walls of the cranial cavity (fig. 6). The anterior end of their endocranial exposure has a deep groove for the superior sagittal sinus, situated between the posterior bifurcations of the parietal/frontal sutural surface. The groove extends posteriorly into a highly irregular, convex region that includes a median tentorial projection. Around and posterior to that projection the endocranial surface of the parietal is heavily pitted. The heavily pitted surface probably housed a vascular rete situated dorsal to the cerebellum, as has been suggested for basilosaurids (Breathnach, 1955) and for the protocetid *Indocetus* (Bajpai et al., 1996). The cranial cavity is transversely constricted anteriorly but widens posteriorly at the level of the foramen ''pseudovale'' (see discussion of this term below). Posterolateral to the groove for the dorsal (superior) sagittal sinus is a shallow fossa for the right cerebral hemisphere. The posterior edge of this fossa forms the division between the middle and posterior endocranial fossae, thus marking the division between the cerebrum and cerebellum. Although not well developed in *Carolinacetus*, this ridge forms a tentorium osseum in *Basilosaurus cetoides* (Kellogg, 1936: fig. 6).

Ventrolateral to the cerebral fossa there is a sharp anteroposterior bulge corresponding to the rhinal sulcus of the brain, which separates a ventrolateral fossa for the piriform lobe from the rest of the cerebral hemisphere. Within the parietal and lateral to the medial bulge that defines the rhinal sulcus, there is a large vascular canal for the cranio-orbital sinus that continues anteriorly toward the orbital region and opens posteriorly into a deep sulcus. That sulcus rapidly widens posteroventrally and forms a pit-like depression on the squamosal/parietal suture anterodorsal to the anterior process of the petrosal. From that pit a small canal continues posteroventrally within the petrosal/squamosal suture and connects with the temporal canal.

SQUAMOSAL: The squamosal forms the posterior half of the temporal fossa and part of the lateral side of the braincase. Its contribution to the endocranial wall is relatively small, consisting only of a narrow strip on the ventral quarter of the lateral side of the braincase. The squamosal is sutured to the parietal dorsally and dorsomedially, to the alisphenoid anteriorly and medially, to the exoccipital and mastoid process of the petrosal posteriorly, and a small portion to the pterygoid medially. Externally, the squamosal/parietal suture traverses the posterior portion of the temporal fossa (fig. 5). As in other archaeocetes (Kellogg, 1936), the squamosal/parietal suture begins at the posterior margin of the temporal fossa and arches dorsally to a point anterior to the nuchal crest. From there it extends anteriorly parallel to the sagittal crest for a distance of ca. 31 mm and then slopes steeply anteroventrally, terminat-

ing at the anteromedial corner of the squamosal fossa. A small foramen possibly for an emissary vein from the dorsal cerebral vein (petrosquamous sinus) is situated on the squamosal/parietal suture anterior to the nuchal crest. On the endocranial surface the squamosal/parietal suture meanders anteroposteriorly near the base of the lateral wall of the braincase immediately dorsal to the petrosal/squamosal suture. The squamosal/parietal suture is highly oblique in cross section with the squamosal extensively overlapping the parietal laterally. The anteroventral corner of the squamosal is sutured to the alisphenoid anteromedially. A small portion of the pterygoid likely sutured to the squamosal dorsomedial to the foramen ''pseudovale'' as in *Zygorhiza* (Kellogg, 1936: fig. 31c) and *Georgiacetus*. We follow Luo and Gingerich (1999: 49) in recognizing that foramen—the external opening for the mandibular branch of the trigeminal nerve—as the foramen ovale (fig. 6: fo). In *Carolinacetus* the foramen ovale is within the squamosal, and its ventral margin is incomplete.

The squamosal is sutured to the supraoccipital medially along the lateral margin and base of the nuchal crest and to the exoccipital posteriorly. In the holotype of *Carolinacetus* the exoccipital and the squamosal are separated by a narrow gap for most of their length and only sporadically contact each other. The lateral portion of the posterior surface of the squamosal is tightly sutured to the mastoid process of the petrosal.

The external surface of the squamosal bears rough-textured rugosities and relatively smooth depressions, is generally concave, and is the origin for the posterior half of the temporal muscle and fascia. A broadly elevated region, herein termed the *squamosal rise* (fig. 5: sqr), ascends anterodorsally to join an elongate elevation on the parietal homologous to the parietal ridge of *Georgiacetus* (Hulbert et al., 1998: 912). The squamosal rise descends posteroventrally across the face of the squamosal. Below the squamosal rise the squamosal is deeply excavated, forming the squamosal fossa. Above it the bone slopes posterodorsally toward the nuchal crest. In the center of the squamosal rise there is a dorsoventrally oriented depression that separates an elevated region along the squamosal/parietal suture from a textured tuberosity anterior to the posterior margin of the temporal fossa. That tuberosity is not homologous to the squamosal prominence of Sanders and Barnes (2003).

In the holotype cranium, the preserved structures on the ventral side of the squamosal are the external auditory meatus, the posttympanic process, the sigmoid fossa, the postglenoid foramen, the falciform process, the medial edge of the glenoid fossa, and the foramen ovale (fig. 6). The postglenoid process, most of the glenoid fossa, and the zygomatic process were not preserved.

The external auditory meatus extends from the tympanic cavity posterolaterally to the edge of the skull and is a deep, narrow trough flaring slightly at its lateral end. Its posterior margin is formed by the ventrally extended posttympanic process of the squamosal. A small sigmoid fossa is situated immediately anterior to the medial end of the external auditory meatus and is separated from the latter by a small ridge (fig. 7: sgf). The sigmoid fossa received the sigmoid process of the tympanic as in basilosaurids (Luo and Gingerich, 1999). The postglenoid foramen occurs in the squamosal/petrosal suture anteromedial to the sigmoid fossa (fig. 7: pgf). On the medial edge of the squamosal immediately anterior to the sigmoid fossa there is a small groove that leads dorsally into the postglenoid foramen. The falciform process of the squamosal is situated anterior to the postglenoid foramen and probably articulated with the anterior margin of the tympanic as in *Georgiacetus* and *Protocetus*. The falciform process is broad and blocky, unlike that of odontocetes, in which it is long, narrow, and ventrally extended. In the holotype of *Carolinacetus* the medial surface of the falciform process is rugose, probably for the attachment of the tympanic bulla. Although the anterior edge of the falciform process is missing, it appears to have partially floored the foramen ovale, which is 7.6 mm in diameter.

ALISPHENOID: Posteriorly, the alisphenoid is sutured to the squamosal and the parietal. On the ventral half of its medial surface there is a broad sutural surface that probably received the pterygoid. Externally, there is a broad longitudinal ridge at the juncture of the

basicranium and the lateral wall of the cranium. Anteriorly, the alisphenoid becomes very thin as it approaches the sphenorbital fissure, which is confluent posteriorly with the fossa for the piriform lobe of the cerebrum. There is no indication of the foramen ovale on the preserved portion of the alisphenoid in this specimen. The foramen rotundum is absent in other archaeocetes (Kellogg, 1936).

OCCIPUT: In certain areas of the occipital region of the holotype cranium the bones are fused, thus obscuring the sutures between them. In posterior view, the supraoccipital forms a dorsally elongate surface from which originated deep epaxial neck musculature that supported the skull (fig. 9). The dorsal edge of the supraoccipital is thrust posteriorly, causing the upper two-thirds to face posteroventrally. The lower third is directed posteriorly and bears a prominent median ridge dorsal to the foramen magnum. Herein termed the *supracondylar ridge* (fig. 9: scr), this prominence probably anchored the nuchal ligament, which separates the right deep neck muscles from the corresponding left muscles in the bovid *Bos taurus* (Dyce et al., 1996). The left half of the ridge is missing in the holotype of *Carolinacetus*, but immediately lateral to the base of the right half is one of presumably a pair of nuchal tubercles as in *Pakicetus inachus* (Gingerich and Russell, 1981). Lateral to the ridge for the nuchal ligament there is a deep, dorsally elongate fossa for the rectus capitus dorsalis muscle, which is probably homologous to the recti postici muscle in extant cetaceans (Schulte, 1916; Schulte and Smith, 1918). The ventral half of the rectus capitus dorsalis fossa contains numerous vascular foramina. On either side of the midline near the dorsal edge of the supraoccipital are two shallow fossae from which the semispinalis capitus probably originated. The ventral margin of the right fossa is V-shaped, points ventrally, and extends posteriorly along the inner edge of the lambdoidal crest. The left fossa appears larger and more wedge-shaped, but its exact shape and extent is unclear due to breakage. In posterior view, the dorsal margin of the supraoccipital forms a tightly rounded arc, somewhat horseshoe-like in shape (fig. 9). The posteriormost point of the lambdoidal crest is thickened and sharply directed inward. Breakage at the vertex of the skull reveals that the supraoccipital is thickest anteroposteriorly along the midline and wedges between the posterior ends of the parietals. The dorsal surface of the supraoccip-

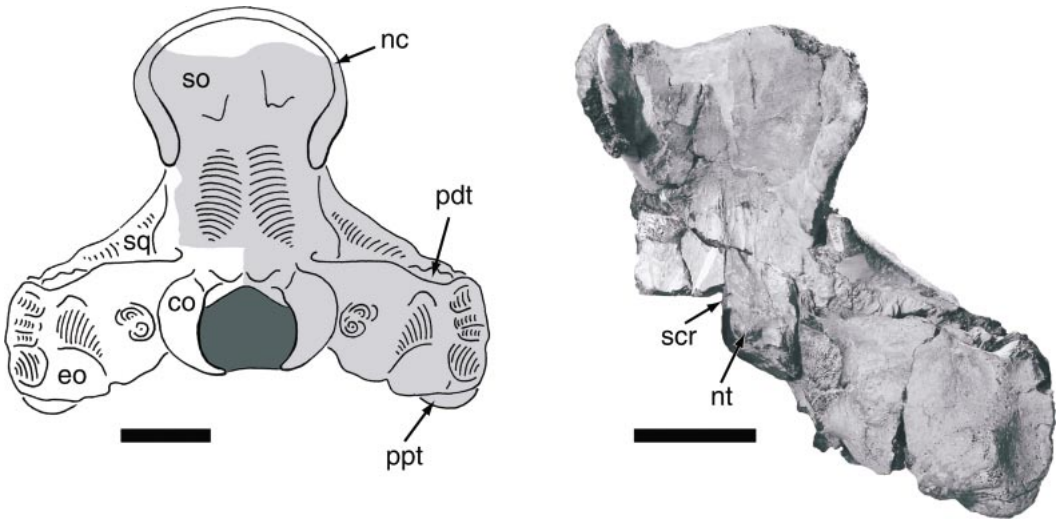

Fig. 9. Line drawing (left) and photograph (right) of the cranium of *Carolinacetus gingerichi* (ChM PV5401) in posterior view. The posterodorsal tongue of the petrosal (pdt) is an autapomorphy of *Carolinacetus*. Scale bars are 5 cm in length. See appendix 3 for anatomical abbreviations.

ital is covered by thin, posterior extensions of the parietals.

The endocranial surface of the occipital contains fossae for various lobes of the cerebellum. Posterior to the median tentorial projection, a dorsoventrally elongate, rugose fossa accommodated a dorsal portion of the lobus medius cerebelli (sensu Dart, 1923), also known as the cerebellar folia (Sisson, 1921). Medial to the dorsoventral fossa, a sagittal ridge divided the cerebellum into right and left halves. Ventral to the dorsal fossa for the lobus medius cerebelli, a transverse ridge 32 mm in length forms the anterior margin of a fossa for another lobe of the cerebellum seated immediately anterior to the roof of the foramen magnum. The posterior wall of the braincase dorsal to the foramen magnum is massively thick, measuring 36 mm along the midline.

Lateral to the foramen magnum, the exoccipital broadens laterally and extends to the lateral edge of the mastoid process of the petrosal, thus obscuring the latter in posterior view. The exoccipital is sutured to the squamosal dorsally and anteriorly, to the mastoid process of the petrosal (lateral to the squamosal) dorsally and anteriorly, and to the posterior process of the tympanic (ventral to the mastoid process) anteriorly and ventrally. The triple junction of the supraoccipital, exoccipital, and squamosal occurs dorsolateral to the broken base of the right occipital condyle. At that junction there is a small pit-like fossa that we interpret as the supracondylar fossa. Extending laterally from that fossa there is a fissure-like separation between the exoccipital and squamosal, terminating at the posterodorsal exposure of the mastoid process of the petrosal. Herein termed the *posterodorsal tongue* of the petrosal (fig. 9: pdt), this exposed portion is sutured to the dorsal edge of the exoccipital, which is notched to receive it. This portion of the mastoid process is 30 mm in transverse diameter and 14 mm in vertical diameter. At the lateral end of the fissure between the squamosal and exoccipital suture there is a foramen that we interpret as the mastoid foramen. We use the term ''mastoid foramen'' as defined by MacPhee (1994) to specify a foramen that transmits an emissary vein from the sigmoid sinus. The mastoid foramen in *Carolinacetus* is formed by the exoccipital ventrally, anteriorly, and laterally, while the roof of the foramen is formed by the squamosal. Continuing from that foramen is a vascular channel that curves ventromedially within the suture between the squamosal and the exoccipital and opens endocranially posterodorsal to the pars cochlearis of the petrosal. Medial to the endocranial opening for the mastoid foramen there is a series of parallel vascular grooves for the occipital diploic veins, which travel posterodorsally into the squamosal/exoccipital suture to enter cancellous bone of the occipital.

The external surface of the exoccipital has several fossae that presumably were the origin or site of insertion for musculature of the neck. Although speculative, myological interpretations can be implied from the morphology of extant cetaceans (Carte et al., 1868; Schulte, 1916; Schulte and Smith, 1918; Howell, 1927) and artiodactyl outgroups (Sisson, 1921; Woodburne, 1968). In the holotype of *Carolinacetus* the right condyle of the skull and most of the condylar neck are missing. A small foramen and a vascular groove of unknown function perforate the base of the condylar neck 22 mm dorsal to the hypoglossal foramen on the posterior surface of the occipital. Ventrolateral to the condylar neck there is a notch in the ventral edge of the exoccipital that forms the dorsal margin of the jugular foramen. The hypoglossal foramen is in the medial wall of the jugular foramen. Lateral to the jugular foramen there is a partially preserved, bulbous paroccipital process. Dorsal to the paroccipital process there is a semicircular depression containing two pits, ca. 9 mm in diameter each, which may mark the insertion of the rectus capitus lateralis muscle. The ventral pit is considerably deeper than the dorsal one and contains a pair of minute foramina. Lateral to those depressions the exoccipital is more posteriorly directed. Lateral to the paroccipital process an ovate prominence of bone forms the base of the exoccipital and defines the edges of two muscular fossae. Dorsal to this region a broad fan-shaped fossa tapers ventrally and marks the likely point of insertion for the obliquus capitus anterior muscle, which inserts in a similar position in the collared peccary (Woodburne, 1968). The

exoccipital extends to the lateral edge of the skull and thus excludes the mastoid process of the petrosal and the postmeatic portion of the squamosal as a surface for muscle attachment. Instead, a vertical row of four muscular fossae occurs on the lateral edge of the exoccipital. The top three are roughly equal in size and the ventral one is twice the size of the others. From dorsal to ventral position they are interpreted as fossae for the longissimus capitus, the splenius mastoideus, sternomastoideus, and the cleidomastoideus muscles. The latter two may be reversed as in extant cetaceans (Schulte, 1916; Howell, 1927).

A fragment of the right side of the basioccipital bearing the basioccipital crest is preserved but cannot be reattached to the skull. However, its position relative to the rest of the skull can be estimated because a matching portion of the hypoglossal foramen was preserved. This fragment indicates that the dorsoventral thickness of the basioccipital rapidly increases laterally. The ventrolateral border is formed by a rounded, protruding basioccipital crest estimated to be 31.5 mm in length and 19 mm in greatest thickness. The dorsal surface of the basioccipital crest has numerous fine pits to which connective tissue to the ectotympanic bulla and petrosal were attached. On the dorsal surface of the basioccipital anterior to the hypoglossal foramen there is a broad, laterally oriented excavation for the peribullary sinus. Anterior to that excavation the dorsoventral thickness increases and the carotid foramen and canal perforate the lateral side of the basioccipital crest, unlike extant cetaceans in which the carotid foramen is within the basisphenoid (Schulte, 1916; Wible, 1984; Fordyce, 1994).

JUGAL: The left jugal is represented only by its posterior portion and the right one only by its anterior portion (fig. 3). The sutural surface for the articulation of the lacrimal is present on the anterior end of the right jugal. The dorsal surface of that bone is flattened adjacent to the orbit, is not sharply recurved, and apparently there was not a postorbital process. Medially, the sutural surface for articulation with the maxilla is present above the lower edge of the right jugal.

PETROSAL: Although only the right petrosal is preserved in the holotype of *Carolinacetus*, it is by far the best preserved petrosal from the archaeocete families of Pakicetidae, Ambulocetidae, Remingtonocetidae, and Protocetidae. The ventral portion of that bone was found separate from the skull, thus allowing both the ventral and dorsal surfaces of the petrosal to be studied before restoration to its original position. In describing the petrosal we employ the term ''mastoid process'' in preference to ''posterior process of petrosal'' because the former stresses homology with other ungulate taxa. We suggest that usage of the term ''posterior process of petrosal'' be restricted to petrosals that have decoupled from the skull (see Fraser and Purves [1960] for a detailed explanation of petrotympanic decoupling).

The ventral view of the petrosal is dominated by a gently convex promontorium that houses the spiral cochlear canal (figs. 7, 8). The medial edge of the promontorium is defined by a broad area (3–5 mm) of rugose bone, the lateral edge by the epitympanic recess, the anterior edge by the groove for the tensor tympani muscle, and the posterior edge by the peribullary sinus. The posteromedial third of the promontorium is flat, while the remaining portion is rounded, convex, and protrudes slightly more ventrally. At the posterior end of the rugose bone and medial to the fenestra rotunda there is a small, pointed process herein termed the *medial tuberosity of the promontorium* (fig. 7: mt). From this tuberosity a short medially directed ridge ascends to the perilymphatic foramen. A narrow sulcus extends from the perilymphatic foramen paralleling the posterior margin of the tube of the internal acoustic meatus (IAM). Anterodorsal to this tuberosity there is a prominent pit within which there is a small foramen of unknown utility. The fenestra rotunda opens onto the posterior face of the pars cochlearis and is highly elliptical, with the long axis being 4.6 mm in length and oriented transversely and horizontally. A shallow groove extends medially from the fenestra rotunda and terminates posterior to the medial tuberosity of the promontorium. Immediately lateral to the fenestra rotunda there is a small posteriorly projecting ledge of bone that might be homologous with the caudal tympanic process of

other mammals as defined by MacPhee (1981) and Wible (1990). Lateral to the promontorium is the fenestra vestibuli, which is situated medial to the epitympanic recess. The fenestra vestibuli faces lateroventrally (fig. 8: fv) and is not visible in a directly ventral view (fig. 7). It is elliptical with the long axis oriented anteroposteriorly and is 2.8 mm in length. In the holotype of *Carolinacetus* the base of the stapes is still lodged within the fenestra vestibuli and appears as a ring of broken bone. Lateral to the fenestra vestibuli is the tympanic aperture of the canal for the facial nerve (fig. 8: VII). The sulcus for the facial nerve begins at its tympanic aperture and proceeds posteriorly along the roof of the epitympanic recess. A deep fossa for the stapedial muscle is located posterior to the fenestra vestibuli, medial to the facial nerve sulcus, and lateral to the fenestra rotunda. The stapedial muscle fossa is at least twice as deep as the facial nerve sulcus.

The tegmen tympani, which is homologous to the superior process of Kellogg (1936) (see Luo and Gingerich, 1999), is the part of the petrosal lateral to the facial nerve canal and has extensive contact with the medial side of the squamosal. The epitympanic recess is situated on the ventral surface of the tegmen tympani and bears a large circular fossa for the head of the malleus, which is situated anterolateral to the tympanic aperture for the facial nerve canal. The presence or absence of the fossa for the incus cannot be determined because that area of the petrosal is missing. The tegmen tympani extends dorsally (dorsal *Schuppe* of tegmen tympani of Pompeckj, 1922), forming a small portion of the endocranial wall of the braincase. The dorsal edge of tegmen tympani is not flush with the squamosal but instead is slightly raised and is penetrated by multiple fossae/foramina. The anterior foramen transmitted the cranio-orbital sinus, the adjacent posterior canal contained the capsuloparietal emissary vein (i.e., postglenoid vein), and the posterior fossa connected to the sigmoid sinus (fig. 7: cos, etc).

As in other cetaceans, the petrosal of *Carolinacetus* has a distinct anterior process (anterior extension of the tegmen tympani; Luo and Gingerich, 1999). In ventral view, most of the anterior process is obscured by the squamosal, which wraps around the anterior end of the former. In basilosaurids the squamosal overlaps the lateral side of the anterior process but does not override it (Luo and Gingerich, 1999). A pronounced deep groove for the tensor tympani muscle extends along the ventromedial edge of the anterior process. This groove begins as a deep fossa posteriorly and narrows to a shallow groove at its anterior end (fig. 7: gtt). Medial to the tensor tympani fossa on the ventromedial edge of the anterior process there is a small hiatus fallopi for the greater superficial petrosal nerve. The posterior end of the anterior process projects toward the tympanic cavity, is flattened, and faces primarily ventrally but slightly posteriorly. That portion of the process likely articulated with the tympanic bulla as in *Protocetus* (Geisler, personal obs.). Anterior to the probable articulating surface with the ectotympanic there is an anterodorsal-to-posteroventral fossa that receives a posterior projection from the falciform process of the squamosal. The postglenoid foramen is visible lateral to the posterior end of the anterior process. The foramen also occurs in basilosaurid archaeocetes but was misidentified by Kellogg (1936: fig. 6) as the fossa epitubaria. The dorsal two-thirds of the anterior face of the anterior process is flat and faces primarily anteriorly but slightly ventrally. The anterior process tapers to a point, homologous to the anterodorsal angle of other taxa (see Fordyce, 1994; Luo and Marsh, 1996; Geisler and Luo, 1996) (fig. 7: ap). This point is homologous to, but not as well developed as, the dorsal spine of *Remingtonocetus* (Kumar and Sahni, 1986).

The mastoid process of the petrosal is elongate and is wedged between and sutured to the squamosal anteriorly and to the exoccipital posteriorly. It has extensive exposure on the lateral and posterior sides of the skull, with a significant portion of the ventrolateral exposure undoubtedly being ectotympanic and not petrosal. Viewed laterally, the mastoid process has a thick wedge-shaped exposure of heavily rugose bone that narrows dorsally to a thin layer between the squamosal and the exoccipital. It then thickens adjacent to the dorsolateral corner of the exoccipital and forms the posterodorsal tongue of the petrosal (fig. 9). In posterior view, that

portion of the petrosal protrudes into the exoccipital/squamosal suture ca. 10 mm medial to the lateral edge of the exoccipital. The ventral surface of the mastoid process is almost completely obscured by the posterior process of the tympanic (fig. 6). That observation, based on a cross-sectional break through the mastoid process in the holotype and upon careful comparison with the basicranium of *Georgiacetus*, demonstrates that in *Carolinacetus* the apparent mastoid process of the petrosal is actually a compound structure composed of the posterior process of the tympanic and the mastoid process of the petrosal as in mysticetes (Kasuya, 1973; Geisler and Luo, 1996). In ventromedial view, the proximal end of the mastoid process is constricted to form the neck of the mastoid process (homologous to neck of posterior process, sensu Luo and Marsh, 1996). The degree of constriction is unclear because a fragment of the petrosal is missing. The petrosal/tympanic suture is situated at the anteromedial end of the mastoid process of the petrosal and anterolateral to the paroccipital process. Adjacent and posterior to that suture there is a short groove that is interpreted as a continuation of the facial nerve sulcus on the ventral surface of the mastoid process as reported in other cetaceans (e.g., Geisler and Luo, 1996; Dooley et al., 2004).

In dorsal view, the rim of the internal acoustic meatus in *Carolinacetus* is elevated to form a cranially elongate tube that projects a maximum of 20 mm from the edge of the pars cochlearis (fig. 7: tiam). The tube is somewhat volcano-shaped, and the meatus itself is analogous to the crater on a volcano's summit. The dorsal lip of the internal acoustic meatus tube projects considerably farther than the ventral lip and has a needle-like process in the posteromedial corner. The internal acoustic meatus tube is present in *Georgiacetus* but is not as well developed as in *Carolinacetus*. The rim of the internal acoustic meatus is elevated in many mysticetes (Geisler and Luo, 1996; Dooley et al., 2004), although this morphology is presumably convergent to the one in *Carolinacetus* and *Georgiacetus*.

The internal acoustic meatus tube transmitted both the vestibulocochlear nerve (cranial nerve VIII) and the facial nerve. The tractus spiralis foramina, for branches of the cochlear nerve, are centered in the IAM at its deepest point. The foramen singulare for the vestibular nerve is slightly anterolateral to the tractus spiralis foramina. The cranial aperture for the facial nerve canal is concealed by sediment, but a break repaired during preparation revealed its position anterior to the foramen singulare ca. 9 mm from the lip of the IAM. That break also exposed a very thin dividing wall (≈0.25 mm) between the facial nerve canal and the IAM proper. The ventralmost surface of the IAM tube is smooth, broadly rounded anteroposteriorly, and forms a nearly flat medial sulcus for the inferior petrosal sinus (Geisler and Luo, 1998: fig. 8). The anterior process of the petrosal and the anterior edge of the IAM tube form, respectively, the lateral and posterior borders of the piriform fenestra, through which the inferior petrosal sinus exited the cranial cavity. The medial side of the piriform fenestra was probably enclosed by the basioccipital and basisphenoid as in other protocetids (e.g., *Protocetus* and *Georgiacetus*). The endocranial surface of the petrosal contains two large fossae: the suprameatal fossa (sensu Luo and Eastman, 1995) dorsal to the IAM, and a second one, located posterior to the IAM, herein termed the *postmeatal fossa* (fig. 7: pmf). Those two fossae are probably excavations for the endocranial portion of the peribullary sinus. A subarcuate fossa is not present. Posterodorsal to the IAM tube and between the postmeatal and suprameatal fossae there is a prominent dorsomedially projecting process herein termed the *suprameatal process* (fig. 7: smp) Between the base of the suprameatal process and the base of the IAM tube there is a small cleft for the endolymphatic foramen.

ECTOTYMPANIC BULLA: Both ectotympanic bullae of ChM PV5410 are preserved, with the right one being more complete than the left. Our description of the bulla of *Carolinacetus* is a composite based on both specimens. In ventral view, a broad anteroposteriorly oriented median furrow divides the bulla into lateral and medial eminences (fig. 10). The thickened and inflated medial edge and eminence is termed the involucrum. In ventral view, the median furrow wraps around the posterior face of the bulla and

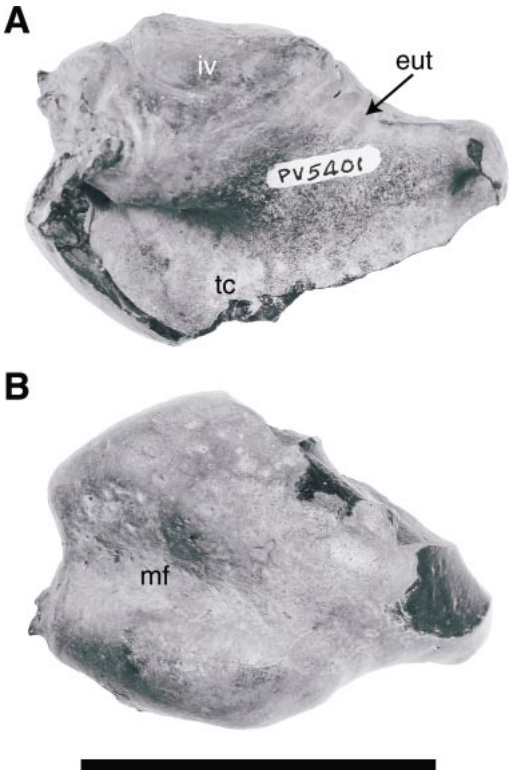

Fig. 10. Right tympanic bulla of *Carolinacetus gingerichi* (ChM PV5401) in dorsal (**A**) and ventral (**B**) view. Most of the outer lip of the bulla was not preserved. Scale bar is 5 cm in length. See appendix 3 for anatomical abbreviations.

forms a broad rounded notch on its posterior edge. The medial margin of the involucrum is deeply indented 47.7 mm anterior to its posterior end, marking the opening for the eustachian tube. That indentation is also evident in medial view where the dorsoventral thickness of the involucrum abruptly thins. The posterior surface of the involucrum is covered with small depressions and rugosities. That area and a similar one along the medial side of the involucrum are points of attachment for tough connective tissue that anchored the bulla to the paroccipital process of the exoccipital and to the basioccipital crest, respectively. In medial view, a deep groove runs dorsally on the surface of the involucrum 8.0 mm anterior to its posterior edge. This groove deepens dorsally and turns anteriorly before reaching the dorsal surface of the involucrum, then terminates 15 mm anterior to the posterior margin of the involucrum.

On the posterior face of the bulla there is a vertical tympanic cleft between the involucrum, or inner lip, and the outer lip of the bulla. A broad sulcus originates near the ventral end of the outer lip and extends dorsally along the lateral margin of the cleft and then enters the tympanic cavity at the ventral edge of the cleft. Broken fragments from the holotype bullae indicate that the lateral edge of the bulla thinned dorsally. The presence of a sigmoid fossa on the squamosal strongly suggests that a large sigmoid process was present but was not preserved. Other features of the outer lip also were not preserved.

As mentioned above, what appears to be the mastoid process is actually a compound process composed ventrally of the posterior process of the ectotympanic and dorsally of the mastoid process of the petrosal. The posterior process of the tympanic is broad, elongate, and almost completely covers the ventral surface of the mastoid process of the petrosal and is sutured to it (figs. 6, 7: ppt). The distal end of the posterior process is exposed on the lateral side of the skull between the exoccipital and squamosal ventral to the mastoid process of the petrosal (fig. 3). The posterior process increases in thickness posterolaterally, and its ventral surface is generally smooth with a few shallow transverse grooves. In the holotype right bulla there are two broken surfaces near the proximal end of its ventral surface; in *Georgiacetus* and in basilosaurids, the inner and outer pedicles of the posterior process of the tympanic connect at similar points. Multiple pits occur in the space between the broken bases of the pedicles and might have been continuous with the sulcus lateral to the vertical tympanic cleft.

MANDIBLE

The posterior regions of both mandibles are preserved, but only the medial halves of the anterior ends were found. The posterior portion of the left mandible is intact as far as the anterior margin for the alveolus of the third molar but is missing that portion of the dentary between the first molar and the canine (fig. 11). Only 114 mm of the anterior

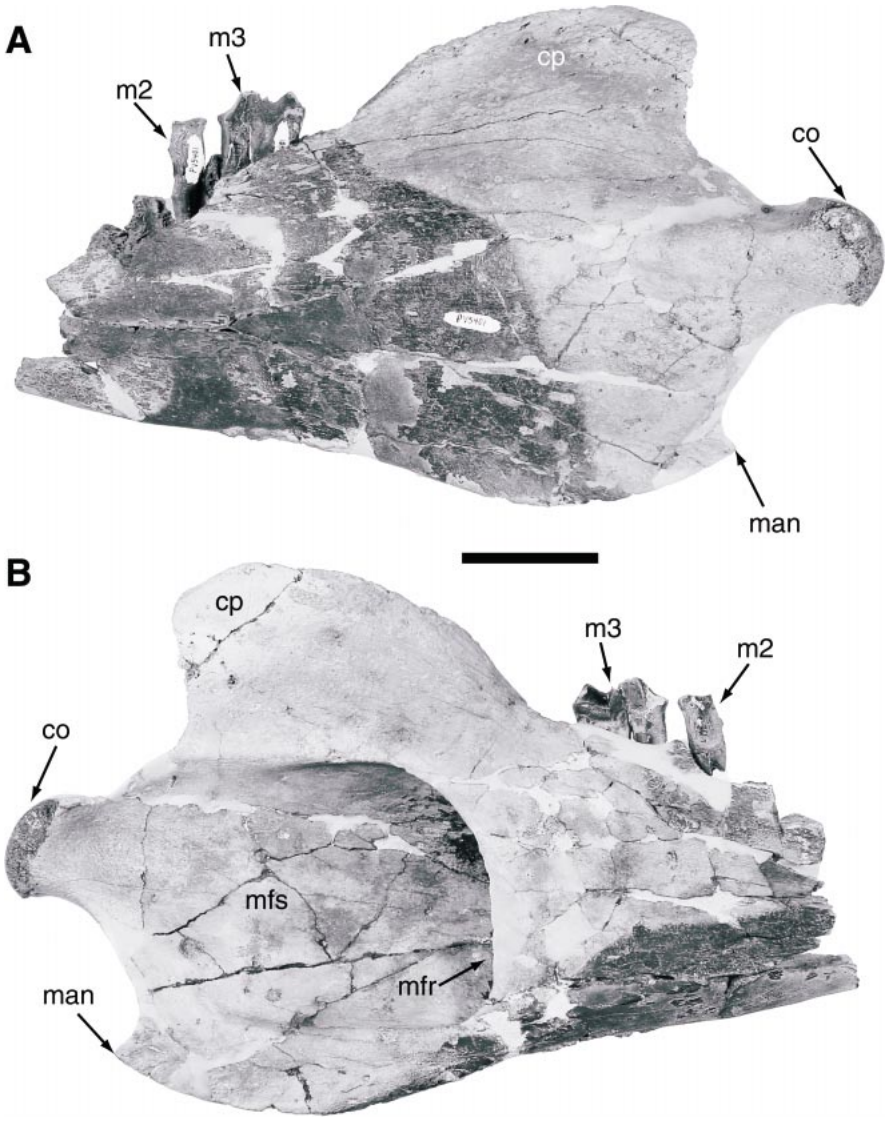

Fig. 11. Posterior portion of the left mandible of *Carolinacetus gingerichi* (ChM PV5401) in lateral (**A**) and medial (**B**) views. The great depth of the mandible between the coronoid process (cp) and the mandibular angle (man) is an autapomorphy of this genus. Scale bar is 5 cm in length. See appendix 3 for anatomical abbreviations.

end is preserved, including a portion of the alveolus for i1 and the alveolus for i2. The posterior region of the right mandible is preserved from the condyle to the anterior edge of the alveolus for p4, but it is missing portions of the coronoid process and the entire angular region (fig. 12). The preserved portion of the anterior end of the right mandible extends from the posterior end of the alveolus for i3 to the middle of the alveolus for i1, a distance of 180 mm. The anterior ends of both mandibles are tightly sutured along the symphysis but are not ankylosed (fig. 13).

The posterior end of the alveolus for i1 is situated immediately anteroventral to the alveolus for i2, with the posterior wall of the former forming the anterior wall of the latter.

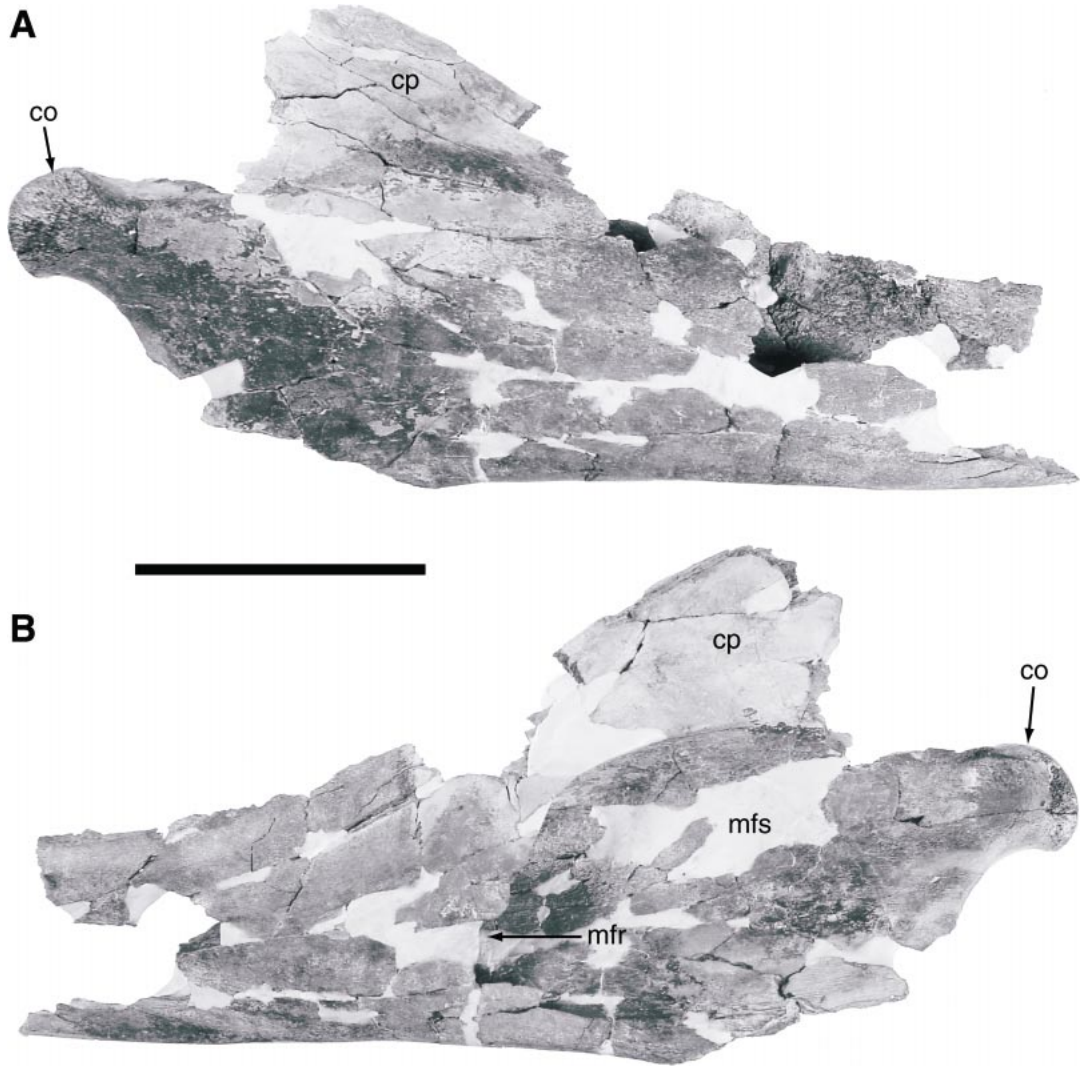

Fig. 12. Posterior portion of the right mandible of *Carolinacetus gingerichi* (ChM PV5401) in lateral (**A**) and medial (**B**) views. Scale bar is 10 cm in length. See appendix 3 for anatomical abbreviations.

Although the anterior part of the alveolus for i1 is missing, it is clear that this tooth was considerably smaller than i2, the alveolus of which is approximately 33 mm in anteroposterior diameter. Posterior to the alveolus for i2 there is a shallow, rounded depression approximately 27 mm in anteroposterior diameter that we think to be the medial wall of the alveolus for i3. The alveolus for the canine lies almost directly behind the alveolus for i3 and has an anteroposterior diameter of approximately 50 mm. The medial wall of the canine alveolus is extremely narrow, measuring only 10.5 mm (fig. 13). Centered on the medial wall of the alveolus of i2 and of the canine there is a low, rounded ridge, suggesting a corresponding groove on the medial surface of these teeth.

The most striking feature of the mandible is its extreme depth in the region of the mandibular fossa, where it is 265% greater than the depth at p4 (table 2). The posterior increase in mandibular depth is caused by the steep ascending (coronoid) process and by the abrupt downward slope of the mandible's ventral edge, which begins at a point below

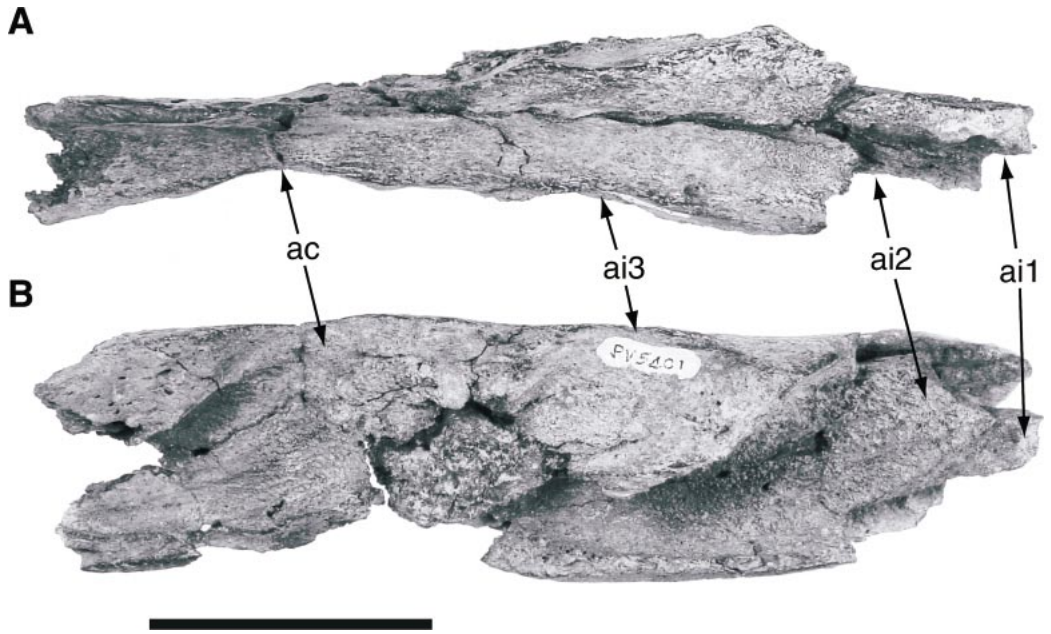

Fig. 13. Sutured anterior ends of the right and left mandibles of *Carolinacetus gingerichi* (ChM PV5401) in dorsal (**A**) and lateral (**B**) views. The lateral sides of the mandibles are not preserved, thus exposing the alveoli for the incisors and canines. Scale bar is 5 cm in length. See appendix 3 for anatomical abbreviations.

the margin of the mandibular foramen and ends at the angular process (fig. 11). The ascending process begins posterior to p4 then rises sharply in the region of m2. The lateral surface of the mandible is highly convex with a broadly rounded longitudinal ridge bisecting the mandible into dorsal and ventral halves. In lateral view, the dorsal edge of the coronoid process begins 15 mm posterior to the posterior edge of the alveolus for m3, rises sharply at an angle of approximately 45°, gradually curves to become nearly horizontal, and finally curves sharply ventrally at its posterior terminus. The anteroposterior length of the coronoid process is roughly twice its dorsal height, and the anterior half of its lateral surface forms a shallow temporalis fossa. The base of the dorsal edge of the coronoid is in line with the lateral edge of the alveolus for the m3. The coronoid process is relatively thin, and the dorsal edge adjacent to the temporalis fossa is curved laterally. Medial to the base of the coronoid and 23 mm posterior to the edge of the alveolus for m3 there is small foramen that leads to an enlarged opening into the mandibular canal.

The medial side of the mandible is dominated by a large rectangular mandibular fossa (fig. 11, 12: mfs). This fossa is continuous anteriorly with a cavernous mandibular foramen. The medial surface of the mandible is flat to slightly concave anterior to the mandibular foramen and highly concave in the region of the mandibular fossa. The mandibular fossa and foramen presumably contained an intramandibular fat body as in extant odontocetes (Norris, 1980). The dorsoventral depth of the mandibular foramen is nearly the height of the mandible at m3. The medial and lateral walls of the mandibular canal are extremely thin just anterior to the mandibular foramen, having an average thickness of 3 and 4 mm, respectively. In medial view, the medial edge of the mandibular foramen is relatively straight and is oriented vertically. This edge is continuous with longitudinal ridges that define the dorsal and ventral edges of the mandibular fossa. The ventral edge of the mandible adjacent to the mandibular

TABLE 2
Measurements (in mm) of Holotype Mandibles of *Carolinacetus gingerichi*, new genus, new species (ChM PV5401)

	Left	Right
Anteroposterior length of preserved portion	310	373
Transverse diameter at margin of mandibular fossa	40.4	40.5
Depth at maximum height of coronoid process	187	—
Depth at anterior base of coronoid process	122.6	—
Depth at posterior margin, alveolus for m3 (lingual side)	103.6	96.6
Depth at anterior margin, alveolus for p4 (lingual side)	—	75.3
Anteroposterior length of coronoid process, anterior base to greatest posterior extremity	132.2	—
Length of coronoid process at base	130.1	—
Transverse diameter of condyle, as preserved	39.3	41.8
Vertical diameter of condyle, as preserved	40.3	38.2
Post. margin of condyle to posterior base of coronoid process	62.6	—
Post. margin of condyle to posterior margin of alveolus for m3	210.5	—
Post. margin of condyle to anterior margin of alveolus for m3	244.9	246
Post. margin of condyle to margin of mandibular fossa	(172.7)[a]	(187.4)
Vertical diameter of mandibular fossa	97.8	96.6
Anteroposterior length, alveolus for m3	35.5	—
Anteroposterior length, alveolus for m2	(27.5)	(27.5)
Anteroposterior length of m3 at base of crown	35	—

fossa bows ventrally in medial view and ends with a posteriorly projecting point that forms the mandibular angle. That angle terminates at a point almost directly ventral to the posterior end of the coronoid process. A rugose ridge extends anteriorly from the mandibular angle for a distance of 51 mm. This ridge and the flattened ventral edge adjacent to it probably served as a point of attachment for the pterygoideus internus muscle. The condyloid process projects approximately 56 mm posteriorly from the plane of the posterior edge of the coronoid process and the tip of the mandibular angle. The condyle is separated from the posterior edge of the coronoid process by the mandibular notch and from the mandibular angle by the curved posterior edge of the mandible. The condyloid process is stout and projects posteriorly approximately along the longitudinal axis of the mandible. On its medial face there is a wide longitudinal fossa for the insertion of the pterygoideus externus muscle. In lateral view, a pronounced ridge separates the condyloid process into a dorsally facing shallow fossa and a broad, flat, ventrally facing surface. In posterior view, the condyle is roughly triangular and is directed ventrally. In dorsal view, the condyle is situated lateral to the long axis of the ramus. Its dorsal edge is approximately level with the dorsal edge of the alveolus for m2, and the edge that forms the mandibular notch is in line with the medial edge of the condyle.

Dentition

Eighteen dental elements were preserved, including both upper canines, a probable right P1, a probable left p1, left p3, right p4, half of the left m1, right and partial left m2, right and left m3, and seven tooth fragments. In general, the enamel of all the teeth is poorly preserved (fig. 14). The tips of the lower

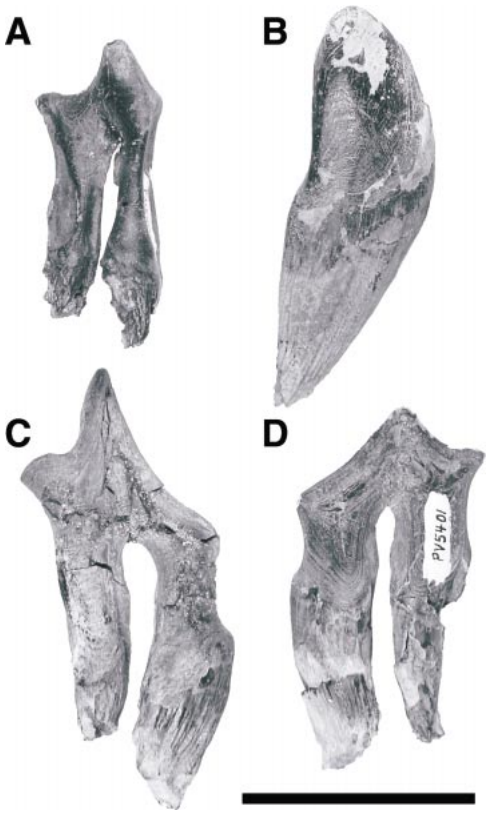

Fig. 14. Teeth of *Carolinacetus gingerichi* (ChM PV5401) in labial view: right m2 (**A**), right C (**B**), right p4 (**C**), and left p3 (**D**). Scale bar is 5 cm in length. See appendix 3 for anatomical abbreviations.

teeth bear numerous fine dorsoventral grooves, and the inner faces of both roots are bisected by a narrow, deep groove. The two teeth that appear to be the upper and the lower first premolars are relatively small, and each is missing the crown and the basal portions of the roots, but the size and the tightly coalesced roots of these teeth indicate that they are first premolars.

UPPER CANINE: The left upper canine is in situ and the right one was isolated (figs. 4, 14B). The root and crown of the canine are transversely compressed, the crown occupying one-half the total length of the tooth on the lingual surface and one-fourth of the labial surface. The anterior half of the labial surface of the crown bears a prominent wear facet from occlusion with the lower canine. The root is finely grooved lengthwise and bears a distinct linear median depression on both the lingual and labial surfaces below the crown base. The root of the canine is directed posteriorly and lies almost parallel to the ventral margin of the maxilla, but the crown is angled anteroventrally.

LOWER THIRD PREMOLAR: The crown of the left p3 is transversely compressed with a broad and low protoconid (fig. 14D). The protoconid is inclined posteriorly and has poorly defined anterior and posterior carinae. The anterior carina forms a long angled cutting surface. Posterior to the protoconid is a posteriorly projecting cusp that is separated from the former on the lingual surface by a broad shallow fossa. In lingual view, the anterior edge of the crown bears a shoulder that separates the cutting edge from the ascending part of the crown below. Between the crown and the dorsal ends of the roots, the tooth is anteroposteriorly and transversely constricted. The tooth is double-rooted with clear separation up to the base of the crown. The anterior root is 7 mm longer than the posterior root and is considerably wider both in transverse and anteroposterior thickness. The lingual face of the anterior root is concave to flat, the posterior face is concave, and the remaining faces are convex. The posterior root is convex on all faces.

LOWER FOURTH PREMOLAR: The right p4 has a narrow pointed protoconid that is inclined posteriorly and a low posteriorly pointed cusp (fig. 14C). The apical end of the protoconid is recurved to a more vertical position. The crown is strongly compressed transversely. Both the anterior and posterior edges of the protoconid have carinae. The posterior carina descends abruptly posterior to the protoconid and continues onto the posterior cusp, which is low, dorsally convex, and hook-like in form. The protoconid and posterior cusp are separated by a shallow furrow on both the labial and the lingual faces. The tooth has two widely separated roots, with the anterior root being significantly longer and much more robust than the posterior one. The lingual sides of the roots are flattened, and the labial sides are strongly convex. Approximately midway down the anterior and posterior roots the transverse and anteroposterior diameters increase abruptly.

LOWER SECOND MOLAR: The complete

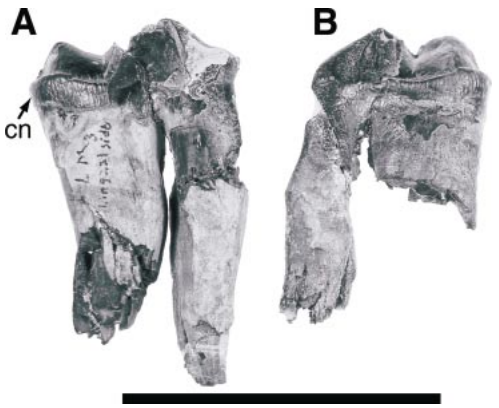

Fig. 15. Left (**A**) and right (**B**) m3s of *Carolinacetus gingerichi* (ChM PV5401) in lingual view. Scale bar is 5 cm in length. See appendix 3 for anatomical abbreviations.

right m2 was found in place in the mandible, but only the posterior half of the left m2 was preserved (figs. 11, 14A). The protoconid is more than twice the height of the hypoconid. The anterior face of the protoconid is flattened, suggesting the original presence of lingual and labial carinae. The protoconid and the hypoconid are connected by a carina, the posterior half of which is also known as the cristid obliqua. In anterior aspect, the protoconid is angled farther lingually than the hypoconid. The hypoconid is directed posteriorly beyond the margin of the posterior root. The anterior root is inflated at the base. The posterior root is more transversely narrow than the anterior one.

LOWER THIRD MOLAR: Both lower m3s were found in place in the mandibles. The crown of the right m3 is better preserved than the left, but it is missing half of its posterior root. Although incomplete in both specimens, the protoconid is clearly not much higher than the hypoconid (fig. 15). As in the lower premolars, both cusps are transversely compressed. A crenulated cingulum 3–5 mm in height wraps around the base and posterior edge of the hypoconid. It continues anteriorly for at least half of the length of the tooth on the lingual side, with the anterior portion remaining only as an eroded remnant. The cingulum has been almost completely removed by wear from the labial side of the tooth. The enamel of the cingulum and the hypoconid has fine, faint wrinkles that become progressively fewer and shallower apically. Along its entire anteroposterior length the hypoconid bears a carina with faint, widely spaced serrations. The hypoconid is separated anteriorly from the protoconid by a small carnassial notch 1 mm in height. The anterior face of the protoconid is formed by labial and lingual carinae that are widely separated at the base but converge dorsally near the apex of the protoconid. On the left m3 the lingual carina ends on a distinct anteriorly projecting cusp, which abuts anteriorly against the hypoconid of m2. The roots are separated by a narrow gap, with the anterior one being compressed anteroposteriorly and the posterior one compressed transversely. The lingual and labial faces of the posterior root are flat. The anterior face of the anterior root is concave, the labial face is convex, and the lingual surface is flat.

VERTEBRAE

Thirteen vertebrae were recovered, including the atlas, axis, and 3rd, 4th, 6th, and 7th cervical vertebrae, and the 1st, 2nd, and 4th–8th thoracics. Three neural arches and six fragments of centra also were found. Each of the cervicals is described separately, but we have selected only the second and sixth thoracic vertebrae for description because most of the preserved thoracics are similar in morphology. Positional determinations of the thoracics were simplified by the preservation of vertebrae from the anterior portion of the series, in which the transitional elevation of the transverse processes posterodorsally can be readily observed (fig. 16). Measurements of the cervical vertebrae are given in table 3; those of the thoracics appear in table 4. In measuring transverse diameters of the thoracics, measurements of the anterior face of the centrum were taken at the approximate centers of the demifacets, and those of the posterior face were taken at the lateral margins of the demifacets.

Epiphyses were missing from both faces of the fourth thoracic and from the posterior face of both the fifth and the seventh thoracics. In both of the latter two vertebrae, portions of the anterior epiphysis were not fully ankylosed and were subsequently glued onto the centrum. Hence, the holotype of *C. gin-*

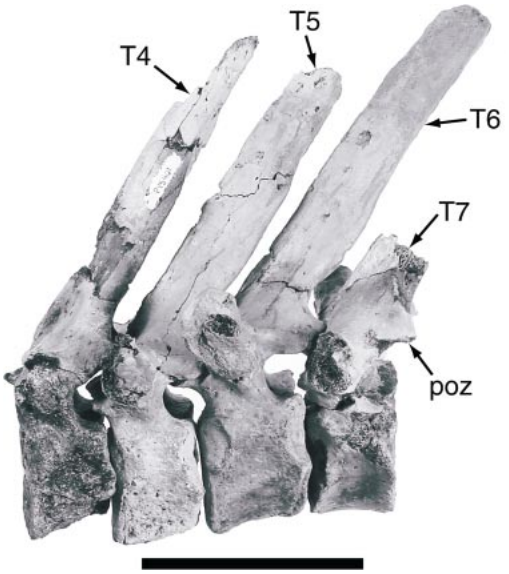

Fig. 16. Lateral views of the thoracic vertebrae (i.e.. T4–T7) of *Carolinacetus gingerichi* (ChM PV5401). Scale bar is 10 cm in length. See appendix 3 for anatomical abbreviations.

gerichi seems to have been a young adult and may not have reached the maximum size attained by this species.

FIRST CERVICAL: The atlas vertebra is approximately 215 mm in width and 101 mm in vertical dimension (fig. 17). It is missing most of the ventral tubercle (hypophysis), the anterolateral portion of the transverse process, and the edges of the transverse processes ventrolateral to the transverse foramina. In general form it is robust and more nearly like the atlas vertebra in artiodactyls than in modern cetaceans. Hence, we have used certain osteological terms generally applied to land mammals, for example, ''transverse foramen,'' is usually termed ''vertebrarterial canal'' in the cetacean literature.

The width of the anterior face is approximately 125 mm, and its height at the midline is 56 mm. The surface is deeply concave with high and narrow lateral and dorsal edges. The anterior margin of the dorsal surface extends forward beyond the lower portion of the anterior face and is deeply emarginated at the midline by a broad notch, herein termed the *supracondylar notch* (fig. 15C: sn). This notch is present in many land mammals, including artiodactyls, perissodactyls, canids, ursids, and hyaenids, inferring that its presence is primitive for cetaceans. Posterior to the notch the dorsal surface grades upward to the dorsal tubercle.

The right transverse process is well preserved, with most of its dorsal surface being depressed below the level of the dorsal tubercle. The transverse process is formed by a horizontal tabular portion and a vertically oriented descending portion, which in lateral view has the form of an inverted ''L''. The deeply excavated region immediately below the horizontal portion of the transverse process is termed the atlantal fossa in land mammals. The distal end of the transverse process is upturned and thickens posteriorly, achieving its greatest thickness at the junction of the horizontal and descending potions.

The right and left halves of the posterior face are separated by the semicircular trough for the reception of the odontoid process of the axis vertebra, herein termed the *odontoid fossa* (fig. 17B: of). Each half has an ovoid articular surface with an upturned lateral edge that forms a thin lip that partially conceals the opening of the transverse foramen. This foramen is vertically elongate, with a maximum diameter of 8.9 mm. It opens anteriorly into the atlantal fossa along the lateral surface of the centrum and at that point is situated 18.5 mm posteroventral to the ventral opening of the alar foramen. This foramen perforates the base of the transverse process at a point 28.3 mm posterior to the dorsal edge of the anterior face of the centrum. At that point it is directly opposite to the mouth of the lateral vertebral foramen, which opens into the neural canal. This canal is broadest (59.5 mm) across its posterior opening and tapers ventrally into the odontoid fossa.

SECOND CERVICAL: The axis vertebra is complete except for the distal ends of the spinous and transverse processes, the lateral edges of the posterior face of the centrum, the right pedicle of the neural arch, and the lateral edge of the right transverse foramen (fig. 18). The right and left articular surfaces for the atlas vertebra are flat dorsoventrally and slightly concave transversely. The odontoid process is bullet-shaped in ventral view and is 30 mm in transverse diameter and 29 mm in anteroposterior length. The ventral

TABLE 3
Measurements (in mm) of Holotype Cervical Vertebrae of *Carolinacetus gingerichi*, new genus, new species (ChM PV5401)

	C1	C2	C3	C6	C7
Anteroposterior diameter	42	86.7[a]	36.6	38.6	34.3
Transverse diameter of centrum, anteriorly	103.5	113.3	49.8	50.1	50.2
Vertical diameter of centrum, anteriorly	31.7[b]	42.7	49	50.3	51.5
Transverse diameter of centrum, posteriorly	102.7	(52)[c]	60.5	66	77.2
Vertical diameter of centrum, posteriorly	62.8	—	51.7	51.9	50.3
Tip of neural spine to ventral face of centrum, anteriorly	102+	129+	90.3	93+	143.7
Distance between outer margins of transverse processes	(233)	—	(156)	179.1	(82.7)
Vertical diameter of neural canal	47.4	36.6	23.3	26.2	26.7
Transverse diameter of neural canal	58	(36.6)	32.8	37.6	37.2
Greatest distance between outer margins of prezygapophyses	—	—	(82.2)	101.8	(102.7)
Distance between inner margins of prezygapophyses	—	—	42	53	61
Greatest distance between outer ends of postzygapophyses	—	77	81.9	104.2	103.5
Least anteroposterior diameter of right pedicle of neural arch	—	—	22.3	18.5	—
Transverse diameter of left transverse foramen (vertebraterial canal)	7.8	(17.5)	11.5	14.9	—
Transverse diameter of right transverse foramen	6.3	—	10.2	13.8	—

[a] Includes odontoid process.
[b] Includes hypophysis.
[c] Measurements in parentheses are estimates.

two-thirds of the odontoid surface is smooth and articulates with the atlas; the dorsal third does not. There is a sharp ridge that begins on the dorsal surface of the odontoid process and extends along the midline for the entire length of the centrum. It increases in height posteriorly and divides the dorsal surface of the centrum into two deep, elongate fossae. It also separates two pairs of foramina, a smaller pair at the base of the odontoid process and a second larger pair close to the posterior end of the centrum. The greatest length of the centrum, including the odontoid process, is 87 mm.

The posterior face of the centrum is poorly preserved, but the remainder shows that it was roughly ovate in shape except for its ventral edge, which is transversely horizontal. From near the posterior bases of the pedicles it slopes posteroventrally at an angle of approximately 39° to intersect the posterior margin of the ventral region of the centrum. The ventral surface bears a large hypophysis that forms an elongate tuberosity occupying most of the length of the centrum. This feature begins anteriorly as a low narrow ridge, 12 mm in width, behind the odontoid process. Posteriorly, it deepens dorsoventrally and widens until it reaches an estimated maximum transverse width of 34 mm at the posterior end of the centrum. Most of the dorsal surface of the hypophysis has been eroded, but its preserved surface is rugose. A deep fossa parallels the hypophysis on each side.

The transverse processes extend posterolaterally from the centrum. Their anterior faces are convex, and the posterior faces are concave. Their ventral edges are thickened and rugose, apparently for muscle attachment. The transverse foramen for the vertebral artery is preserved only on the left side of the holotype axis vertebra. In posterior

TABLE 4
Measurements (in mm) of Holotype Thoracic Vertebrae of *Carolinacetus gingerichi*, new genus, new species (ChM PV5401), and ChM PV6088, Probable Sixth Thoracic Vertebra Referred to *C. gingerichi*

	T1	T2	T4	T5	T6	T7	T8	PV6068
Anteroposterior diameter of centrum	35.5	38.5	(41.5)[a]	42.3	43.7	(43.5)	—	49.5
Transverse diameter of centrum, anteriorly	—	60.6	64.6	63.6	67.7	67.2	—	73.4
Vertical diameter of centrum, anteriorly	—	48.8	53.3	51.2	53.5	52.5	—	55.1
Transverse diameter of centrum, posteriorly	68.4	76.4	(76)	77.4	83	84	—	89.5
Vertical diameter of centrum, posteriorly	46	44.1	47	54.4	60.8	56.2	—	63.1
Tip of spinous process to ventral face of centrum, anteriorly	—	—	187.7+	196.5+	206.5	—	—	195+
Distance between outer margins of transverse processes	—	—	(115)	(122)	(115)	—	—	—
Vertical diamter of neural canal	—	24.3	22	26.8	30.4	29.7	—	27
Transverse diameter of neural canal	—	34.1	32.3	32.4	32.4	31.9	(34)	36.1
Greatest distance between outer margins of prezygapophyses	—	(105)	(62)	64.5	67.8	(66.4)	(66.8)	68.8
Distance between inner margins of prezygapophyses	—	(50)	(30)	24	(28)	(26)	—	29.7
Greatest distance between outer margins of postzygapophyses	—	67	60.4	60.6	61	(61)	—	61.7
Least anteroposterior diameter of right pedicle of neural arch	—	23.2	27.2	24.1	26.1	25.7	—	28.5
Angle of spinous process from vertical axis of anterior face of centrum	—	25°	37°	41°	45°	45°	—	50°
Anteroposterior length of spinous process	—	27.9	28	29.4	29	26.1	—	30

[a] Measurements in parentheses are estimates.

view it is situated at the upper end of the base of the left transverse process and is ovoid with a vertical diameter of 20 mm and a transverse diameter of 14 mm. Posteriorly, it forms a short canal that curves and narrows anterolaterally. The anterior aperture is much smaller than the posterior one, with a dorsoventral diameter of 16.4 mm and a transverse diameter of 9 mm. This opening is obscured in anterior view by the lateral margin of the surface that articulates with the atlas. The lateral margin of the foramen is formed by a bony strut that joins the transverse process to the left pedicle of the neural arch. The left pedicle is robust, with a transverse width of 25 mm.

In anterior view the neural canal has the shape of an inverted heart. Its anteroposterior length varies considerably and is greatest (42 mm) along the roof of the neural arch. The postzygapophyses are nearly circular and face posteroventrally and slightly laterally.

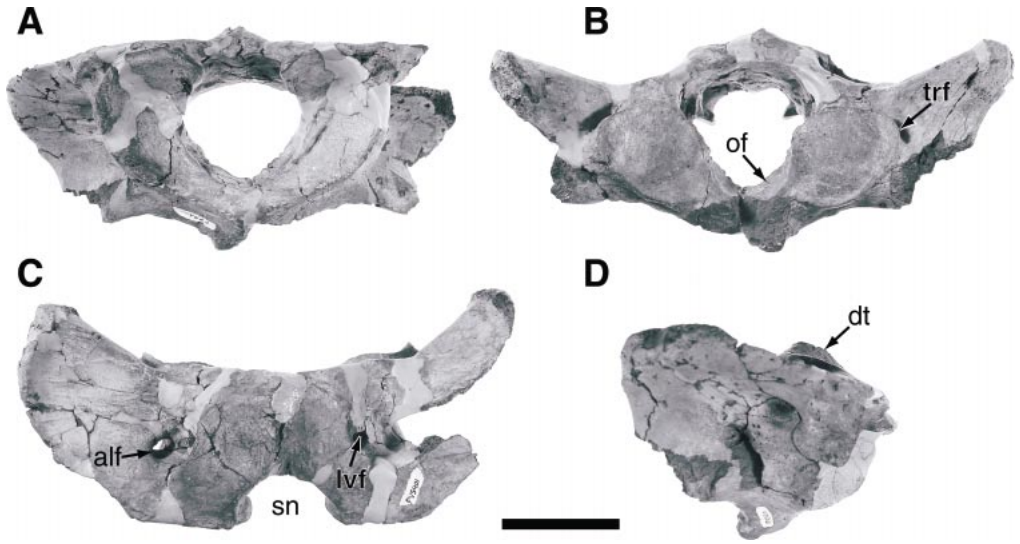

Fig. 17. Atlas vertebra (C1) of *Carolinacetus gingerichi* (ChM PV5401) in anterior (**A**), posterior (**B**), dorsal (**C**), and right lateral view (**D**). Scale bar is 5 cm in length. See appendix 3 for anatomical abbreviations.

The distal end of the spinous process is missing, but its general shape can be discerned. Its base is anteroposteriorly long, is triangular in cross section, and is sharply hooked posterodorsally. On the posterior face of the preserved portion of the spinous process there is a shallow medial sulcus that extends into a narrow, slit-like foramen in the base of the neural arch just above the dorsal margin of the neural canal. This foramen is 6.7 mm in dorsoventral diameter and 1.9 mm in transverse diameter.

THIRD CERVICAL: This vertebra is nearly complete, and both epiphyses are firmly ankylosed. As seen in lateral view, the anterior and posterior faces of the centrum are not aligned. Instead, the posterior face is in a more ventral position. Whereas the anterior face is somewhat cordiform (fig. 18D), the posterior face is nearly circular. In lateral view, both faces are similar in having a sigmoidal profile with the dorsal two-thirds concave and the ventral third convex. A faint, dorsoventral groove ca. 9 mm in length is centered on the anterior epiphysis. Nutrient foramina on the dorsal side of the centrum are separated by a span of bone that straddles the sagittal plane, and the ventral side bears a hypophysis along its posterior margin.

As seen in anterior view, the base of the transverse process is directed ventrolaterally while its distal end is slightly recurved to point laterally. The anteroposterior thickness of the process thins distally, and its posterior face bears a deep and wide transverse sulcus. The ventral edge of the sulcus is delineated by an elongate tubercle. A short transverse canal perforates the base of the transverse process. In anterior view, the canal is ovoid with the long axis being oriented dorsoventrally. Within the canal, the lateral side of the centrum forms a deep pit. The pedicles of the neural arch are stout and are joined to the transverse processes by bridges of bone that form the lateral walls of the transverse canals. The neural arch bears large prezygapophyses that face dorsomedially and large postzygapophyses that face ventrolaterally. The neural spine is absent, although a bump occurs in a homologous position, and the neural canal is ovoid.

SIXTH CERVICAL: The sixth cervical vertebra is well preserved, missing only the distal portion of the lateral branch of the right transverse process and the tip of the spinous process (fig. 19A). The shapes of the anterior and posterior faces of the centrum differ considerably. The anterior face is squarish, measuring 50.5 mm transversely and 51 mm dorsoventrally, and is bisected transversely by a

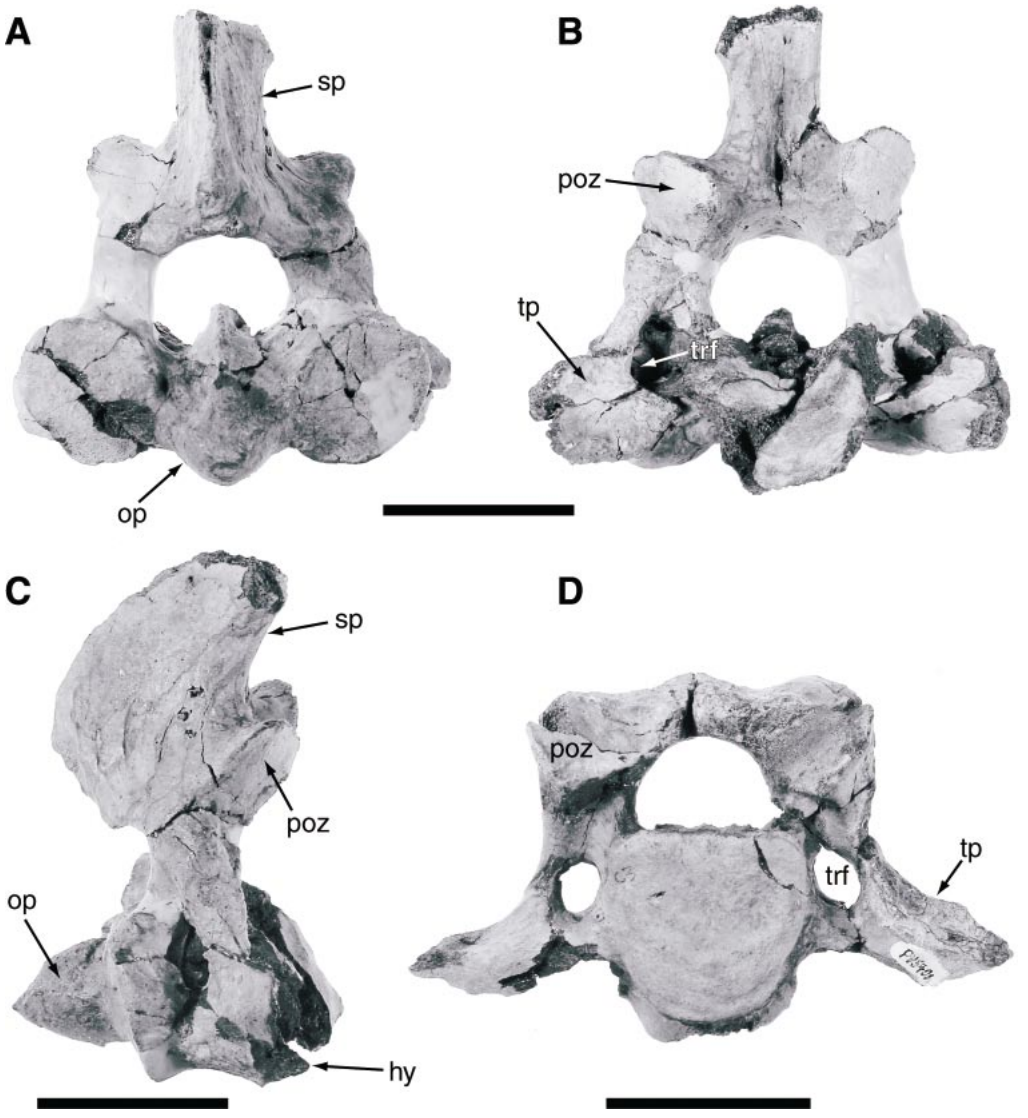

Fig. 18. Axis vertebra (C2) of *Carolinacetus gingerichi* (ChM PV5401) in anterior (**A**), posterior (**B**), left lateral view (**C**), and anterior view of third cervical vertebra (**D**). Scale bars are 5 cm in length. See appendix 3 for anatomical abbreviations.

shallow channel-like depression. The posterior face is ovate, is 60.5 mm in transverse diameter and 50.7 mm dorsoventrally, and is concave at its center. The ventral side of the centrum bears a low median keel. Along the midline of the dorsal surface an elevated hourglass-shaped platform of bone ca. 8 mm in width extends between the anterior and posterior faces of the centrum and separates a pair of bilaterally symmetrical foramina.

The transverse processes are bifid, with the lateral (upper) branch being much smaller than the ventral branch, which is robust and dorsoventrally compressed and extends for 79 mm ventrolaterally from the centrum. The anteroposterior width of the right ventral branch widens distally from 36 mm at its base to a width of 57 mm at its distal end. On the ventral side of each ventral branch there is an anteroposteriorly elongate tuber-

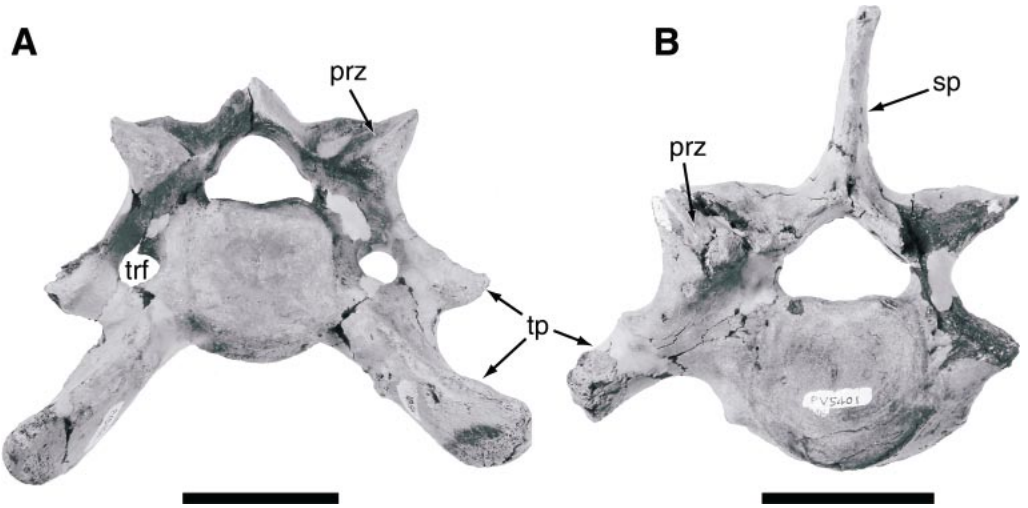

Fig. 19. Anterior views of sixth (**A**) and seventh (**B**) cervical vertebrae of *Carolinacetus gingerichi* (ChM PV5401). Scale bars are 5 cm in length. See appendix 3 for anatomical abbreviations.

cle for muscle attachment situated approximately 26 mm distal to the centrum. The tubercle on the left side is much better developed than the one on the right side. The well-preserved left lateral branch of the transverse process is short (16.2 mm), projects laterally, is hooked slightly dorsally, and its dorsoventral depth exceeds its anteroposterior width (12.1 mm).

The bridge of bone between the dorsal and ventral branches is anteroposteriorly compressed. Posterior to the junction of the dorsal and ventral branches there is an ovate muscular fossa, with its medial margin formed by a low ridge that ascends toward the base of the dorsal branch. That ridge forms the posterolateral margin of a broad sulcus leading into the transverse foramen, which perforates the base of the transverse process medial to its lateral branch and immediately lateral to the centrum. As a conduit for the vertebral artery, this foramen is nearly circular and has a maximum diameter of approximately 15 mm. The pedicles of the neural arch support a pair of large, flat prezygapophyses. The prezygapophyses are ovate, are 32–33 mm in anteroposterior length, and the dorsal plane of each is concomitantly sloped dorsomedially and posteroanteriorly. Both facets face dorsomedially, and the transverse plane of their dorsal margins intersects the peak of the roof of the neural canal. Immediately posterior to the prezygapophyses the postzygapophyses project posteriorly beyond the posterior face of the centrum. They are ovate, face ventrolaterally, and overhang the posterior entrance to the transverse foramen. The long axis of each postzygapophysis is oriented dorsolaterally, and the right one is 30.8 mm in length.

In anterior view, the neural canal is pentagonal with rounded corners and is 26.2 mm in greatest height and 37.6 mm in transverse diameter. The spinous process is incomplete, but its preserved portion shows that it was low and shaped like a spear point, with the apex being situated anteriorly. Laterally, it is flanked by narrow expanses of rugose bone bounded by steep posterodorsally and anteromedially directed escarpments that converge above the peak of the neural arch. The point of convergence is uneven, however, with the left escarpment being higher than the right one. Although not demonstrable within the light of present knowledge, the triangular shape of the area enclosing the spinous process may be diagnostic for the sixth cervical vertebra of *Carolinacetus*.

SEVENTH CERVICAL: This vertebra is complete except that it is missing the left prezygapophysis, the left transverse process, and the posterior epiphysis, which was not ankylosed (fig. 19B). The centrum of C7 rapidly increases in size posteriorly, resulting in

its posterior face being much larger than its anterior face. The anterior and posterior faces are different in shape; the anterior face is square-shaped, except for a broadly rounded ventral side, while the posterior face is oval with a width 1.5 times its height. Centered on the anterior face is a narrow, dorsoventral groove ca. 10 mm in length. In lateral view, the anterior face of the centrum has a sigmoidal profile; the anterior two-thirds are concave while the ventral third is convex. Several small foramina lie on the centrum adjacent to the lateral margins of the anterior epiphysis. Other features of the centrum include: bilateral nutrient foramina on its dorsal side, a weak sagittal keel on its ventral side, and elevated capitular facets for the 1st rib on the lateral sides adjacent to the margins of the posterior face.

Extending dorsolaterally from the centrum is a wide, dorsoventrally compressed plate of bone that bifurcates into the transverse process and the pedicle for the neural arch. In posterior view, there is an oval pit on that plate between the base of the transverse process and the postzygapophysis. The transverse process is about 35 mm in length, is oriented ventrolaterally, and has a fairly flat distal end. The transverse foramen is absent. In anterior view, the neural canal is pentagonal in shape with rounded corners. Above the canal is a gracile neural spine that bears bilateral pits on the anterior face of its base, one on either side of the sagittal place. The pre- and postzygapophyses are large; the left postzygapophysis has a transverse diameter of 33 mm, and whereas the prezygapophyses face dorsomedially, the postzygapophyses face ventrolaterally. Medial to the postzygapophysis and just inside the neural canal is an ovoid area of rugose bone probably for muscle attachment.

SECOND THORACIC: Most of the holotype second thoracic vertebra is preserved, but it is missing both transverse processes, the edges of the right metapophysis, and the distal half of the spinous process (fig. 20). The anterior face of the centrum is slightly trapezoidal, with a transverse diameter of 60.6 mm and a vertical diameter of 48.8 mm. Most of the anterior face is gently convex except for the dorsalmost portion, which is concave transversely. Just above the ventral

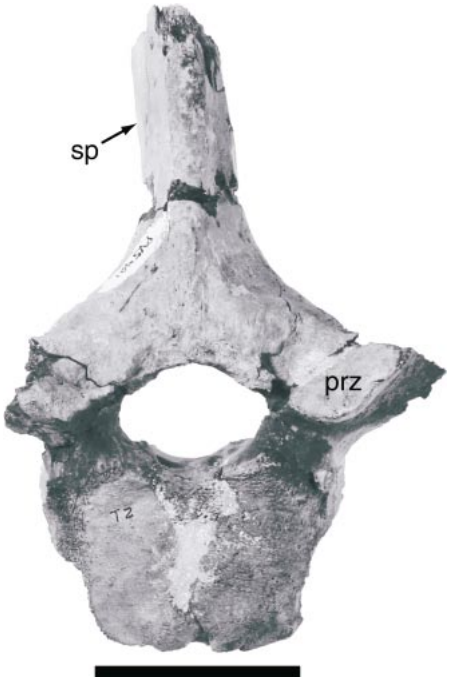

Fig. 20. Anterior view of second thoracic vertebra of *Carolinacetus gingerichi* (ChM PV5401). Scale bar is 5 cm in length. See appendix 3 for anatomical abbreviations.

margin there is a low tuberosity on each side of the sagittal plane. The demifacets for the capitula of the second ribs are situated at the dorsal margins of the anterior face. Posteriorly, each demifacet is bordered by a shallow fossa. The posterior face of the centrum is much broader than its vertical height, having a transverse diameter of 76.4 mm and a vertical diameter of 44.1 mm. The left demifacet for the capitulum of the third rib is present, but the right one is less distinct.

The neural canal is ovate, with a transverse diameter of 34.1 mm and a vertical diameter of 24.3 mm. The left prezygapophysis is virtually complete; its articular surface is flat, faces dorsomedially, and is approximately 26 mm wide. The right prezygapophysis is missing its lateral and medial edges but is 20.2 mm in anteroposterior length, virtually the same measurement as its counterpart on the left. The distance between the two prezygapophyses was ca. 50 mm, estimated by doubling the distance from the inner margin of the left prezygapophysis to the midline

of the neural canal. Posterior to the articular surface of each prezygapophysis there is an ovoid fossa at the base of the neural arch. Medial to each of these fossae there is a shallow angular recess bordering the dorsal margin of the neural canal.

The preserved portion of the spinous process is triangular in cross section, with the apex of the triangle being directed anteriorly. It is inclined posteriorly at an angle of ca. 25° from the vertical axis of the anterior face of the centrum. The posterior face of the process is fairly flat, but ventrally it grades into a narrow groove leading to a rectangular, concave fossa between the medial edges of the postzygapophyses. Each postzygapophysis is ovate, slightly concave, and faces ventromedially.

SIXTH THORACIC: This vertebra is virtually complete except for the distal end of the right transverse process and the anterior tip of the right prezygapophysis (fig. 21B). The vertebra is 206.5 mm in height from the ventral base of the centrum to the tip of the spinous process. It is approximately 115 mm in width between the lateral margins of the transverse processes. The centrum is 67.7 mm in greatest transverse width anteriorly and 83 mm posteriorly. The neural canal is circular and is 30.4 mm in vertical diameter and 32.4 mm transversely.

The anterior face of the centrum is nearly circular except for its slightly emarginated dorsal edge, and it is slightly concave at its center. The demifacets for the capitula of the sixth ribs are somewhat larger than the demifacets on most of the other preserved thoracics of *Carolinacetus*. The ventral surface of the centrum is featureless, and there is no pronounced median keel. On the dorsal surface there is a low median ridge flanked by vascular foramina. Unlike the more circular anterior face, the posterior face of the centrum has the shape of a transversely expanded heart and is concave over most of its surface. The demifacets for the capitula of the seventh ribs are much larger than the anterior demifacets but are similar in size to the demifacets for the seventh ribs on the anterior face of the seventh thoracic.

The neural canal is circular in shape and relatively large, with its vertical diameter (30.4 mm) being 57% of the vertical diameter of the anterior face at the midline (53.5 mm). The pedicles are stout and thicken posteriorly. The prezygapophyses extend anteriorly from the base of the junction of the transverse processes with the neural arch and slope dorsolaterally. The left prezygapophysis is flat and circular and is 19 mm in anteroposterior diameter and 18.9 mm in transverse diameter. Immediately behind it a pair of ventrolaterally elongate fossae deeply indent the base of the transverse process. Posterior to the right prezygapophysis there is only a single shallow, circular fossa. The medial edges of the prezygapophyses extend posteromedially to join the anterior margin of the neural arch at the midline. Immediately above the midline of the arch there is a shallow, broadly triangular recess. At its center a hood-like transversely broadened projection extends anteriorly and overhangs the midline of the neural canal. We herein term this feature the *supraneural prominence* (fig. 21: snp).

The transverse processes extend dorsolaterally from the juncture of the pedicles and the neural arch. The distal end of the well-preserved left process flares slightly upward at its outermost extremity, which is 57.5 mm from the median ridge at the base of the spinous process. The articulating facet for the tuberculum of the left sixth rib is vertically elongate, faces laterally and slightly ventrally, and is 39.7 mm in dorsoventral diameter. The vertical axis of the facet is directed anteriorly, so that the dorsal end of the process projects forward beyond the vertical axis of the anterior face. The left postzygapophysis is larger than the right one, which is virtually complete but may have lost the edge of its lateral margin through erosion. The left one is slightly concave and is quadrangular with rounded corners.

The spinous process is inclined posteriorly at an angle of approximately 45° from the vertical axis of the anterior face of the centrum and is 142.6 mm in length measured from the plane of the bases of the postzygapophyses. The proximal two-thirds of the process is triangular in cross section, with the posterior face as the base. The posterior face is irregular in width, ranging from 23 to 23.5 mm in transverse diameter. Proceeding from its margins, the lateral faces of the process

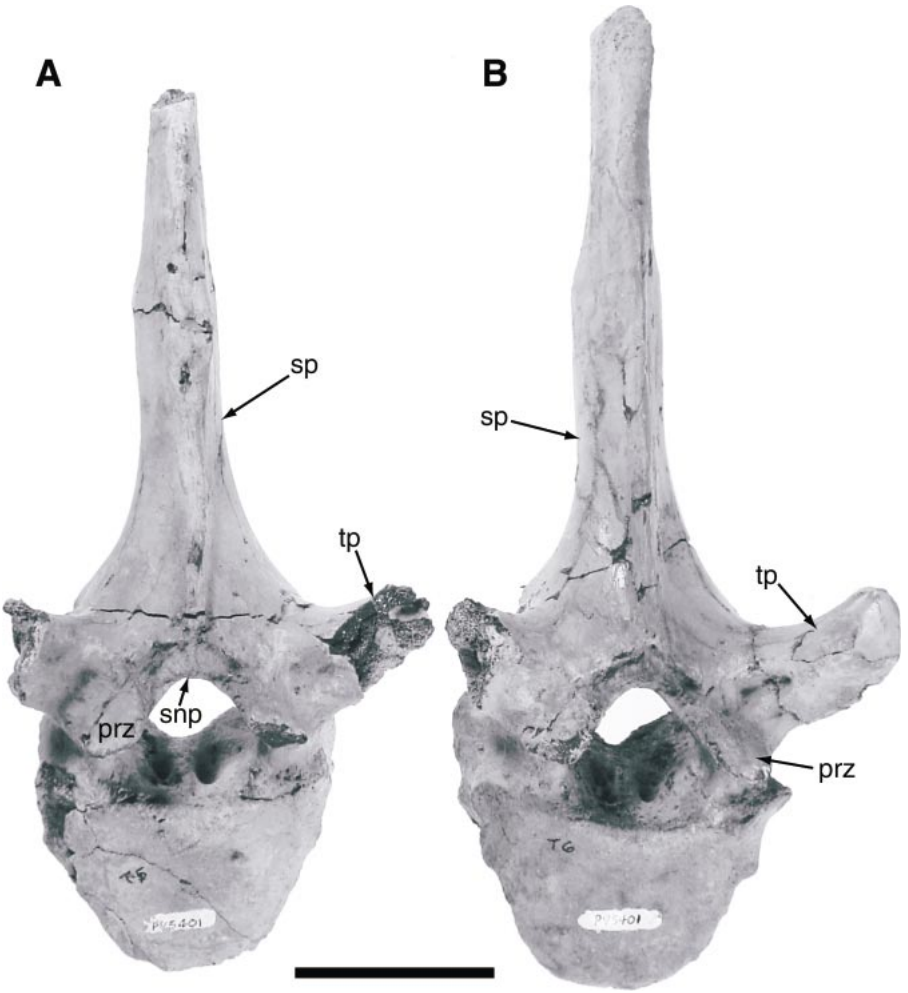

Fig. 21. Anterior views of the fifth (**A**) and sixth thoracic (**B**) vertebrae of *Carolinacetus gingerichi* (ChM PV5401). Scale bar is 5 cm in length. See appendix 3 for anatomical abbreviations.

converge anteromedially to form the apex of the triangular configuration. Proximally, the narrow, blade-like anterior edge of the spinous process forms a wall dividing the left and right sides of the neural arch. Distally, the spinous process narrows and becomes elliptical in cross section, with the posterior face tapering from a width of 23.5 mm to 16.3 mm at a point 60.5 mm from the distal end. Along most of the posterior face there is a longitudinal median ridge. At the base of the spinous process between the postzygapophyses there is a cave-like recess floored by a shelf of bone that extends posteriorly and overhangs the posterior entrance to the neural canal. We herein term this projection the *supraneural shelf*. This feature is not present in the second thoracic vertebra, but the beginnings of it are evident in T4. It is further developed in T5, is most pronounced in T6 and T7, and has begun to disappear in T8.

OTHER THORACIC VERTEBRAE: The preserved portions of the other holotype thoracic vertebrae of *Carolinacetus* are similar in morphology to T6. Three trends are evident in the thoracic series. The shape of the neural canal ranges from ovate with a wide transverse diameter in the anteriormost thoracics (T2–T5) to nearly circular in T6–T8 and pre-

sumably in the remaining thoracics. As shown in table 4, the vertical diameter of the neural canal increases from 24.3 mm in T2 to 30.4 mm in T6, resulting in its more circular shape in the latter vertebrae. That trend seems merely a reflection of the progressive increases in the height of the pedicles that accompanied the gradual elevation of the transverse processes and their facets for articulation of the capitula of the ribs. In most cetaceans the elevation of the rib facets reaches its peak at or about the middle of the thoracic series, after which they begin a sequential descent to the level of the transverse processes of the lumbar vertebrae.

As demonstrated by T2 and T4 (fig. 22), the anterior face of the centrum in the anteriormost thoracics continues the squarish shape of that face in the cervicals, but in T5 the shape is more cordiform (fig. 23). The anterior face of T4 is intermediate in morphology between that of T2, which is nearly square, and that of T6, which is nearly circular. Additionally, the supraneural prominence between the prezygapophyses is poorly defined in T2 and T4 and is most prominent in T5–T8, although it is somewhat eroded in the latter vertebra (fig. 23). Seemingly by more than sheer coincidence, the supraneural shelf between the postzygapophyses is most strongly developed in T5–T7, suggesting that it and the supraneural prominence of the following vertebra were common points for the attachment of connective tissue.

As shown in table 4, the spinous processes of the thoracics undergo a progressive posteroventral incline from the vertical axis of the posterior face of the vertebra, beginning at 25° in T2 and continuing to a slope of 45° in T6 and T7. The narrow, posteriorly inclined spinous processes are characteristic of protocetid vertebrae and are more typical of terrestrial ungulates than of crown cetaceans.

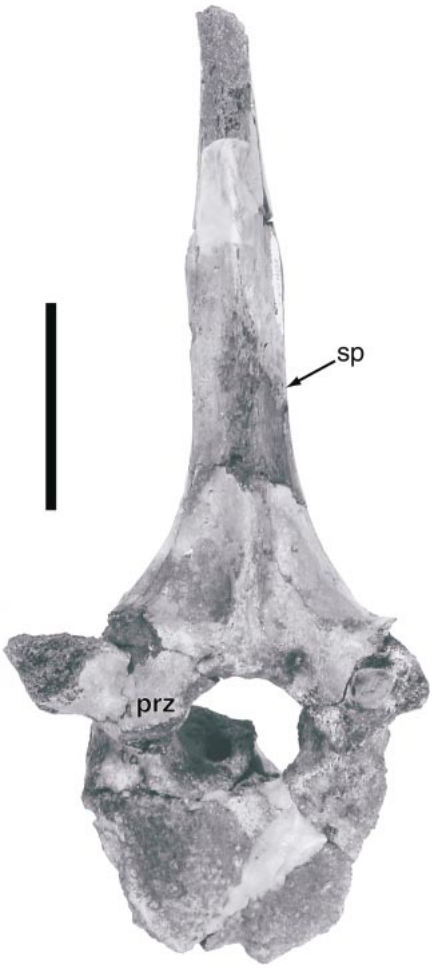

Fig. 22. Anterior view of the fourth thoracic vertebra of *Carolinacetus gingerichi* (ChM PV5401). Scale bar is 5 cm in length. See appendix 3 for anatomical abbreviations.

Ribs

The holotype ribs of *Carolinacetus gingerichi* consist of 15 partial elements with heads, two individual rib heads, and five shaft fragments (fig. 24). All of the rib elements were randomly distributed among the rest of the skeletal remains, making it difficult to determine the correct anatomical position of individual specimens. Without careful study, even a provisional interpretation of the preserved material would not have been feasible.

The ribs of *Carolinacetus* are somewhat unusual in that a well-formed tuberculum persists through virtually the entire rib sequence, as we have determined it. In most cetaceans the posteriormost two, three, or even four ribs lack a well-defined capitulum and tuberculum, but only one of the preserved rib heads of *Carolinacetus*—the probable last (13th) rib—lacks these structures in their conventional form. In all of the pre-

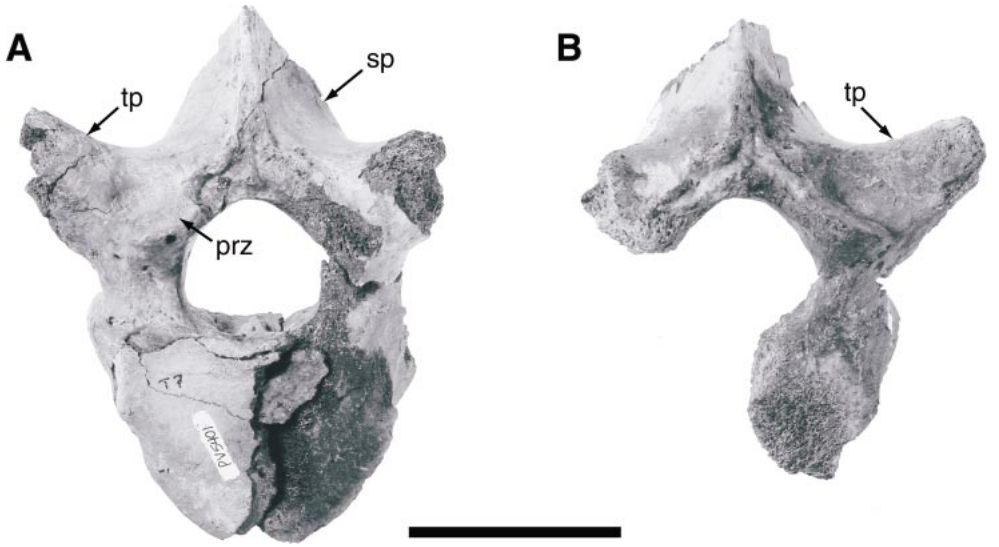

Fig. 23. Anterior views of the seventh (**A**) and the eighth (**B**) thoracic vertebrae of *Carolinacetus gingerichi* (ChM PV5401). Scale bar is 5 cm in length. See appendix 3 for anatomical abbreviations.

served ribs of *Carolinacetus* except the latter one, the capitulum is globose and is much broader than the neck. The better preserved specimens can be assigned to the right or left side of the ribcage based on the curvature of the shaft and the direction in which the neck of the capitulum is twisted, that is, to the left in right ribs and to the right in left ribs. Among all of the rib elements for which assignments can be attempted, including the two detached rib heads, 10 left ribs and 7 right ones are represented. Measurements of the length of the ribs as preserved were taken on a straight line from the articular facet of the tuberculum to the distal end of the shaft as preserved, with the exception of three ribs (L3, R7, L8) in which the tuberculum is missing; in those ribs the measurement was taken from the dorsal side of the capitulum.

The change in angle (CIA) of the dorsal edge of the rib is preserved in 10 of the ribs and is quite prominent. That feature is common in varying degrees in the ribs of cetaceans (e.g., *Kogia*, *Tursiops*) and in many artiodactyls (e.g., *Cervus*, *Odocoileus*) and certain other land mammals, but it is especially well developed in *Carolinacetus*. In the holotype ribs of *Carolinacetus* the CIA becomes progressively more distal to the tuberculum from anterior to posterior through the probable 7th rib, but in the probable 8th rib, it begins a retreat toward the tuberculum that continues through the much shorter 9th and 10th ribs. Its position in the probable 11th and 12th ribs could not be determined because most of the shaft is missing in those specimens. Nevertheless, the position of the CIA seems clearly related to the length of the rib, that is, closer to the tuberculum in the shorter anterior and posterior ribs and farther from it in the longer ribs in the middle of the rib cage. Hence, this feature was used to determine the probable position that the preserved rib elements occupied in the sequence of dorsal ribs of *Carolinacetus* (table 5). For example, in L2 the CIA occurs only 50 mm distal to the base of the tuberculum, while in the probable R3 the CIA is 93 mm from the base of the tuberculum. In R3 and all subsequent ribs the CIA measurement was taken along the dorsal curvature of the rib.

In the two detached rib heads (i.e., the capitulum and its neck) the direction of the twist of one of them shows it to be from a right rib. Despite its fragmentary nature, the latter specimen can be assigned a provisional place in the rib series. The length of its neck (29.2) compares favorably with that of probable L4 (27.4), so we have tentatively referred this rib head to R4. The other detached

Fig. 24. Posterior views of the ribs of *Carolinacetus gingerichi* (ChM PV5401). The left 4th, 6th, 7th, and 13th and the right 2nd and 9th–12th ribs were not preserved. Anterior is to the top of the page, and the scale bar is 10 cm in length. See appendix 3 for anatomical abbreviations.

rib head has only suggestions of the capitulum and the tuberculum and is clearly a posterior rib, possibly the last rib in the series.

The dorsoventral depth of the shaft at the base of the tuberculum was useful in placing the anterior ribs and in recognizing two partial ribs with shallow depths as probable L11 and L12.

The location of the CIA was the principal—and most reliable—means of determin-

TABLE 5
Key Measurements (in mm) of Holotype Rib Elements of *Carolinacetus gingerichi*, new genus, new species

Rib	Capitulum length	Diameter of shaft	Distance to change in angle
L1	23.3	42.9	—
R1	23	(35)	—
L2	31.6	37.3	50
L3	26.1	—	(93)
R3	27.9	36	93
(R4)	29.6	—	—
L5	27.4	34.6	139
R5	33.7	34.1	144
R6	33.5	28.9	168
R7	—	23.6	191
L8	29.2	—	(178)
R8	28.6	26.7	—
L9	30.9	27	58
L10	26	26.3	61
L11	25.1	24	—
L12	20.7	15.6	—
R13	—	—	—

Note: Left (L) and right (R) ribs are identified by upper case prefixes. Rib heads (capitulum and neck only) are in parentheses, for example, (R4). Numberical sequence of ribs is provisional and is based on the three measurements listed below: (1) relative length of the capitulum neck, (2) dorsoventral diameter of shaft at distal base of tuberculum, and (3) distance from distal base of tuberculum to dorsal change in angle (CIA). Neck of capitulum was measured from proximal base of tuberculum to epiphysial suture of capitulum. With the exception of the second rib, all CIA measurements were made along the curve of the dorsal surface. Parentheses indicate estimated measurements. Dash (—) indicates measurement not possible because of breakage. Additional measurements are given in the text.

ing probable positions in the rib sequence. That feature first appears in R2 and is well preserved in 11 of the 13 ribs apparently present in *Carolinacetus*, and, as seen in table 5, it provides a valuable landmark for placement of the ribs. The morphology of the dorsal surface of the rib immediately lateral to the tuberculum also is useful in recognizing anterior and posterior ribs. In the specimens that we have identified as the first five ribs the dorsal surface of the shaft adjoining the tuberculum is rounded, but in the rest of the ribs it is flat for a short distance (ca. 25 mm) extending laterally from the tuberculum. This feature is especially prominent in the probable 8th–12th ribs.

Using the criteria described above, the holotype ribs and detached rib heads of *Carolinacetus* were sorted into the following pattern of probable identity, with detached heads shown in italics:

R1 R3 *R4* R5 R6 R7 R8 *R13*
L1 L2 L3 L5 L8 L9 L10 L11 L12

FIRST AND SECOND RIBS: Although approximately half of the shaft is missing in the left first rib (L1) and nearly all of it in the right first rib (R1), these bones are easily recognized by the very large tuberculum and very short neck of the capitulum. Those features are characteristic of the first rib in cetaceans and in many land mammals (e.g., *Bison*, *Equus*).

The preserved portion of the holotype L1 of *Carolinacetus* measures 152.6 mm in a straight line from the articular face of the tuberculum to the broken end of the shaft. In this rib the tuberculum actually exceeds the capitulum in size and robustness, with the former measuring 30.1 mm mediolaterally and 25.1 mm anteroposteriorly and the latter 27.2 mm vertically and 23.1 mm anteroposteriorly. On the dorsal surface of L1 there is an elongate, anteroposteriorly compressed tubercle at the base of the tuberculum. This feature is present also on R1 but is not as large as in L1. Among the other holotype ribs of *Carolinacetus*, that structure appears only on the one that we have identified as R2, where it is associated with the CIA, but it is not as robust as in the first ribs.

The holotype R1 is fragmentary, measuring only 72.5 mm from the broken base of the tuberculum to the broken edge of the shaft. The tuberculum is missing in R1, but the size of its base indicates that it was smaller than its counterpart in L1. The capitulum in R1 is 30.9 mm vertically, but its anterior face has been eroded and yields an incomplete measurement of only 19.3 mm anteroposteriorly.

The probable R2 also lacks most of its shaft, measuring only 144.6 mm on a straight line from the articular face of the tuberculum to the broken end of the shaft. It is also missing the epiphysis of the capitulum. In R2 the tuberculum is 30.9 mm mediolaterally and

18.1 mm in anteroposterior diameter. The capitulum is 24.1 mm vertically and 19.4 mm anteroposteriorly, and its neck is 31.8 mm in length and is longer and more slender than the neck in the first ribs. The CIA of the dorsal side is preserved in R2 and is situated 46 mm distal to the tuberculum. Both the dorsal and ventral surfaces of the shaft are rounded at the base of the tuberculum dorsally and at the beginning of the neck of the capitulum ventrally.

THIRD, FOURTH, AND FIFTH RIBS: The ribs that we recognize as the probable L3, R3, L5, and R5 differ from the rest of the preserved ribs of *Carolinacetus* in having a greater depth of the shaft at the distal base of the tuberculum, averaging 34.9 mm in dorsoventral diameter at that point. A detached rib head is tentatively regarded as that of the right fourth rib.

Most of the probable right third rib is preserved and measures 251.5 mm on a straight line from the articular face of the tuberculum to the preserved distal end. This rib appears to be missing not more than 60 or 70 mm of the distal end of the shaft. The capitulum is 22 mm in vertical depth and 25 mm anteroposteriorly, and its ventral face is flattened. Though not nearly as robust as in L2, the tuberculum of R3 is large, measuring 22.8 mm in mediolateral length and 15.4 mm anteroposteriorly. The CIA is more distal than in L2, being 93 mm from the tuberculum. The probable L3 is missing the tuberculum and less than half of its shaft and measures 200.9 mm on a straight line from the dorsal side of the capitulum to the broken end of the shaft. The capitulum is 22.5 mm in vertical depth and 24 mm anteroposteriorly. When L3 is placed against R3 with the heads of the two ribs aligned evenly, the CIA of the two occurs at exactly the same point, and the dorsal and ventral degrees of curvature are almost identical, leaving little doubt that these two ribs are opposites. Using the head of R3 as a gauge, it is possible to obtain a measurement of the dorsoventral depth of L3 very close to the base of the missing tuberculum. In L3 the dorsoventral depth is 35.8 mm and is 36 mm in R3, adding further support to the placement of this rib as the opposite of R3. This measurement in L3 was not placed in table 5, however, because the position of the distal base of the tuberculum cannot be determined as precisely as in the ribs in which the tuberculum is present; nevertheless, we are confident that the measurement of the dorsoventral depth of L3 was taken very close to, if not immediately behind, the distal base of the missing tuberculum. In both of these ribs the dorsal surface immediately behind the tuberculum is rounded, and directly below that point the ventral surface is keeled, with the keel continuing for approximately half the length of the preserved portion of the shaft of the more completely preserved R3.

The detached rib head that we regard as probably belonging to R4 consists only of the capitulum and its neck and is 50.5 mm in total length from the articular face of the capitulum to the broken end of the specimen. The neck of the capitulum measures 29.2 mm from the medial remnant of the base of the missing tuberculum to the epiphysial suture of the capitulum. That measurement is close to the measurement of the neck of L4 (27.4 mm) and for that reason is thought to represent its opposite. The capitulum is 23 mm in vertical diameter and 20.8 mm anteroposteriorly.

The probable left fifth rib is missing approximately half of its shaft and is 192 mm in length on a straight line from the articular face of the tuberculum to the broken end of the shaft. The head is well preserved although slightly eroded in places. The capitulum is 22.4 mm in vertical depth and 22.7 mm anteroposteriorly, and its ventral face is flattened. The tuberculum measures 24.8 mm in mediolateral length and 15.3 mm anteroposteriorly. The dorsal surface of the shaft immediately behind the tuberculum is rounded, and directly below that point the ventral surface is sharply keeled along its anterior edge and rounded along its posterior margin. In that regard L5 differs from R3, in which the ventral keel is located medially instead of along the anterior edge of the shaft. The dorsoventral depth of the shaft at the distal base of the tuberculum is 34.6 mm. There is also a marked difference in the location of the CIA, which is 93 mm distal to the tuberculum in R3 and 140 mm in L5, as the CIA continues to move farther distally in the rib sequence.

The probable R5 is missing perhaps a third of its shaft and is 222.8 mm in length on a straight line from the articular face of the tuberculum to the broken end of the shaft. The capitulum is 21.5 mm in vertical depth and 22.2 mm anteroposteriorly. The tuberculum is poorly preserved and is missing its medial third, precluding a mediolateral measurement; its preserved portion is 12.1 mm anteroposteriorly, but that is an incomplete measurement. The dorsoventral depth of the shaft at the distal base of the tuberculum is 34.1 mm, and the CIA is 144 mm distal to the tuberculum, slightly farther than in L5 (139) but not appreciably so.

As we have determined them, the first five ribs differ from the remaining ones in having a deeper dorsoventral depth immediately distal to the tuberculum. This characteristic can be seen in the anterior ribs of other cetacean taxa and thus lends support to our placement of this portion of the holotype ribs of *Carolinacetus*.

SIXTH, SEVENTH, EIGHTH, AND NINTH RIBS: It is within this series that the ribs of *Carolinacetus* reach their greatest length and then begin to shorten as they approach the posterior proton of the rib cage. The probable right sixth and seventh ribs are the best preserved of all of the holotype ribs of *Carolinacetus*. The R7 is missing its tuberculum, however, so to obtain comparative lengths of R6 and R7 the overall measurement of each of these two ribs has been taken from the dorsal surface of the capitulum instead of from the articular face of the tuberculum.

The R6 measures 298.1 mm on a straight line from the dorsal side of the capitulum to the preserved distal end of the shaft. The projected terminus of the curvature of its anterior and posterior faces indicates that it is missing approximately 25 mm of its distal end, the addition of which would place its original length at approximately 323 mm. The capitulum is 23.4 mm in vertical depth and 24 mm anteroposteriorly. The tuberculum is missing its medial half, and thus a mediolateral measurement is not possible. Its anteroposterior diameter is 11.5 mm, though this may not be a complete measurement because of the breakage. The dorsoventral depth of the shaft at the distal base of the tuberculum is 28.9 mm, the first measurement at this point that does not exceed 30 mm. The CIA is 168 mm from the tuberculum, continuing the movement of the CIA distally from the proximal end of the rib.

The probable right seventh rib measures 302.6 mm on a straight line from the dorsal side of the capitulum to the preserved distal end of the shaft. Although the lateral edge of the distal end the shaft is missing, the medial edge is present and appears to be the natural end of this rib, and thus it seems to be essentially complete. It is clearly shorter than R6, indicating that it represents the beginning of the posterior rib series. It is in this rib that the CIA achieves its greatest separation from the tuberculum, a distance of 191 mm. Although the tuberculum is missing in R7, a remnant of the edge of its distal base can be detected, permitting a measurement of the CIA. The dorsoventral depth of the shaft at that point is 23.6 mm. The area immediately distal to the tuberculum is flattened, typical of the posterior ribs of *Carolinacetus*. The capitulum is 23.9 mm in vertical depth and 25.8 mm anteroposteriorly.

The probable left eighth rib is virtually complete, lacking only the tuberculum and less than 20 mm of its distal end. It is 243.3 mm in length on a straight line from the dorsal side of the capitulum to the preserved distal end of the shaft. The capitulum is 21.1 mm in vertical depth and 24 mm anteroposteriorly. Placement of this rib in correct alignment in juxtaposition to R8, in which the tuberculum is preserved, permits an approximate measurement of the CIA of L8 as 178 mm distal to the presumed lateral margin of its missing tuberculum. Thus, it is in the probable eighth rib that the CIA begins to retreat medially toward the tuberculum. Missing bone behind the tuberculum prohibits a measurement of the depth of L8 at that point.

As preserved, the probable R8 lacks part of the capitulum and most of its shaft, measuring only 130.4 mm on a straight line from the articular face of the tuberculum to the preserved distal end. The flattened area on the lateral side of the tuberculum identifies this specimen as a posterior rib. The absence of the CIA on the preserved portion places this rib between R7, in which the CIA is 191 mm distal to the tuberculum, and the prob-

able L9, in which the CIA is just 58 mm from the tuberculum. When placed in juxtaposition with L8, the two ribs are virtually identical in curvature and lateromedial diameter, leaving little question that that these two ribs are opposites. The capitulum is 24.9 mm in vertical depth and 21.5 mm anteroposteriorly. The tuberculum is 19.5 mm in mediolateral length and 12 mm anteroposteriorly.

The probable left ninth rib evinces a pronounced shortening of the shaft characteristic of the last few ribs in the sequence. This rib is virtually complete, missing only the distalmost tip of the shaft, and as preserved it measures 205.6 mm on a straight line from the articular face of the tuberculum to the preserved distal end. There is a pronounced flattening of the dorsal surface immediately lateral to the tuberculum, a characteristic of the posterior ribs of *Carolinacetus*. At this point the dorsolateral depth of the shaft is 27 mm. Doubtless because the shortness of the rib, the CIA is located only 58 mm distal to the tuberculum. The capitulum is 20.5 mm in vertical depth and 25.5 mm anteroposteriorly. The length of its neck (30.9 mm) is slightly greater than the necks of the other posterior ribs, but this difference merely reflects the variation that occurs in the lengths of the necks throughout the rib cage of *Carolinacetus*. The tuberculum is somewhat eroded but yields measurements of 19.3 mm in mediolateral length and approximately 11 mm anteroposteriorly.

TENTH, ELEVENTH, TWELVETH, AND THIRTEENTH RIBS: The small sizes of the specimens that we think to be the probable 10th–13th ribs clearly place them near the posterior end of the rib cage. Remarkably, the 10th–12th ribs of *Carolinacetus* all have as well-developed capitula and tubercula as any of the preceding ribs. All three of those ribs also display a prominent flattening of the dorsal surface of the shaft immediately lateral to the tuberculum.

The probable left 10th rib is virtually complete, lacking not more than 15 or 20 mm of its distal end. As preserved, it measures 162.8 mm on a straight line from the articular face of the tuberculum to the broken edge of the distal end. The head of this rib seems inordinately large compared to its relatively short shaft, with the capitulum measuring 22.2 mm in vertical depth and 24.7 mm anteroposteriorly. The tuberculum is 18.3 mm in mediolateral length and 16.2 mm anteroposteriorly. The flattening of the dorsal surface of the shaft immediately lateral to the tuberculum is quite pronounced in this rib, measuring 12.1 mm anteroposteriorly and 24.2 mm in its lateral extent. The dorsoventral depth of the shaft lateral to the base of the tuberculum is 26.3 mm. In this rib the CIA occurs 64 mm distal to the tuberculum.

The probable L11 is missing most of its shaft and measures only 79.6 mm from the medial edge of the tuberculum to the preserved end of the shaft. The capitulum is 21.4 mm in vertical depth and 23 mm anteroposteriorly. The tuberculum is considerably smaller than in the preceding rib, measuring 14.6 mm in mediolateral length and 14.1 mm anteroposteriorly. In L11 the dorsoventral depth of the shaft lateral to the base of the tuberculum continues its decrease in the posterior ribs and is just 24 mm in this rib.

The smallest of all of the preserved ribs with both capitulum and tuberculum, the probable L12 is also missing much of its shaft, but apparently not more than about 60%. It is 92.5 mm from the medial edge of the tuberculum to the preserved end of the shaft. The capitulum is 18.3 mm in vertical depth and 26.7 mm anteroposteriorly, remarkably large for such a small rib. The tuberculum is eroded but is approximately 15 mm in mediolateral length and about 12 mm anteroposteriorly. The dorsoventral depth of the shaft lateral to the base of the tuberculum is a mere 15.6 mm. The diminutive size of the shaft of this rib and the greatly reduced size of the tuberculum compared to that of the capitulum strongly suggest that it is the last of the ribs of *Carolinacetus* in which both of those structures are well defined.

One single-headed rib element was preserved among the holotype ribs of *Carolinacetus*. Only 32 mm in length, this specimen is strongly convex on one side (apparently the posterior face), and on the other side there is a median gutter separating two rounded elevations, with the larger presumably representing a relict capitulum and the smaller one seemingly being a remnant of the

tuberculum. If this interpretation is correct, this side would be the posterior face and this rib head would thus be from the right side. Even on the opposite (anterior) side there is a narrow groove that outlines the presumed tuberculum and separates it from the presumed capitulum. We feel fairly confident that such is indeed the case, and accordingly we regard it as the head of the probable right 13th rib.

Whether there were additional single-headed ribs in the rib sequence of *Carolinacetus* is, of course, impossible to determine with absolute certainty, but judging from the small size of the probable 12th and 13th rib elements it seems rather unlikely that the ribcage of *Carolinacetus* contained more than 13 ribs.

Referred Specimen

An isolated probable sixth thoracic vertebra (ChM PV6088) from the Tupelo Bay Formation at the type locality of *Carolinacetus* is here referred to *C. gingerichi*. Both morphometrically and in its preservation, this specimen so closely agrees with the holotype thoracics of *Carolinacetus* that it could easily be mistaken for one of the holotype series, but it was collected at a different location within the Berkeley Quarry. The length/width ratio of the centrum of this vertebra (1.48) is only slightly less (0.07) than that of the holotype T6 (1.55) of *Carolinacetus* but is considerably greater than that of the T6 of *Georgiacetus* (1.34), which is also smaller in overall dimensions. Both the supraneural prominence and the supraneural shelf are as well developed as they are in the holotype sixth thoracic of *Carolinacetus*, suggesting that the referred specimen occupied a similar position in the thoracic series. All of the measurements of this specimen exceed those of the holotype T6, and the epiphyses are well ankylosed to the centrum, indicating that it belonged to a slightly larger and more mature individual than the holotype of *Carolinacetus*. The referred specimen differs from the holotype T6 in having a less circular neural canal and a greater posterior slope (50°) of the spinous process.

Although it is possible that PV6088 belongs to another as-yet-unknown taxon, the dimensions and morphology of this specimen are so similar to the thoracics of *Carolinacetus* that we feel safe in referring it to that form until its identity can be demonstrated otherwise.

DISCUSSION

Taxonomic Placement and Comparisons

Several characters diagnostic of Cetacea are apparent in the holotype of *Carolinacetus* and support its placement in this group, including a greatly reduced postglenoid foramen situated on the petrosal/squamosal suture (Geisler and Luo, 1998); presence of an anterior process of the petrosal (Luo and Gingerich, 1999); involucrum of ectotympanic bulla (Thewissen, 1994); and incisors subequal to canine. In addition, *Carolinacetus* is a member of the clade that includes protocetids, basilosaurids, and crown cetaceans but excludes pakicetids, ambulocetids, and remingtonocetids (fig. 25). This clade has a Bremer support of 4 and is diagnosed by six unequivocal synapomorphies: anterior margin of external nares over or just posterior to I3 (character 4, $1 > 2$), wide rostrum (13, $1 > 0$), supraorbital processes present but short (16, $0 > 1$), anterior edge of orbit over M2 or the division between M2/M3 (19, $0 > 1$), postorbital process forms a 90° angle with the sagittal crest (20, $0 > 1$), and short cervical vertebrae (87, $0 > 1$).

Carolinacetus is further recognized as a member of Protocetidae, which is a paraphyletic family of early cetaceans (Uhen, 1999), and, as interpreted here, includes the following taxa: *Artiocetus clavus*, *Carolinacetus gingerichi*, *Protocetus atavus*, *Eocetus schweinfurthi*, *E. wardii*, *Georgiacetus vogtlensis*, *Pappocetus lugardi*, *Babiacetus indicus*, *Rodhocetus kasrani*, *R. balochistanensis*, *Indocetus ramani*, *Takracetus simus*, *Natchitochia jonesi*, *Gaviacetus razai*, and *G. sahnii*. Plesiomorphic features that support the inclusion of *Carolinacetus* in the Protocetidae are: (1) external nares above the canine; (2) supraoccipital narrow, tubular, and oriented posterodorsally; (3) accessory cusps absent on m3; (4) broad articulation between the ectotympanic bulla and the falciform process of the squamosal; and (5) large vertebral foramen in the axis vertebra.

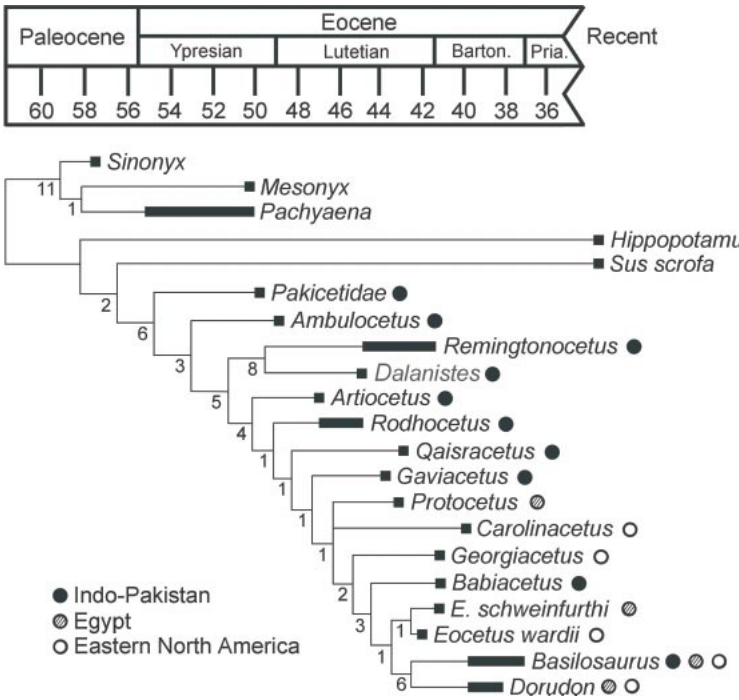

Fig. 25. Strict consensus of two most parsimonious trees of 229 steps; thick lines/black boxes to the left of taxon names indicate known temporal ranges, circles to the right of cetacean taxa indicate geographic occurrence(s). Bremer support values are placed below and to the left of each node. Note that the branching order of taxa is generally concordant with the first geologic occurrence of taxa, and we can infer that the immigration of cetaceans to North America occurred in the latter half of the Lutetian. The geologic durations of taxa are from Gingerich et al. (1997, 2001a, 2001b) and Uhen (1998a, 1998b).

Carolinacetus has multiple differences with every described taxon in the Protocetidae for which comparisons can be made. Although the autapomorphies described in the diagnosis are sufficient to distinguish this new taxon, we describe below further comparisons between *Carolinacetus* and the three protocetids described from North America, *Georgiacetus vogtlensis*, *Eocetus wardii*, and *Natchitochia jonesi*. Presently, the best preserved and most informative protocetid from North America is *Georgiacetus vogtlensis*, known from the middle Eocene ''Blue Bluff Unit'' of Georgia. Hulbert et al. (1998) and Hulbert (1998) described the holotype skeleton of the genus, which includes a complete skull, left mandible, 23 vertebrae, 12 ribs, and both innominates. *Carolinacetus* is between 8 and 15% larger than *Georgiacetus*, and the former differs from the latter in the following cranial characters: (1) posterior margin of the external nares above the canine, not P1; (2) palatal process of the premaxilla terminates between the canine and P1, not posterior to P1; (3) ascending process of the premaxilla terminates dorsal to P1, not above P3; and (4) parietal ridge is rounded, not acute. There is considerable difference between the length-to-width ratios of the centrum in the vertebrae of *Carolinacetus* and *Georgiacetus* (table 5). Ratios for the thoracic series T2–T7 range from 1.54 to 1.58 in *Carolinacetus* and 1.34 to 1.46 in *Georgiacetus*. The higher ratios of the vertebral centra of *Carolinacetus* reflect their proportionately shorter length compared to those of *Georgiacetus*. In addition, the spinous processes of the anterior thoracics of *Carolinacetus* are much larger and more robust than those of *Georgiacetus*, and the ribs of *Carolinacetus* have a more prominent CIA than those of *Georgiacetus*.

Eocetus wardii Uhen, 1999 is the only protocetid from North America to have been placed in an Old World genus. The type species of *Eocetus*, *E. schweinfurthi* Fraas, 1904, was described from a skull (SNMS 10986) from the mid-Bartonian Guishi Formation from Gebel Mokattam near Cairo, Egypt (Gingerich, 1992: 72, figs. 5, 52). Two isolated vertebrae from Gebel Mokattam were referred to *Eocetus* by Fraas (1904), but they have since been referred to *Basilosaurus drazindae* by Uhen (1998a). The affinities of two other isolated vertebrae from Gebel Mokattam, described by Stromer (1908) as ''Frankfurt #1'' and also referred to *Eocetus*, remain unclear, partly because they have been missing for many years, thus precluding any comparisons with vertebrae of other taxa. Uhen (1999) reported two vertebrae in the Staatliches Museum für Naturkunde that appeared to fit the description of ''Franfurt #1'', and the similarity of these vertebrae to those of *E. wardii* was the primary basis for his assignment of *E. wardii* to *Eocetus*. We follow previous authors (Barnes and Mitchell, 1978; Hulbert, 1998) in treating the referral of any isolated vertebrae to *Eocetus* with skepticism because no vertebrae were found with the holotype skull of *E. schweinfurthi* and thus are unknown for *Eocetus*. Therefore, we hereinafter refer to the taxon described by Uhen (1999) as ''*Eocetus*'' *wardii*. Although it clearly represents a form distinct from all other known North American cetacean taxa, a better understanding of the systematic position of ''*E.*'' *wardii* must await the discovery of additional remains with a fairly complete skull.

The holotype of ''*E.*'' *wardii* (USNM 310633), from late Lutetian (NP 16) beds in the Castle Hayne Formation of North Carolina, includes only a fragment of the anterior end of the rostrum, 11 vertebrae, a partial sacrum, and 3 partial ribs. Most of the precaudal axial skeleton of this taxon is now known from referred specimens (NCSM 11284) reported by Uhen (2001). There are several differences between the vertebrae of *Carolinacetus* and ''*E.*'' *wardii*. The cortical bone of the vertebrae in the former is thin and smooth externally, but in the latter it is thick and bears numerous external depressions that lead into vascular canals. Where comparisons are possible, the relative proportions of the vertebrae of *Carolinacetus* differ considerably from those of ''*E.*'' *wardii*, with those of the former being much shorter than those of the latter. For example, the width/length ratio of the centrum of the sixth thoracic vertebra in *Carolinacetus* is 1.55, while in ''*E.*'' *wardii* the ratio for that vertebra is 0.90 (table 6). Unlike C7 in *Carolinacetus*, the transverse processes of that vertebra in ''*E.*'' *wardii* are deeper dorsoventrally and are directed laterally instead of ventrolaterally. Beginning with T4, there is an extreme difference in the anteroposterior diameter of the spinous process of the thoracic vertebrae in these two taxa. In *Carolinacetus* it is very narrow (table 4), but in the thoracics of ''*E.*'' *wardii* the anteroposterior diameter of the neural spine is greater than in any known protocetid and is more similar to those of basilosaurids, as is the broad, fan-shaped scapula of ''*E.*'' *wardii* (Uhen, 2001: figs. 3, 8).

Little comparison can be made between *Natchitochia jonesi* Uhen (1998b) and *Carolinacetus* because the holotype vertebrae of the former consist only of four thoracics, five lumbars, one sacral, two caudals, and three ribs, while the holotype of the latter includes thoracic vertebrae but no lumbars, sacrals, or caudals. The relative positions of the thoracic vertebrae of *N. jonesi* are ambiguous, further compounding the problem. The only currently reportable difference between these two taxa is in the relative size of the vertebrae, with the anterior thoracics of *Natchitochia* being ca. 15% larger than those of *Carolinacetus*. *Natchitochia* has a single sacral vertebra with short transverse processes, no pleurapophyses, and broad articulation with the sacrum (Uhen, 1998b). The morphology of the sacrum is intermediate between *Gaviacetus*, which has a sacral vertebra with short transverse processes, and *Protocetus*, which has a sacral vertebra with long transverse processes. *Natchitochia* and *Carolinacetus* may represent a similar evolutionary grade, but that issue cannot be settled without additional skeletal material.

Phylogenetic Analysis

The branch-and-bound analysis found two most parsimonious trees of 299 steps, each

TABLE 6

Measurements (in mm) and Width/Length Ratios of Holotype Vertebral Centra of *Carolinacetus gingerichi*, n.gen, n.sp. (ChM PV5401) and Referred ~T6 (ChM PV6088), *Georgiacetus vogtlensis* (GSM 350), and Referred Specimens of *"Eocetus" wardii* (NCSM 11284)

	Carolinacetus			*Georgiacetus*			*"Eocetus" wardii*		
	AW	APL	Ratio	AW	APL	Ratio	AW	APL	Ratio
C3	49.8	36.6	1.36	—	—	—	—	—	—
C4	—	—	—	46.3	28.1	1.65	—	—	—
C5	—	—	—	42+	28.6	(1.47)	—	—	—
C6	50.1	38.6	1.30	—	—	—	—	—	—
C7	50.2	34.3	1.46	45.6	28.5	1.60	56.4	32	1.76
T1	—	35.5	—	—	—	—	62.3	51	1.22
T2	60.6	38.5	1.57	—	—	—	59.4	63.3	0.94
T3	—	—	—	54.2	37.2	1.46	67.1	63.7	1.05
T4	64.6	(41.5)	(1.56)	—	—	—	64.2	60.3	1.06
T5	66.9	42.3	1.58	—	—	—	68	58.4	1.16
T6	67.7	43.7	1.55	54.1	40.5	1.34	66.8	74.3	0.90
~T6*	73.4*	49.5*	1.48*	—	—	—	—	—	—
T7	67.2	(43.5)	(1.54)	54.0	40.4	1.34	72.2	74	0.98
T8	—	—	—	57.1	40.7	1.40	73	78.2	0.93
T9	—	—	—	—	—	—	84.2	80.5	1.05
T10	—	—	—	—	—	—	93	89.5	1.04
T11	—	—	—	—	—	—	85.9	111	0.77
T12	—	—	—	68.2	47.8	1.43	97	118.1	0.82
T13	—	—	—	76+	48.3	1.57	—	—	—
L1	—	—	—	—	—	—	95.9	134	0.71
L2	—	—	—	—	54.8	—	104.1	135.1	0.77
L3	—	—	—	—	—	—	—	—	—
L4	—	—	—	78	59.1	1.32	—	—	—
L5	—	—	—	—	—	—	—	—	—
L6	—	—	—	—	—	—	—	—	—
L7	—	—	—	81.5	71.2	1.14	—	—	—
L8	—	—	—	78+	72.3	1.08	—	—	—

Notes: Ratios derived from dividing anterior width (AW) of centrum by anteroposterior length (APL). Atlas vertebra (C1) and axis vertebra (C2) are omitted because their disparate morphology makes it difficult to compare their measurements with those of the remaining cervical vertebrae. Dashes (—) indicate missing elements. Measurements for *Georgiacetus* are from Hulbert (1998: 241, table 1); those for "*E.*" *wardii* are from Uhen (2001: 137, table 1). Asterisk (*) indicates the measurements for the referred specimen (ChM PV6088), thought to be a T6.

with a CI of 0.59 and a RI of 0.75. A strict consensus of the two trees is shown in figure 25. In both trees, *Carolinacetus* and *Protocetus* are adjacent members of a pectinate series of stem taxa to Basilosauridae; however, in the first most parsimonious tree, *Carolinacetus* is more basal than *Protocetus*, while the opposite is true in the second one. The first topology is supported by the position of the posterior edge of the external bony nares; in *Carolinacetus* it is over the canines, while in *Protocetus* it is just anterior to P1. The second shortest tree is supported by the morphology of embrasure pit between the canine and P1; in *Carolinacetus* it is deep, like that of *Georgiacetus*, while in *Protocetus* this pit is shallow, similar to the morphology in *Qaisracetus*. In all other respects, the most parsimonious trees are identical, including a monophyletic Cetartiodactyla, Cetacea, Remingtonocetidae, Basilosauridae, and *Eocetus*.

Carolinacetus occupies a fairly central position among protocetids and is more basal than the North American protocetids *Georgiacetus* and "*Eocetus*" *wardii*. *Natchitochia* is too poorly known to determine whether it is more derived than *Carolinacetus*. The phylogenetic position of *Carolinacetus*, as

supported by the present study, is consistent with previous studies of *Carolinacetus* as the ''Cross Whale'' that placed it between *Protocetus* and Remingtonocetidae among a series of cetacean stem taxa (Geisler and Luo, 1998; O'Leary and Geisler, 1999). In our study, the most exclusive clade of which *Carolinacetus* is a member includes *Protocetus*, *Georgiacetus*, and *Babiacetus* but excludes *Gaviacetus* and *Qaisracetus*. This clade has a Bremer support of 1 and is only diagnosed by a foramen ovale that is not enclosed on its ventral side (character 23, $2 > 1$). Better support is found for the clade excluding *Carolinacetus* and *Protocetus* but including *Georgiacetus*, *Babiacetus*, ''*Eocetus*'' *wardii*, and Basilosauridae. It has a Bremer support of 2 and is diagnosed by three unambiguous synapomorphies: posterior margin of bony nares over P1 (character 5, 1 or $2 > 3$), palatal processes of premaxillae terminate near P1 (7, $1 > 2$ or 3), and ascending process of premaxilla terminates over or posterior to P3 (8, $2 > 3$).

Our phylogenetic analysis corroborates previous studies that found Protocetidae to be paraphyletic (Uhen, 1998a, 1999; Geisler, 2001; Geisler and Uhen, 2003). In addition, we corroborated the phylogenetic arrangement (Pakicetidae (Ambulocetidae (Remingtonocetidae (Protocetidae (Basilosauridae))))) advocated by Uhen (1998a, 1999), Geisler and Luo (1998), O'Leary and Geisler (1999), Geisler (2001), and Geisler and Uhen (2003). A notable exception is the phylogenetic analysis of Thewissen and Hussain (2000), which proposed a sister-group relationship between Basilosauridae and Remingtonocetidae to the exclusion of protocetids. The authors of that study were skeptical of their results, and we can confirm their skepticism by noting that, in the present study, forcing monophyly of Basilosauridae + Remingtonocetidae increases the length of the shortest trees by 28 steps.

Contrary to Uhen (1999), we found *Georgiacetus* to occupy a more basal position than *Babiacetus*. The clade including *Babiacetus*, *Eocetus*, and Basilosauridae to the exclusion of *Georgiacetus* is relatively well supported, as indicated by a Bremer support of 3 (fig. 25) and by seven unequivocal synapomorphies, including embrasure pit between C and P1 indents ventral and lateral surfaces of rostrum (character 11, $2 > 3$); frontal with large nasal process (15, $1 > 2$); postorbital process directed laterally and slightly posteriorly (20, $1 > 2$); exoccipital does not extend beyond lateral margin of mastoid process of petrosal (29, $1 > 0$); lateral margin of exoccipital lacks a dorsoventral row of muscular fossae (38, $1 > 0$); P1 and p1 subequal to canine (character 66, $0 > 1$); and absence of molar protocones (75, $1 > 2$). Forcing *Georgiacetus* to be the sister group to a Basilosauridae + *Eocetus* clade to the exclusion of *Babiacetus* increases the tree length by a minimum of six steps.

Gingerich et al. (2001b) noted that sacral characters do not unambiguously indicate whether *Rodhocetus* or *Qaisracetus* is more closely related to extant cetaceans. We agree that this anatomical region contains contradictory evidence; nevertheless, our parsimony analysis resolved the relationship between these taxa and supports a more derived position for *Qaisracetus*. The clade including *Qaisracetus*, *Georgiacetus*, and later cetaceans but excluding *Rodhocetus* and *Artiocetus* has a Bremer support of 1 and is diagnosed by two synapomorphies: three or fewer postlumbar vertebrae articulate via pleurapophyses (character 96, $1 > 2$), and ventromedial expansion of pubis (106, $0 > 1$). Under this topology, it is equally parsimonious to infer that the fusion of two sacral vertebrae in *Qaisracetus* is a reversal or that the lack of fusion in *Rodhocetus* is convergent with more derived cetaceans (e.g., *Georgiacetus*).

The systematic position of the Eocene cetacean genus *Gaviacetus* warrants discussion here because its status is in dispute. *Gaviacetus* was described by Gingerich et al. (1995b) as a protocetid, but in their description of *Gaviacetus sahnii*, Bajpai and Thewissen (1998) removed that genus from the Protocetidae and placed it in the Basilosauridae. Their revision was based on the apparent absence of the alveolus for M3 in the holotype of *G. sahnii* and on the length of two elongate caudal vertebrae that they referred to that species. *Basilosaurus*, the type genus of Basilosauridae, lacks M3 and has elongate lumbar and caudal vertebrae (Kellogg, 1936). Bajpai and Thewissen (1998:

231) stated that ''M3 is probably absent'' in *G. sahnii*; however, we note that the thin bone that forms the alveoli of the second and third upper molars may not be preserved (e.g., *Georgiacetus*). More informative is the single tooth preserved with the holotype, a right P1 that the authors of that taxon figured in drawings but did not compare with other taxa. Their figure 7d shows a tooth that is triangular, low-crowned, and broad-based, far more similar to the P1 of protocetids (e.g., *Protocetus*) than that of basilosaurids, in which the crown of P1 is much higher, has accessory denticles, and is proportionately more narrow at the base (see Fraas, 1904: fig. 2, left P1, and Kellogg, 1936, figs. 3, 31a). Bajpai and Thewissen (1998: 226 [fig. 9], 228, 230) also referred four elongate caudal vertebrae to *G. sahnii* because they ''are of an animal of the size of *Gaviacetus*'', but we regard it as equally probable that the specimens could belong to another taxon similar in size to *Gaviacetus*. We do not think that there is sufficient evidence to refer those vertebrae to *Gaviacetus*; therefore, *G. sahnii* has no unambiguous basilosaurid characters.

Among the characters upon which Gingerich et al. (1995b) based their assignment of *Gaviacetus* to the Protocetidae were the ''sphyroid shape of frontals and confirmation of exoccipitals and bulla'' in the type species of the genus, *Gaviacetus razai*. The supraoccipital of *G. razai* has the narrow, tubular, and posteriorly elongate form typical of protocetids, quite unlike the broader, more vertically directed occiput of basilosaurid archaeocetes. Other characters in the holotype of *G. razai* indicate that it is excluded from Basilosauridae, including a rudimentary pterygoid sinus that has not extended beyond the tympanic bulla; broad articulation between the falciform process of the squamosal and the ectotympanic bulla (Luo and Gingerich, 1999); and a short, robust transverse process of the sacral vertebra (Gingerich et al., 1995b; Hulbert, 1998). Our cladistic analysis shows that the shortest trees that include *Gaviacetus* within Basilosauridae require an additional 28 steps. Thus, based on strong morphological evidence and the results of our phylogenetic analysis (fig. 25), we restore the genus *Gaviacetus* to the Protocetidae.

BIOGEOGRAPHY

All Ypresian and most Lutetian cetaceans are currently known only from Indo-Pakistan, but by Bartonian or Priabonian times, cetaceans had achieved a cosmopolitan distribution, with taxa known from North America (McLeod and Barnes, 1996; Hulbert et al., 1998; Uhen, 1998b, 1999), Egypt (Fraas, 1904), New Zealand (Köhler and Fordyce, 1994), and Europe (Kellogg, 1936; Uhen and Tichy, 2000). Those distributional patterns clearly indicate that protocetids moved out of Indo-Pakistan at some time during the Lutetian. There is, however, no direct evidence of the routes of their dispersal, especially of those that eventually made their way to North America.

Although there are several possible routes of protocetid dispersals, we will consider only two of the most obvious avenues by which they could have dispersed from the Tethys region to the Western Hemisphere. The first was a course across the North Atlantic Ocean from the west coast of Africa to the north coast of South America, and then northward to the east coast of North America. The second route was a northerly one along the west coast of Europe, then westward along the southern coast of Greenland, and down the coast of Labrador to the eastern shores of the present-day United States.

Uhen (1999) was the first to suggest a path of dispersal to North America from the western Mediterranean via the open Atlantic Ocean. In support of that hypothesis, he cited Feldmann et al. (1998), who noted that fossil decapods from Lutetian beds in North Carolina are closely related to Old World forms. Feldmann et al. (1998) used a computer-based ocean circulation model to estimate the temperatures, salinities, and circulation of the Atlantic during the middle Eocene. Their model suggested a gyre in the North Atlantic similar to the present-day pattern of circulation (e.g., Sanders et al., 1976: fig. 12.6), and they suggested that westward larval dispersal via the southern branch of the Eocene gyre could explain the close phylogenetic relationships between European and eastern North American decapods. Earlier, Blow and Manning (1996: 1) had observed that the assemblage of crabs from both the Castle Hayne

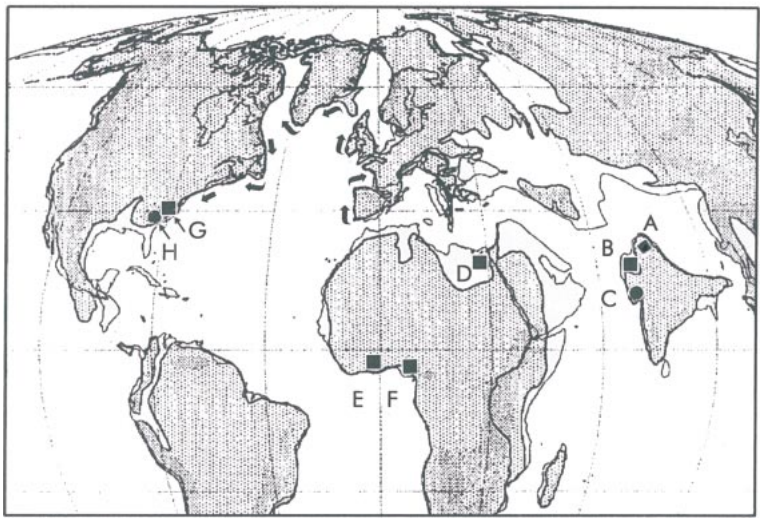

Fig. 26. Paleocoastline map, Middle Eocene (Lutetian), ca. 45 Ma, showing paleogeographic distribution of selected protocetid taxa (**A-H**) from Ypresian (Early Eocene) (♦), Lutetian (Middle Eocene) (■), and Bartonian (Late Middle Eocene) (●) rocks, and probable route (☁) of protocetid dispersal from Tethys Sea to North America. **A.** *Himalayacetus subathuensis*, Subathu Fm. (ca. 53.5 Ma), Kuthar Nala, India. **B.** ''Habib Rahi Limestone Whale'', Habib Rahi Fm. (ca. 48 Ma), Sulaiman Range, Pakistan. **C.** Various remingtonocetids and protocetids, Harudi Fm. (ca. 41 Ma), Kutch, India. **D.** *Protocetus atavus*, Mokattam Fm. (ca. 43.5 Ma), Gebel Mokattam, Egypt. **E.** ''Togo whale'', unspecified stratigraphic unit (ca. 45 Ma), Kpogame-Hahotoe Basin, Togo. **F.** *Pappocetus lugardi*, Ameki Fm. (ca. 42 Ma), Ombialla District, Nigeria. **G.** *''Eocetus'' wardii*, Castle Hayne Fm. (ca. 42 Ma), Maple Hill, North Carolina, U.S. **H.** *Carolinacetus gingerichi*, new genus and species, Tupelo Bay Fm. (ca. 40 Ma), Martin Marietta Berkeley Quarry, South Carolina, U.S.

Limestone of North Carolina and the Santee Limestone of South Carolina ''as a whole, has greater affinities with faunas of the Eocene of Hungary, Italy, and Spain than with known American Eocene faunas.'' While currents could affect the distribution of certain invertebrates, particularly those with a larval stage, we do not think that currents would substantially influence the distribution of active swimmers, such as protocetids.

In trying to determine the most probable route that these early migrants would have taken, perhaps the most important factor to consider is the locomotor capabilities of protocetids, but current opinions regarding their locomotion are controversial. Protocetids have been described as efficient swimmers with propulsion via undulation of the body and tail (Buchholtz, 1998; Fish, 1998) or as having a more primitive means of aquatic movement that involved alternate hindlimb paddling (Gingerich, 2003). Despite the lack of consensus, it is clear that protocetids were not nearly as well adapted to the marine environment as are extant cetaceans or even basilosaurids. As Gingerich et al. (2001a: 2241) noted regarding *Rodhocetus*, ''The forelimbs and hands could not be extended as broad pectoral flippers, which would be required to control recoil from undulation or oscillation of a caudal fluke . . . hence, it is doubtful that *Rodhocetus* had such a fluke.'' If such were the case, the absence of a fluke would seem to have mitigated against the movement of early Lutetian protocetids out into the open sea. Coastal waters are typically more productive than pelagic surface waters; therefore, successful dispersal across the open ocean is unlikely for taxa that do not move efficiently in the marine environment. For these reasons, we think that the most likely route along which protocetids would have migrated to North America during the middle Eocene would have been northward along the coast of Europe and thence westward along the southern coast of

Greenland. As seen in figure 26, that course presented only two relatively narrow water barriers that would have been far more easily negotiated than the open ocean between Africa and South America, and in the warm climatic conditions of the middle Eocene there would have been no appreciable temperature deterrents (Cronin, 1999).

The timing of the movement of protocetids toward North America is suggested by the age of the oldest cetaceans from North America. ''*Eocetus*'' *wardii*, from late Lutetian (NP 16) beds in the Castle Hayne Formation of North Carolina (fig. 25), and undescribed material in the Charleston Museum from the late Lutetian Santee Limestone (NP 16) at Cross Quarry in South Carolina demonstrate that protocetids were present in North America by the late Lutetian, ca. 42 Ma. The undescribed material from the Santee Limestone seems to include representatives of at least two (and possibly three) different taxa, suggesting that protocetid diversification in North America was well underway by the late Lutetian. *Carolinacetus* and two undescribed ChM specimens from the middle to late Bartonian (NP 17) Cross Member of the Tupelo Bay Formation overlying the Santee Limestone, *Georgiacetus*, from the early Bartonian McBean Formation, and *Natchitochia*, from the early Bartonian Cook Mountain Formation of Louisiana, document a protocetid fauna of at least five taxa along the late middle Eocene coastline of the southeastern United States, and there is no reason to think that other taxa were not present as well. Given the stratigraphic age (ca. 42–40 Ma) and the diversity of North American protocetids by mid-Bartonian times, the initial dispersal of cetaceans into the Western Hemisphere seems to have taken place between 45 and 43 Ma.

Anatomical innovations in locomotion may have played a role in the timing of protocetid dispersal to North America. Hypotheses regarding specific evolutionary developments that might have been involved were tested by optimizing characters onto our most parsimonious trees. On the cladogram supported by the present study, the first cetacean lineage that had representatives outside of Indo-Pakistan branched from an unresolved trichotomy between *Protocetus*, *Carolinacetus*, and the clade including derived protocetids and basilosaurids. Surprisingly, no postcranial characters are optimized to have evolved on this branch. The loss of fusion between sacral vertebrae is optimized to have evolved lower on the tree, on one of the three internal branches at the base of Protocetidae. Hence, we cautiously suggest that the development of caudal flukes may have been a key anatomical innovation that assisted *Carolinacetus*-grade cetaceans in their dispersal out of Indo-Pakistan. What little is known of the caudal vertebrae of early cetaceans is consistent with this hypothesis.

Buchholtz (1998) inferred the presence or absence of flukes in extinct taxa from variations in the ratios of centrum width/height among caudal vertebrae, noting that extant cetaceans with flukes have relatively narrow caudal vertebrae anteriorly and wide vertebrae within the region of the flukes. If the correlation observed among extant taxa holds for extinct forms, then basilosaurids had flukes (Buchholtz, 1998) and primitive cetaceans like *Kutchicetus* (Bajpai and Thewissen, 2000) did not. Therefore, caudal flukes would seem to have evolved within the protocetid grade of cetaceans, but only after the loss of iliosacral articulation had committed them to an aquatic existence. However, our hypothesis can be tested only by the discovery of protocetid skeletal remains with most of the caudal vertebrae preserved. Theoretically, the distalmost caudals of a protocetid with flukes would be short and broad, much like those of basilosaurids, and their flukes may have been ''small rounded, lateral outgrowths of the tail'', similar to stage 2 in figure 7 of Fish (1998: 316).

CONCLUSIONS

Carolinacetus gingerichi is the basalmost cetacean from North America known from cranial and postcranial material. Hence, its lineage is expected to have existed during the late Lutetian, even though it is currently known only from the Bartonian. The morphology of *Carolinacetus* is distinctly different from that of *Georgiacetus* and ''*Eocetus*'' *wardii*, and all three taxa appear to represent distinct grades of protocetid evolution. If the dispersal capabilities of protocetids were lim-

ited, one might expect that there was a single dispersal of protocetids to the east coast of North America and that all taxa found there would form a clade. The phylogenetic analysis presented here shows that the North American taxa do not form a clade, with several synapomorphies indicating that ''*Eocetus*'' *wardii* is more closely related to basilosaurids than to *Georgiacetus* or *Carolinacetus*. Alternatively, was there a single dispersal after which several grades of protocetids evolved in North America, with one lineage being ancestral to basilosaurids and extant cetaceans? A detailed study of the meager but growing Middle Eocene record from North America suggests that such was not the case.

Given an adequate fossil record for a particular group, one might expect that in the primary region of its evolution and speciation the stratigraphic position of its various taxa would correlate with their relative positions in a cladogram; that is, the oldest forms should be the basalmost taxa on the cladogram. In general, that appears to be the case with the Eocene deposits of Indo-Pakistan (fig. 25). Using the most up-to-date correlation chart for this region (Gingerich et al., 1997: fig. 14) and adding the discoveries of *Artiocetus* (Gingerich et al., 2001a) and *Qaisracetus* (Gingerich et al., 2001b), the first stratigraphic occurrence of taxa follows quite closely the position of taxa in the cladogram of the present study. *Artiocetus*, which is the oldest known protocetid (Gingerich et al., 2001a), is also the basalmost protocetid in our cladogram. *Babiacetus*, which, according to our study, is the most derived of the Indo-Pakistan pakicetids, is found in the youngest (i.e., Bartonian) rocks that produce fossil cetaceans in that region. Thus, the Indo-Pakistan record is consistent with the hypothesis that the eastern Tethys was an area of origin for several early cetacean lineages.

In North America, the record of early cetaceans is quite different from that of Indo-Pakistan. ''*Eocetus*'' *wardii* appears in the fossil record at approximately the same time as *Georgiacetus*, which branches from our cladogram two nodes below ''*E.*'' *wardii*. *Carolinacetus*, which is more basal than both, is presently known only from rocks younger than those that have produced other North American protocetids. Thus, the stratigraphic sequence of protocetid occurrence in North America—as currently understood—is not consistent with their respective phylogenetic positions as implied by the cladogram of the present study. It is, however, a pattern that would be expected of animals evolving in one region and migrating to another. In such a case, the order of appearance could be more reflective of dispersal capability than of evolutionary grade.

An important caveat to the preceding biogeographic observations is the fact that we are still in the early stages of discovering and studying the protocetid faunas of North America. There is at least one undescribed protocetid from North Carolina (McLeod and Barnes, 1990), and an initial assessment of protocetid specimens in the Charleston Museum indicates that there are at least three other undescribed species in the Cross Quarry fauna. We think that the as-yet-undescribed diversity of the protocetid faunal remains from this quarry will indicate that there were multiple immigrations of protocetids to eastern North America and that one or more of those dispersals were followed by endemic speciation and evolution. If we are correct, North America will provide a unique window into early cetacean evolution, supplementing the excellent record from Indo-Pakistan with knowledge of the earliest developments in cetacean evolution in the New World.

ACKNOWLEDGMENTS

We are especially grateful to Sonny King, plant manager of the Martin Marietta Berkeley Quarry, and others of the Martin Marietta Company for allowing representatives of the Charleston Museum full access to the quarry to search for fossil cetacean remains during the past decade. Mr. King has been ever helpful with information about the quarry, and during the excavation of the holotype skeletal remains of *Carolinacetus gingerichi* he diverted mining activities from the excavation site so that our work would not be interrupted. We also thank Bricky Way, Sam Davis, and Johnny Hanlon for their valuable assistance in the excavation.

We express our sincere thanks to Robert E. Weems and Lucy Edwards (U.S. Geological Survey) and Ralph Willoughby (South Carolina Geological Survey) for their helpful suggestions and discussions regarding the stratigraphic relationships of the Eocene units on the coastal plain of South Carolina. Philip Gingerich (Univ. of Michigan) and J.G.M. ''Hans'' Thewissen (Northeastern Ohio Universities, College of Medicine) graciously provided access to described and undescribed specimens in their care. We greatly appreciate the constructive comments of two anonymous reviewers.

It is with utmost gratitude that we acknowledge the contributions of Charleston Museum volunteer Billy Palmer. His tireless collecting efforts in the South Carolina quarries have provided a crucial body of Eocene cetacean remains that gives us an unprecedented perspective of the North American protocetid fauna.

Much of this research was conducted while J.H. Geisler was a graduate student. During that time, he was supported by a National Science Foundation Graduate Fellowship, a Faculty Fellowship in the Department of Earth and Environmental Sciences at Columbia University, and the Office of Grants and Fellowships at the American Museum of Natural History. Recent fossil discoveries were integrated into this study during the summer of 2003, with support from a faculty research grant from Georgia Southern University. Zhe-Xi Luo's research was supported by the National Science Foundation (grant DEB 94–19898).

REFERENCES

Albright, L.B. 1996. A protocetid cetacean from the Eocene of South Carolina. Journal of Paleontology 70: 519–523.

Bajpai, S., and J.G.M. Thewissen. 1998. Middle Eocene cetaceans from the Harudi and Subathu Formations of India. *In* J.G.M. Thewissen (editor), The emergence of whales, evolutionary patterns in the origin of Cetacea: 213–233. New York: Plenum Press.

Bajpai, S., and J.G.M. Thewissen. 2000. A new, diminuitive whale from Kachchh (Gujarat, India) and its implications for locomotor evolution of cetaceans. Current Science (New Delhi) 79: 1478–1482.

Bajpai, S., J.G.M. Thewissen, and A. Sahni. 1996. *Indocetus* (Cetacea, Mammalia) endocasts from Kachchh (India). Journal of Vertebrate Paleontology 16: 582–584.

Barnes, L.G., and E.D. Mitchell. 1978. Cetacea. *In* V.J. Maglio and H.B.S. Cooke (editors), Evolution of African mammals: 582–602. Cambridge, MA: Harvard University Press.

Barnes. L.G. 1984. Whales, dolphins, and porpoises: origin and evolution of Cetacea. *In* T.W. Broadhead (editor), Mammals. Notes for a short course organized by P.D. Gingerich and C.E. Badgley: 139–154. University of Tennessee Department of Geological Sciences. Studies in Geology 8(1–4).

Baum, G.R., J.S. Collins, R.M. Jones, B.A. Madlinger, and R.J. Powell. 1980. Correlation of the Eocene strata of the Carolinas. South Carolina Geology 24: 19–27.

Berggren, W.A., D.V. Kent, C.C. Swisher III, and M-P. Aubry. 1995. A revised Cenozoic geochronology and chronostratigraphy. *In* W.A. Berggren, D.V. Kent, and J.A. Hardenbol (editors), Geochronology, time scales and global stratigraphic correlation: 129–212. SEPM Society for Sedimentary Geology Special Publication No. 54.

Blow, W.C., and R.B. Manning. 1996. Preliminary descriptions of 25 new decapod crustaceans from the middle Eocene of the Carolinas, U.S.A. Tulane Studies in Geology and Paleontology 29: 1–26.

Breathnach, A.S. 1955. Observations on endocranial casts of recent and fossil cetaceans. Journal of Anatomy 89: 532–546.

Bremer, K. 1988. The limits of amino acid sequence data in angiosperm phylogenetic reconstruction. Evolution 42: 795–803.

Bremer, K. 1994. Branch support and tree stability. Cladistics 10: 295–304.

Buchholtz, E.A. 1998. Implications of vertebral morphology for locomotor evolution in early Cetacea. *In* J.G.M. Thewissen (editor), The emergence of whales, evolutionary patterns in the origin of Cetacea: 325–351. New York: Plenum Press.

Carte, A., A. MacAlister, and W.H. Flower. 1868. On the anatomy of *Balaenoptera rostrata*. Philosophical Transactions of the Royal Society of London 158: 201–262.

Cifelli, R.L. 1982. The petrosal structure of *Hyopsodus* with respect to that of some other ungulates, and its phylogenetic implications. Journal of Paleontology 56(3): 795–805.

Cooke, C.W. 1936. Geology of the coastal plain of South Carolina. U.S. Geological Survey Bulletin 867: 1–196.

Coombs, M.C., and W.P. Coombs, Jr. 1982. Anatomy of the ear region of four Eocene artiodactyls: *Gobiohyus*,? *Helohyus*, *Diacodexis* and

Homacodon. Journal of Vertebrate Paleontology, 2: 219–236.
Cronin, T.R. 1999. Principles of paleoclimatology. New York: Columbia University Press.
Dart, R.A. 1923. The brain of the Zeuglodontidae (Cetacea). Proceedings of the Zoological Society of London 1923: 615–648.
Dennstedt, A. 1904. Die Sinus durae matris der Haussäugetiere. Anatomische Hefte 25(75): 1–96.
Dooley, A.C., Jr., N.C. Fraser, and Z.-X. Luo. 2004. The earliest member of the rorqual-gray whale clade (Mammalia, Cetacea). Journal of Vertebrate Paleontology 24: 453–463.
Dyce, K.M., W.O. Sack, and C.J.G. Wensing. 1996. Textbook of veterinary anatomy, 2nd ed. Philadelphia: WB Saunders.
Edwards, L.E., L.M. Bybell, G.S. Gohn, and N.O. Frederiksen. 1997. Paleontology and physical stratigraphy of the USGS–Pregnall no. 1 core (DOR-208), Dorchester County, South Carolina. USGS Open-file Report 97–145: 1–35.
Feldmann, R.M., K.L. Bice, C.S. Hopkins, E.W. Salva, and K. Pickford. 1998. Decapod crustaceans from the Eocene Castle Hayne Limestone, North Carolina: paleoceanographic implications. Journal of Paleontology, The Paleontological Society Memoir, 48: 1–28.
Fish, F.E. 1998. Biochemical perspective on the origin of cetacean flukes. *In* J.G.M. Thewissen (editor), The emergence of whales, evolutionary patterns in the origin of Cetacea: 303–324. New York: Plenum Press.
Fordyce, R.E. 1994. *Waipatia maerewhenua*, new genus and new species (Waipatiidae, new family), an archaic late Oligocene dolphin (Cetacea: Odontoceti: Platanistoidea) from New Zealand. *In* A. Berta and T. Deméré (editors), Contributions in marine mammal paleontology honoring Frank C. Whitmore, Jr.: 147–176. Proceedings of the San Diego Society of Natural History 29.
Fraas, E. 1904. Neue zeuglodonten aus dem unteren Mitteleocän vom Mokattam bei Cairo. Geologische und Palaeontologische Abhandlungen, Neue Folge 6(3): 199–220.
Fraser, F.C., and P.E. Purves. 1960. Hearing in cetaceans: evolution of the acessory air sacs and the structure and function of the outer and middle ear in recent cetaceans. Bulletin of the British Museum (Natural History), Zoology 7: 1–140.
Gatesy, J. 1997. More DNA support for a Cetacea/Hippopotamidae clade: the blood-clotting protein gamma-fibrinogen. Molecular Biology and Evolution 14: 537–543.
Gatesy, J., C. Hayashi, A. Cronin, and P. Arctander. 1996. Evidence from milk casein genes that cetaceans are close relatives of hippopotamid artiodactyls. Molecular Biology and Evolution 13: 954–963.
Gatesy, J., M. Milinkovitch, V. Waddell, and M. Stanhope. 1999. Stability of cladistic relationships between Cetacea and higher-level artiodactyl taxa. Systematic Biology 48: 6–20.
Geisler, J. 2001. New morphological evidence for the phylogeny of Artiodactyla, Cetacea, and Mesonychidae. American Museum Novitates 3344: 1–53.
Geisler, J.H., and Z.-X. Luo. 1996. The petrosal and inner ear of *Herpetocetus* sp. (Mammalia: Cetacea) and their implications for the phylogeny and hearing of archaic mysticetes. Journal of Paleontology 70: 1045–1066.
Geisler, J.H., and Z.-X. Luo. 1998. Relationships of Cetacea to terrestrial ungulates and the evolution of cranial vasculature in Cete. *In* J.G.M. Thewissen (editor), The emergence of whales, evolutionary patterns in the origin of Cetacea: 163–212. New York: Plenum Press.
Geisler, J.H., A.E. Sanders, and Z.-X. Luo. 1996. A new protocetid cetacean from the Eocene of South Carolina, U.S.A.; phylogenetic and biogeographic implications. *In* J.E. Repetski (editor), Sixth North American Paleontological Convention abstracts of papers: 139. Paleontological Society Special Papers 8.
Geisler, J.H., and M.D. Uhen. 2003. Morphological support for a close relationship between hippos and whales. Journal of Vertebrate Paleontology 23: 991–996.
Getty, R. 1975. The anatomy of the domestic animals, 5th ed. Philadelphia: W.B. Saunders.
Gingerich, P.D. 1992. Marine mammals (Cetacea and Sirenia) from the Eocene of Gebel Mokattum and Fayum, Egypt: stratigraphy, age, and paleoenvironments. University of Michigan Papers of Paleontology 30: 1–84.
Gingerich, P.D. 2003. Land-to-sea transition of early whales: evolution of Eocene Archaeoceti (Cetacea) in relation to skeletal proportions and locomotion of living semiaquatic mammals. Paleobiology 29: 429–454.
Gingerich, P.D., M. Arif, M.A. Bhatti, H.A. Raza, and S.M. Raza. 1995a. *Protosiren* and *Babiacetus* (Mammalia, Sirenia and Cetacea) from the middle Eocene Drazida Formation, Sulaiman Range, Punjab (Pakistan). Contributions from the Museum of Paleontology, University of Michigan 29: 331–357.
Gingerich, P.D., M. Arif, and W.C. Clyde. 1995b. New archaeocetes (Mammalia, Cetacea) from the middle Eocene Domanda Formation of the Sulaiman Range, Punjab (Pakistan). Contributions from the Museum of Paleontology, University of Michigan 29: 291–330.
Gingerich, P.D., M. Arif, M.A. Bhatti, M. Anwar, and W.J. Sanders. 1997. *Basilosaurus drazindai* and *Basiloterus hussaini*, new Archaeoceti

(Mammalia, Cetacea) from the middle Eocene Drazinda Formation, with a revised interpretation of ages of whale-bearing strata in the Kirthar Group of the Sulaiman Range, Punjab (Pakistan). Contributions from the Museum of Paleontology, University of Michigan 30: 55–81.

Gingerich, P.D., S.M. Raza, M. Arif, M. Anwar, and X. Zhou. 1993. Partial skeletons of *Indocetus ramani* (Mammalia, Cetacea) from the lower middle Eocene Domanda Shale in the Sulaiman Range of Punjab (Pakistan). Contributions from the Museum of Paleontology, University of Michigan, 28: 393–416.

Gingerich, P.D., S.M. Raza, M. Arif, M. Anwar, and X. Zhou. 1994. New whale from the Eocene of Pakistan and the origin of cetacean swimming. Nature 368: 844–847.

Gingerich, P.D., and D.E. Russell. 1981. *Pakicetus inachus* a new archaeocete (Mammalia, Cetacea) from the early-middle Eocene Kuldana Formation of Kohat (Pakistan). Contributions from the Museum of Paleontology, University of Michigan 25: 235–246.

Gingerich, P.D., and D.E. Russell. 1990. Dentition of early Eocene *Pakicetus* (Mammalia, Cetacea). Contributions from the Museum of Paleontology, University of Michigan 28: 1–20.

Gingerich, P.D., D.E. Russell, and S.M.I. Shah. 1983. Origin of whales in epicontinental remnant seas: new evidence from the early Eocene of Pakistan. Science 220: 403–406.

Gingerich, P.D., B.H. Smith, and E.L. Simons. 1990. Hind limbs of Eocene *Basilosaurus*: evidence of feet in whales. Science 249: 154–157.

Gingerich, P.D., M. ul-Haq, I.S. Zalmout, I.H. Khan, and M.S. Malkani. 2001a. Origin of whales from early artiodactyls: hands and feet of Eocene Protocetidae from Pakistan. Science 293: 2239–2242.

Gingerich, P.D., M. ul-Haq, I.H. Khan, and I.S. Zalmout. 2001b. Eocene stratigraphy and archaeocete whales (Mammalia, Cetacea) of Drug Lahar in the eastern Sulaiman Range, Balochistan (Pakistan). Contributions from the Museum of Paleontology, University of Michigan 30: 269–319.

Harris, W.B., V.A. Zullo, and R.A. Laws. 1993. Coastal onlap stratigraphy of the onshore Paleogene, southeastern Atlantic Coastal Plain, U.S.A. *In* H.W. Posamentier, C.P. Summerhayes, B.U. Haq, and G.P. Allen (editors), Sequence stratigraphy and facies associations: 537–561. International Association of Sedimentologists, Special Publication 18.

Hendy, M.D., and D. Penny. 1982. Branch and bound algorithms to determine minimal evolutionary trees. Mathematical Biosciences 59: 277–290.

Howell, A.B. 1927. Contribution to the anatomy of the Chinese finless porpoise, *Neomeris phocaenoides*. Proceedings of the United States National Museum 70(13): 1–43.

Hulbert, R.C., Jr. 1998. Postcranial osteology of the North American Middle Eocene protocetid *Georgiacetus*. *In* J.G.M. Thewissen (editor), The emergence of whales, evolutionary patterns in the origin of Cetacea: 235–267. New York: Plenum Press.

Hulbert, R.C., Jr., R.M. Petkewich, G.A. Bishop, D. Bukry, and D.P. Aleshire. 1998. A new middle Eocene protocetid whale (Mammalia: Cetacea: Archaeoceti) and associated biota from Georgia. Journal of Paleontology 72: 905–925.

Kasuya, T. 1973. Systematic consideration of recent toothed whales based on the morphology of tympano-periotic bone. Scientific Reports of the Whale Research Institute 25: 1–103.

Kellogg, R. 1936. A review of the Archaeoceti. Carnegie Institute of Washington Publication 482.

Köhler, R., and R.E. Fordyce. 1997. An archaeocete whale (Cetacea: Archaeoceti) from the Eocene Waihao Greensand, New Zealand. Journal of Vertebrate Paleontology 17: 574–583.

Kumar, K., and A. Sahni. 1986. *Remingtonocetus harudiensis*, new combination, a middle Eocene archaeocete (Mammalia, Cetacea) from western Kutch, India. Journal of Vertebrate Paleontology 6: 326–349.

Luo, Z.-X. 1998. Homology and transformation of cetacean ectotypmpanic structures. *In* J.G.M. Thewissen (editor), The emergence of whales, evolutionary patterns in the origin of Cetacea: 269–301. New York: Plenum Press.

Luo, Z.-X., and E.R. Eastman. 1995. Petrosal and inner ear of a squalodontoid whale: implications for the evolution of hearing in odontocetes. Journal of Vertebrate Paleontology 15: 431–442.

Luo, Z.-X., and P.D. Gingerich. 1999. Terrestrial Mesonychia to aquatic Cetacea: transformation of the basicranium and evolution of hearing in whales. University of Michigan Papers in Paleontology 31: 1–98.

Luo, Z.-X., and K. Marsh. 1996. The petrosal (periotic) and inner ear of a Pliocene kogiine whale (Kogiinae, Odontoceti): implications on relationships and hearing evolution of toothed whales. Journal of Vertebrate Paleontology 16: 328–348.

Lyell, C. 1845. On the White Limestone of South Carolina and Georgia, and the Eocene strata of other parts of the U.S., with appendix, on the corals, by Mr. Lonsdale. Proceedings of the Geological Society of London 4(1843–1845): 563–576.

McLeod, S.A., and L.G. Barnes. 1996. The systematic position of *Pappocetus lugardi* and a new taxon from North America (Archaeoceti:

Protocetidae). *In* J.E. Repetski (editor), Sixth North American Paleontological Convention abstracts of papers: 270. Paleontological Society Special Papers 8.

MacPhee, R.D.E. 1981. Auditory regions of primates and eutherian insectivores. Contributions to Primatology 18: 1–282.

MacPhee, R.D.E. 1994. Morphology, adaptations, and relationships of *Plesiorycteropus*, and a diagnosis of a new order of eutherian mammals. Bulletin of the American Museum of Natural History 220: 1–214.

Nikaido, M., A.P. Rooney, and N. Okada. 1999. Phylogenetic relationships among cetartiodactyls based on insertions of short and long interspersed elements: hippopotamuses are the closest extant relatives of whales. Proceedings of the National Academy of Sciences U.S.A. 96: 10261–10266.

Norris, K.S. 1980. Peripheral sound processing in odontocetes. *In* R.-G. Busnel and J.F. Fish (editors), Animal sonar systems: 495–509. New York: Plenum Press.

Novacek, M.J. 1986. The skull of leptictid insectivorans and the higher-level classification of eutherian mammals. Bulletin of the American Museum of Natural History 183: 1–111.

Nummela, S., J.G.M. Thewissen, S. Bajpai, S.T. Hussain, and K. Kumar. 2004. Eocene evolution of whale hearing. Nature 430: 776–778.

O'Leary, M.A., and J.H. Geisler. 1999. The position of Cetacea within Mammalia: phylogenetic analysis of morphological data from extinct and extant taxa. Systematic Biology 48: 455–490.

O'Leary, M.A., and K.D. Rose. 1995. Postcranial skeleton of the early Eocene mesonychid *Pachyaena* (Mammalia: Mesonychia). Journal of Vertebrate Paleontology 15: 401–430.

Padget, D.H. 1957. The development of the cranial venous system in man, from the viewpoint of comparative anatomy. Contributions to Embryology, Carnegie Institution 36: 81–153.

Pompeckj, J.F. 1922. Das Ohrskelett von *Zeuglodon*. Senckenbergiana 4: 44–100.

Prothero, D.R., E.M. Manning, and M. Fischer. 1988. The phylogeny of the ungulates. *In* M.J. Benton (editor), The phylogeny and classification of the tetrapods, mammals: 201–234. Systematic Association Special Volume 35B, vol. 2.Oxford: Clarendon Press.

Radinsky, L.B. 1965. Evolution of the tapiroid skeleton from *Heptodon* to *Tapirus*. Bulletin of the Museum of Comparative Zoology 134(3): 69–106.

Reid, M.S., W.R. Aucott, R.W. Lee, and R.A. Renken. 1986. Hydrologic and geologic analysis of a well in Dorchester County, South Carolina. U.S. Geological Survey Water-Resources Investigations Report 86–4161.

Rose, K.D. 1982. Skeleton of *Diacodexis*, oldest known artiodactyl. Science 216: 621–623.

Rose, K.D. 1985. Comparative osteology of North American dichobunid artiodactyls. Journal of Paleontology 59: 1203–1226.

Sanders, A.E., and L.G. Barnes. 2003 (2002). Paleontology of the late Oligocene Chandler Bridge and Ashley formations of South Carolina, 3: Eomysticetidae, a new family of primitive mysticetes (Mammalia: Cetacea). *In* R. Emry (editor), Cenezoic mammals of land and sea: tributes to the career of Clayton E. Ray. Smithsonian Contributions to Paleobiology 93: 313–356.

Sanders, A.E., and M.P. Katuna. 2000. Proposal for revision of the stratigraphic nomenclature of the Santee Limestone (Eocene) of South Carolina. Abstracts with Programs, Geological Society of America, 49th Annual Meeting, Southeastern Section, March 2000, 32(2): A-71.

Sanders, J.E., A.H. Anderson, Jr., and R. Carola. 1976. Physical geology. New York: Harper and Row.

Schulte, H. von. 1916. Anatomy of a fetus of *Balaenoptera borealis*. Memoirs of the American Museum of Natural History 1: 389–502.

Schulte, H. von, and M. de Forest Smith. 1918. The external characters, skeletal muscles, and peripheral nerves of Kogia breviceps (Blainville). Bulletin of the American Museum of Natural History 38: 7–72.

Shimamura, M., H. Yasue, K. Ohshima, H. Abe, H. Kato, T. Kishiro, M. Goto, I. Munechika, and N. Okada. 1997. Molecular evidence from retroposons that whales form a clade within even-toed ungulates. Nature 388: 666–670.

Sisson, S. 1921. The anatomy of the domesticated animals. Philadelphia: W.B. Saunders.

Slijper, E.J. 1936. Die cetacean vergleichend-anatomisch und systematisch. Capita Zoologica 7: 1–590.

Sloan, E. 1908. Catalogue of the mineral localities of South Carolina. South Carolina Geological Survey Bulletin 2, series 4: 1–505.

Smith, A.G., D.G. Smith, and B.M. Funnell. 1994. Atlas of Mesozoic and Cenozoic coastlines. Cambridge: Cambridge University Press.

Sorenson, M.D. 1996. TreeRot. University of Michigan, Ann Arbor. Can be downloaded from http://people.bu.edu/msoren/TreeRot.html.

Spoor, F., S. Bajpai, S.T. Hussain, K. Kumar, and J.G.M. Thewissen. 2002. Vestibular evidence for the evolution of aquatic behaviour in early cetaceans. Nature 417: 163–166.

Stromer, E. 1903. Zeuglodon-reste aus dem Oberen Mittleocän des Fayum. Beiträge zur Paläntologie und Geologie Österreich-Ungarns und des Orients 15: 65–100.

Stromer, E. 1908. Die Archaeoceti des ägyptiscen Eozäns. Beiträge zur Paläontologie und Geo-

logie Österreich-Ungarns und des Orients 21: 106–178.
Swofford, D.L. 2002. PAUP*, Phylogenetic analysis using parsimony (* and other methods). Sinauer Associates, vers. 4.0b10. Available at http://paup.csit.fsu.edu/.
Thewissen, J.G.M. 1994. Phylogenetic aspects of cetacean origins: a morphological perspective. Journal of Mammalian Evolution 2: 157–184.
Thewissen, J.G.M., and D.P. Domning. 1992. The role of phenacodontids in the origin of the modern orders of ungulate mammals. Journal of Vertebrate Paleontology 12(4): 494–504.
Thewissen, J.G.M., and S.T. Hussain. 1993. Origin of underwater hearing in whales. Nature 361: 444–445.
Thewissen, J.G.M., and S.T. Hussain. 2000. *Attockicetus praecursor*, a new remingtonocetid cetacean from marine Eocene sediments of Pakistan. Journal of Mammalian Evolution 7: 133–146.
Thewissen, J.G.M., S.T. Hussain, and M. Arif. 1994. Fossil evidence for the origin of aquatic locomotion in archaeocete whales. Science 263: 210–212.
Thewissen, J.G.M., S.I. Madar, and S.T. Hussain. 1996. *Ambulocetus natans*, an Eocene cetacean (Mammalia) from Pakistan. Courier Forschungsinstitut Senckenberg 191: 1–86.
Thewissen, J.G.M., D.E. Russell, P.D. Gingerich, and S.T. Hussain. 1983. A new dichobunid artiodactyl (Mammalia) from the Eocene of north-west Pakistan. Proceedings of the Koninklijke Nederlandse Akademie van Wetenschappen, Series B, 86(2): 153–180.
Thewissen, J.G.M., E.M. Williams, L.J. Roe, and S.T. Hussain. 2001a. Skeletons of terrestrial cetaceans and the relationship of whales to artiodactyls. Nature 413: 277–281.
Uhen, M.D. 1998a. Middle to late Eocene basilosaurines and dorudontines. *In* J.G.M. Thewissen (editor), The emergence of whales, evolutionary patterns in the origin of Cetacea: 29–61.New York: Plenum Press.
Uhen, M.D. 1998b. New protocetid (Mammalia: Cetacea) from the late middle Eocene Cook Mountain Formation of Louisiana. Journal of Vertebrate Paleontology 18(3): 664–668.
Uhen, M.D. 1999. New species of protocetid archaeocete whale, *Eocetus wardii* (Mammalia: Cetacea) from the middle Eocene of North Carolina. Journal of Paleontology 73(3): 512–528.
Uhen, M.D. 2001. New material of *Eocetus wardii* (Mammalia: Cetacea) from the middle Eocene of North Carolina. Southeastern Geology 40: 135–148.
Uhen, M.D., and G. Tichy. 2000. A new basilosaurid archaeocete from Austria. Journal of Vertebrate Paleontology 20(suppl.): 74A–75A.
Vogl, A.W., and H.D. Fisher. 1981. Arterial circulation of the spinal cord and brain in the Monodontidae (Order Cetacea). Journal of Morphology 170: 171–180.
Vogl, A.W., and H.D. Fisher. 1981. The internal carotid artery does not directly supply the brain in the Monodontidae (Order Cetacea). Journal of Morphology 170: 207–214.
Ward, L.W., B.W. Blackwelder, G.S. Gohn, and R.Z. Poore. 1979. Stratigraphic revision of Eocene, Oligocene, and lower Miocene formations of South Carolina. Geologic Notes 23: 2–23.
Weems, R.W., J.M. Self-Trail, and L.E. Edwards. 2004. Supergroup stratigraphy of the Atlantic and Gulf coastal plains (Middle? Jurassic through Holocene, eastern North America). Southeastern Geology 42: 191–216.
Wible, J.R. 1984. The ontogeny and phylogeny of the mammalian cranial arterial system. Ph.D. dissertation, Duke University, Durham, North Carolina, 705 pp.
Wible, J.R. 1986. Transformations in the extracranial course of the internal carotid artery in mammalian phylogeny. Journal of Vertebrate Paleontology 6: 313–325.
Wible, J.R. 1987. The eutherian stapedial artery: character analysis and implications for superordinal relationships. Zoological Journal of the Linnean Society 91: 107–135.
Wible, J.R. 1990. Petrosals of late Cretaceous marsupials from North America, and a cladistic analysis of the petrosal in therian mammals. Journal of Vertebrate Paleontology 10: 183–205.
Wilkinson, M. 1992. Ordered versus unordered characters. Cladistics 8: 375–385.
Woodburne, M.O. 1968. The cranial myology and osteology of *Dicotyles tajacu*, the collared peccary, and its bearing on classification. Memoirs of the Southern California Academy of Sciences 7: 1–48.
Zhou, X., W.J. Sanders, and P.D. Gingerich. 1992. Functional and behavioral implications of vertebral structure in *Pachyaena ossifraga* (Mammalia, Mesonychia). Contributions from the Museum of Paleontology, University of Michigan 28: 289–319.
Zhou, X., R. Zhai, and P.D. Gingerich. 1995. Skull of a new mesonychid (Mammalia, Mesonychia) from the late Paleocene of China. Journal of Vertebrate Paleontology 15: 387–400.

APPENDIX 1

Characters for Phylogenetic Analysis

Character codings for characters 14, 76, 77, 79, 80, 82, 92, 102, and all postcranial codings for *Sinonyx* are from Uhen (1999).

Cranial Characters

1. Premaxillae: (0) short with incisors arranged in transverse arc, (1) elongate, incisors aligned longitudinally with intervening diastemata (Prothero et al., 1988; Thewissen, 1994).

2. Palatine fissures: (0) present, (1) absent (Uhen, 1998a; O'Leary and Geisler, 1999).

3. Skull length (ordered): (0) short, length $<$ 700% of condylar breadth, (1) moderate length, 700% $<$ length $<$ 800% of condylar breadth, (2) elongate, $>$800% condylar breadth (Uhen, 1998a, 1999).

4. Anterior margin of external nares (ordered): (0) anterior to I2, (1) dorsal to I2, (2) dorsal or immediately posterior to I3, (3) dorsal to I3 to canine diastema, (4) dorsal to canine.

5. Posterior margin of external nares (ordered): (0) anterior to the canine, (1) over C, (2) immediately anterior to P1, (3) dorsal to P1, (4) between P1 and P2 (modified from Geisler and Luo, 1998).

6. Palate (ordered): (0) concave transversely, (1) flat transversely, (2) convex transversely (Gingerich et al., 1995b; Uhen, 1998a).

7. Palatal process of premaxilla (ordered): (0) short, terminates anterior or at posterior edge of canine, (1) between canine and P1, (2) at P1, (3) posterior to P1.

8. Ascending process of premaxilla (ordered): (0) terminates posteriorly, anterior to or over P1, (1) over P2, (2) over diastema between P2 and P3, (3) over or posterior to P3.

9. Embrasure pits between I1–I2 and I2–I3: (0) absent, (1) present.

10. Embrasure pit between C and I3 (ordered): (0) absent, (1) shallow, (2) deep.

11. Embrasure pit between P1 and C (ordered): (0) absent, (1) small, located on ventral surface of maxilla, (2) deep but contained on ventral surface, (3) occurs on lateral and ventral surfaces of maxilla.

12. Embrasure pits between upper cheekteeth: (0) absent, (1) present (Thewissen, 1994).

13. Rostrum breadth: (0) wide, width at M2 $>$ 140% the condylar width, (1) narrow, width at M2 $<$ 120% the maximum width across the occipital condyles (modified from Uhen, 1999).

14. Palate narrows (ordered): (0) posterior to M3, (1) at M3, (2) at M2, (3) at M1, (4) at P4 (Uhen, 1998a).

15. Nasal process of frontal: (0) absent, (1) present, frontal with small ($<$3 mm) process that lies medial to the posterior end of the nasal, (2) frontal with large nasal process (derived from Uhen, 1998a).

16. Supraorbital process (ordered): (0) absent, frontal shield width $<$ 180% the condylar breadth, (1) present but small, 180% $<$ frontal shield width $<$ 290% of condylar breadth, (2) present, 190% $<$ frontal shield width $<$ 240% of condylar breadth, (3) greatly enlarged, $>$245% of condylar breadth (Barnes, 1984; modified from Uhen, 1998a).

17. Orbit size: (0) small, vertical diameter of orbit $<$ 30% of condylar breadth, (1) large, vertical diameter of orbit $>$ 30% of condylar breadth (Gingerich et al., 1995b; Uhen, 1998a).

18. Orbit: (0) elevated well above toothrow, (1) elevated slightly above toothrow (Thewissen and Hussain, 2000).

19. Anterior edge of orbit: (0) over or posterior to M3, (1) over M2 or M2/M3 division, (2) over M1 or M1/M2 division, (3) over P4 or P4/M1 division (Geisler, 2001).

20. Posterior edge of postorbital process (ordered): (0) forms highly obtuse angle with sagittal crest (angle of anterior border of temporal fossa), (1) oriented at approximately 90° to sagittal crest, (2) forms acute angle with sagittal crest due to posterior swelling of lateral end (modified from Uhen, 1998a).

21. Foramen rotundum: (0) present, (1) absent, maxillary division of trigeminal nerve exits skull through sphenorbital fissure (Novacek, 1986; Thewissen and Domning, 1992).

22. Alisphenoid canal: (0) present, (1) absent (Novacek, 1986; Thewissen and Domning, 1992).

23. Foramen ovale: (0) within the alisphenoid, (1) at squamosal and alisphenoid suture but open ventrally, (2) at squamosal/alisphenoid suture but completely enclosed, (3) merged with piriform fenestra. Use of the term ''foramen ovale'' follows Luo and Gingerich (1999) and corresponds to the ''foramen pseudoovale or pseudo-ovale'' of some other authors (Köhler and Fordyce, 1997; Hulbert et al., 1998).

24. Pterygoid sinus (ordered): (0) absent, (1) present but obscured in ventral view by the bulla, occupies region between anterior end of involucrum and alisphenoid portion of pterygoid ridge, (2) breaches posterior wall of tube for foramen ovale and extends slightly anterior to the anterior edge of the tympanic bulla, (3) enlarged, forms a deep anteroposterior trough which approaches the

internal nares (modified from Luo and Gingerich, 1999).

25. Preglenoid process: (0) absent, (1) present, forms transverse, ventrally projecting ridge at anterior edge of glenoid fossa (modified from Thewissen, 1994; Geisler and Luo, 1998).

26. Postglenoid foramen (ordered): (0) large, (1) greatly reduced in size, only slightly larger than the fenestra vestibuli, (2) absent (modified from Novacek, 1986; Geisler and Luo, 1998).

27. Basioccipital crests (falcate processes): (0) absent, (1) present, forming ventrolaterally flaring basioccipital processes, (2) present and extremely wide transversely and narrow anteroposteriorly (modified from Barnes, 1984; Thewissen, 1994; Geisler and Luo, 1998).

28. External auditory meatus (ordered): (0) absent or very short, length less than 7% of half of the basicranial width, (1) short, 17% < length of meatus < 25% half of the basicranial width, (2) long, 25% < length of meatus < 40%, (3) very long, 40% < length of meatus < 47% (4) elongate, >50% of half of the basicranial width (modified from Luo and Gingerich, 1999).

29. Lateral extent of exoccipital in ventral view: (0) same as or less than the mastoid process of petrosal, (1) greater than mastoid process of petrosal.

30. Hypoglossal foramen: (0) closer to occipital condyle, (1) closer to jugular foramen or notch (Thewissen et al., 1996; Uhen, 1998a).

31. Nuchal crests: (0) oriented laterally, (1) lateral ends are gently curved posterolaterally, (2) form a horseshoe shape in dorsal view that is open posteriorly.

32. Orientation of supraoccipital shield: (0) posterodorsally, (1) vertical above foramen magnum, (2) anterodorsally (modified from Uhen, 1998a).

33. Cerebellar rete (as determined in endocasts or a visible cranial cavity) (ordered): (0) absent or indistinguishable from the rest of the endocast, (1) occurs dorsal and medial to petrosal, (2) occurs dorsal and medial to petrosal as well dorsal to the cerebellum, (3) hypertrophied, completely surrounding the dorsal surface of the cerebellum and the trigeminal nerve and towers above the endocast of the cerebral hemispheres (derived from Geisler and Luo, 1998).

34. Nuchal tubercles: (0) absent, (1) present on dorsal edge of foramen magnum.

35. Exoccipital in posterior view: (0) small finger-like lateral process, dorsoventral diameter < 75% of vertical diameter of foramen magnum, (1) large rectangular process, >80% the vertical diameter of foramen magnum.

36. Fossa for insertion of rectus capitus lateralis muscle (ordered): (0) absent, (1) present as ovoid pit lateral to occipital condyle, (2) present and divided into two smaller fossae which share the larger depression.

37. Fan-shaped fossa on exoccipital dorsal to paroccipital process (narrow part of fan points medially, see description in text): (0) absent, (1) present.

38. Dorsoventral row of muscular fossae on lateral edge of exoccipital: (0) absent, (1) present.

Petrosal Characters

39. Size (transverse width) of tegmen tympani: (0) small or moderately inflated, <80% the transverse width of the promontorium, (1) massive and inflated, >90% the transverse width of the promontorium (modified from Cifelli, 1982; Geisler and Luo, 1998; Luo and Gingerich, 1999).

40. Anterior process of petrosal (anterior extension of tegmen tympani): (0) absent, (1) present, anterior edge of tegmen tympani extends far anterior to the edge of the pars cochlearis (Luo and Marsh, 1996; Geisler and Luo, 1998; Luo and Gingerich, 1999).

41. Anterior process of petrosal: (0) articulates laterally with the entoglenoid (falciform) process of the squamosal but is exposed ventrally, (1) anterior two-thirds of the anterior process completely overlapped ventrally by the entoglenoid process (Luo and Gingerich, 1999).

42. Epitympanic recess: (0) uniformly concave without a fossa for the malleus, (1) with distinct fossa for the head of the malleus (derived from Luo and Eastman, 1995).

43. Hiatus epitympanicus: (0) poorly developed or absent, (1) forms a deep transverse groove between the tegmen tympani and mastoid process of the petrosal (Geisler and Luo, 1996; Luo and Gingerich, 1999).

44. Transpromontorial sulcus for internal carotid artery: (0) absent, (1) present (Cifelli, 1982; Thewissen and Domning, 1992).

45. Fossa for tensor tympani muscle: (0) shallow, bowl-shaped pit, (1) deep groove that is partially hidden in ventral view by a medial shelf of the tegmen tympani, (2) deep groove that is clearly visible, (3) absent (modified from Luo and Marsh, 1996).

46. Articulation of pars cochlearis with basisphenoid/basioccipital: (0) present, (1) absent (Thewissen and Domning, 1992; Geisler and Luo, 1998; Luo and Gingerich, 1999).

47. Edge of internal acoustic meatus: (0) flush or nearly flush with the surrounding endocranial surface of petrosal, (1) forms a tube that projects mediodorsally into the endocranial cavity.

48. Lambdoidal exposure of mastoid process of petrosal: (0) present, triangular exposure visible

in posterior view with exposure bounded medially by the supraoccipital, ventrally by the exoccipital, and dorsolaterally by the lambdoidal crest of the squamosal, (1) absent, squamosal contacts exoccipital in this region.

Ectotympanic Characters

49. Stylomastoid foramen: (0) forms a large open notch, petrosal does not contact the petrosal either anterior or posterior to the fenestra rotunda, (1) is complete, ectotympanic contacts tympanohyal laterally and the petrosal medially, in some cases ectotympanic separated from petrosal by a narrow (<1 mm) fissure (Geisler and Luo, 1998; O'Leary and Geisler, 1999; Luo and Gingerich, 1999).

50. Ectoympanic: (0) simple ring or a annulus of thin bone projects from dorsal surface of the bulla, (1) annulus not visible, instead the middle conical process present in the homologous position (Luo, 1998; Luo and Gingerich, 1999).

Ectotympanic Bulla Characters

51. Involucrum of bulla: (0) absent, (1) present (Thewissen, 1994; Luo and Gingerich, 1999).

52. Position of external opening of the eustachian tube: (0) at anterior end of bulla, (1) on medial side of bulla (Luo and Gingerich, 1999).

53. Meatal portion of ectoympanic: (0) tympanic does not extend ventral to external auditory meatus, (1) tympanic extends laterally forming the floor of the external auditory meatus (Luo and Gingerich, 1999).

54. Sigmoid process (medial part of anterior wall of ectotympanic meatal tube) (ordered): (0) absent, (1) present, forms a thin, splint-like, transversely oriented plate that projects laterally from the anterior crus of the tympanic ring, (2) present and robust, base has clearly defined posterior edge which is marked by a dorsoventral groove (Geisler and Luo, 1998; Luo and Gingerich, 1999).

55. Tip of sigmoid process: (0) points posterodorsally, (1) forms anteroposteriorly broad, transverse plate (modified from Luo and Gingerich, 1999).

56. Lateral furrow of tympanic: (0) absent, (1) present (Kasuya, 1973).

57. Median furrow of tympanic: (0) absent, (1) present, forms narrow notch on posterior edge of bulla, bulla in ventral view, (2) present, forms broad embayment of postrior edge of bulla, (3) bisects bulla into a smaller posteromedial and a larger posterolateral portions (modified from Geisler and Luo, 1998; Luo and Gingerich, 1999).

58. Medial eminence of tympanic (ordered): (0) absent, (1) present (modified from Luo and Gingerich, 1999).

59. Base of posterior process of tympanic: (0) forms a single columnar pedicle, (1) perforated and forms medial and lateral pedicles (Kasuya, 1973; Luo and Gingerich, 1999).

60. Entoglenoid process (ordered): (0) absent with broad articulation of squamosal to tympanic, (1) short with circular facet for articulation with tympanic, (2) entoglenoid process forms ridge which contacts tympanic (Luo and Gingerich, 1999).

61. Articulation of anterior part of tympanic ring or bulla to the tegmen tympani of petrosal (ordered): (0) absent, ectotympanic ring or bulla articulates with squamosal only, (1) articulation present immediately anterolateral to epitympanic recess (Luo and Marsh, 1996; Luo and Gingerich, 1999).

62. Articulation of medial edge of the tympanic bulla with basioccipital (ordered): (0) present along entire medial edge of bulla, (1) present but small, (2) absent, wide gap separates both bones (Luo and Gingerich, 1999).

63. Contact between ectotympanic and mastoid process of petrosal (ordered): (0) absent, ectotympanic ring or bulla contacts tegmen tympani just anterior to junction of mastoid process with rest of petrosal, (1) present but restricted to ventromedial end of mastoid process, (2) extensive, posterior process of ectotympanic covers greater part of mastoid process in ventral view (Luo and Gingerich, 1999).

64. Posterior edge of tympanic: (0) does not contact exoccipital, (1) contacts paraoccipital process of exoccipital (Geisler and Luo, 1998; Luo and Gingerich, 1999).

Dental Characters

65. Incisors (uppers and lowers): (0) substantially smaller than canines, (1) subequal to canines.

66. P1 and p1: (0) substantially smaller than canines, (1) subequal to canine in size.

67. Accessory cusps on posterior premolars and molars (lowers and uppers) (ordered): (0) absent, (1) present but small, (2) present and large (modified from Uhen, 1998a).

68. p1 roots: (0) absent, (1) one root, (2) two roots (Uhen, 1999).

69. P1 roots: (0) one root, (1) two roots (Uhen, 1999).

70/ P3 length: (0) shorter than length of P4, (1) subequal to P4 length, (2) longer than P4 (Thewissen and Hussain 2000).

71. Paraconid on lower molars (ordered): (0) present and large, (1) small and much lower than protoconid, (2) absent.

72. Carnassial notch on lower molars: (0) ab-

sent, (1) present and located on cristid obliqua between protoconid and hypoconid.

73. Trigonid of molars: (0) flat anterior border, (1) concave with a reentrant groove, accommodates posterior convex border of the talonid or adjacent tooth (modified from Thewissen, 1994; Geisler and Luo, 1998).

74. Talonid of m1 and m2: (0) slightly longer to or subequal to length of trigonid, (1) distinctly shorter than length of trigonid (Thewissen and Hussain, 2000).

75. M1 and M2 protocone: (0) present and large, (1) present but is minute cusp, (2) absent (Thewissen and Hussain, 2000).

76. M1 roots (ordered): (0) four completely separate, (1) three completely separated, (2) three partially divided, (3) two, and an anterior and a posterior root (modified from Uhen, 1998a).

77. M2 roots (ordered): (0) four completely separate, (1) three completely separated, (2) three partially divided, (3) two, and an anterior and a posterior root (modified from Uhen, 1998a).

78. M3 (ordered): (0) present and distinctly larger than M2, (1) present and roughly equal in size to M2, (2) present but small, maximum mesodistal $<$ 60% the length of M2, (3) absent (modified from Zhou et al., 1995; Geisler and Luo, 1998).

79. M3 roots (ordered): (0) four completely separate, (1) three completely separated, (2) three partially divided, (3) two, and an anterior and a posterior root (Uhen, 1998a). Cannot be scored if M3 is absent.

Mandibular Characters

80. Mandibular symphysis posterior termination (ordered): (0) below p1, (1) below p2, (2) below diastema between p2 and p3, (3) below p3, (4) below or posterior to p4 (Uhen, 1998a).

81. Mandibular symphysis: (0) suture visible, (1) fused (Uhen, 1998a)

82. Mandibular foramen size: (0) small, maximum height of opening 25% or less the height of mandible at m3, (1) greatly enlarged, maximum height greater than 50% the height of the mandible at m3 (modified from Thewissen, 1994; Geisler and Luo, 1998).

Vertebral and Rib Characters

83. Surface texture of posterior thoracic and postthoracic vertebrae: (0) smooth, (1) pockmarked with verebrae having multiple layers of dense, cortical bone with vascular channels that invade these layers (Uhen, 1999).

84. Hypophysis of axis in ventral view: (0) steep-sided cone, transverse width $<$ 1.5 times its anteroposterior length, (1) low with no clear separation from lateral articulation facets for the atlas, transverse width $>$ 2 times its anteroposterior length.

85. Articulation facets on the atlas for the axis: (0) convex, (1) concave.

86. Vertebral canal in axis vertebra: (0) wide, straight canal, (1) small, curved canal.

87. Cervical vertebra: (0) long, length of centra greater than or equal those of anterior thoracics, (1) short, length shorter than anterior thoracics (Gingerich et al., 1995b).

88. Number of thoracic vertebrae (ordered): (0) $<$10, (1) 12, (2) 13, (3) 14–15, (4) $>$15 (modified from Uhen 1998a).

89. Spinous processes of T6 and T7: (0) steeply inclined from plane of the anterior face of the centrum, $>$25°, (1) gently inclined to vertical, $<$15°.

90. Number of lumbar vertebrae (ordered): (0) 6, (1) 7, (2) 8, (3) $\geq$13 (modified from Uhen, 1998a).

91. Length of posterior lumbar or anterior sacral vertebrae, whichever is longer (ordered): (0) short, centrum length $\leq$ 150% the length of T1, (1) slightly elongate, 150% $\leq$ centrum length $\leq$ 200% the length of T1, (2) elongate, 200% $\leq$ centrum length $\leq$ 250% the length of T1, (3) greatly elongate, centrum length $\geq$ 250% the length of T1.

92. Lumbar zygapophyses (ordered): (0) revolute, (1) curved, (2) flat, (3) absent (Uhen, 1998a).

93. Articulation between sacral vertebrae and ilium of pelvis (ordered): (0) broad area of articulation between pelvis and one or two sacral vertebrae, (1) no articulation between vertebrae and pelvis (Uhen, 1998a).

94. Number of vertebrae fused together to form a sacrum (ordered): (0) no fusion, (1) two, (2) three, (3) four, (4) four or more (modified from Uhen, 1998a).

95. Transverse processes of sacral vertebrae: (0) short, (1) long. Cannot be scored when homology of sacral vertebrae unclear (derived from Hulbert, 1998).

96. Number of postlumbar vertebrae articulating via pleuropophyses: (0) more than four, (1) four, (2) three, (3) two, (4) none, no vertebrae have them (derived from Hulbert, 1998).

97. First five ribs: (0) distal ends similar in diameter to proximal portions, (1) distal ends expanded and bulbous.

98. Radius: (0) circular to slightly ovoid in cross section, (1) flattened mediolaterally, highly elliptical in cross section (Uhen, 1998a).

99. Olecranon process: (0) has the same, or slightly narrower, anteroposterior diameter as the shaft of the ulna, (1) much larger anteroposterior diameter than the shaft (Uhen, 1998a).

100. Distal end of ulna: (0) pointed, (1) broad anteroposteriorly (Uhen, 1998a).

101. Trapezoid and magnum: (0) separate, (1) fused (Uhen, 1998a).

102. Distal carpal articular surfaces (e.g., unciform, magnum): (0) curved to allow for substantial movement, (1) flat (Uhen, 1998a).

Pelvic Characters

103. Pelvis size: (0) large, has well-developed ilium with total length $>$ 300% the length of the first sacral vertebra, (1) greatly reduced with a small ilium, total length $\leq$ the length of the first sacral vertebra.

104. Obturator foramen, (0) larger than acetabulum, (1) smaller than acetabulum (derived from Hulbert, 1998a).

105. Dorsal edge of acetabulum: (0) high and sharp, (1) low and rounded (Gingerich et al., 1995b).

106. Ventromedial expansion of pubis ventromedial to obturator foramen (ordered): (0) absent, (1) present but small expansion, (2) present and extreme expansion (Hulbert, 1998; Uhen, 1999).

107. Femur (ordered): (0) large, (1) moderate, (2) small (Uhen, 1998a).

APPENDIX 2
THE 107 MORPHOLOGICAL CHARACTERS SCORED FOR 21 TAXA[a]

	1	11	21	31	41	51
Sinonyx	000001?000	0000101110	0000120300	00?00?????	?????0?01?	0011?01000
Mesonyx	0000000000	010??01110	0000120400	00?00???00	?001010?0	0011?????0
Pachyaena	00?0000000	00001?111?	?0001B04??	????0?????	??????????	??????????
Sus scrofa	1000010300	0010001000	1130020411	1101100000	-000110110	001B?010N0
Hippopotamus	000B112200	0010021020	1130020 4?0	00001???10	N??0?10110	001B?0AN03
Pakicetidae	10?010??00	?0?AA0?0?0	1120010311	0001111 0?1	11?0100110	1101001001
Ambulocetus	??????????	?11??01000	????0?0D?1	???1??????	??????????	1?????A???
Rodhocetus	11A21?0201	010?121121	???A??111?	???11210??	?????1?10?	?10B??3??1
Remingtonocetus	112B12?011	3110100100	11E00121??	20?1????11	11?0111 1??	1002?130?1
Dalanistes	1121120?01	3111?0010?	????0B111?	0111120 0??	?????1?10?	1102113 1?1
Gaviacetus	???G?0?I??	?1021311A1	1121011311	20B11211??	?????1?101	1102113111
Carolinacetus	11?21?1001	2????F1??1	??1?011411	2021121111	1110111101	110??13111
Protocetus	1?23211 2?1	1102?3?111	1112011311	20?01B1??1	11?0111 10?	1102013111
Georgiacetus	1112313301	2101121111	1112011311	20?1121 1?1	11?0111101	1102113111
Babiacetus	1??3312 3?1	31?12F1102	1??20??D0?	????1210??	?????1?10?	??0B11F111
Basilosaurus	1123413312	3104231132	???3011201	2130100011	0110210101	1002112112
Dorudon	1113312312	C104231132	1133011201	2131100011	0110210101	1002112112
Eocetus wardii	11?4H???0B	??????????	??????????	??????????	??????????	??????????
E. schweinfurthi	11B33?3302	31?F?F11??	????0?????	20?????????	??????????	??????????
Artiocetus	1112111100	?101111111	?1210B1101	20?1121??1	?1??A11101	1102N13101
Qaisracetus	11N3112202	1102121121	1?20?A1?01	20?1111??1	???011?1?1	1102N1310?

	61	71	81	91	101
Sinonyx	?010000101	0100000103	00????0G?G	A002?B?000	000???0
Mesonyx	10A?00010?	01?00003?C	000???0301	10020B0000	00000?0
Pachyaena	??A?000100	010000010D	0000000102	00020B?000	0000000
Sus scrofa	12N100NN11	1000000000	1000?00D0A	A00D0A0010	0000000
Hippopotamus	?211000002	20010AA1A3	100???0D00	??040A0000	00000A0
Pakicetidae	0021100112	1001011111	000?0?0?0?	?00301?01?	??00000
Ambulocetus	??????0???	??010111A?	?10????402	1103010010	0000000
Rodhocetus	?12110020?	2111?11111	0100101201	1100?10011	0000001
Remingtonocetus	?1211?0201	20N02FF2F4	1?00100???	0?0301????	???????
Dalanistes	??2110?101	??N?212133	0?0???0???	0?0301????	??000A0
Gaviacetus	A121100 1?2	?????11??1	010????????	??00040???	???????
Carolinacetus	1B21100???	2111??????	0100101G0?	??????0???	???????
Protocetus	1121?00?12	????B1122?	??00001B?F	1200140???	??0????
Georgiacetus	1221101212	2111122123	010???1203	2210140???	??0001?
Babiacetus	??21110 2?2	21012BB1B2	11????????	??????????	???????
Basilosaurus	2220102212	21N12333?1	0101111414	3210?41111	1111122
Dorudon	22201122A2	21N12333?1	0101111414	?210?41111	11?????
Eocetus wardii	??????????	??????????	??1???110?	32???N0???	????1??
E. schweinfurthi	????110?1?	?????1????	??1????????	3????N????	???????
Artiocetus	1121100102	????01B1?1	01????1???	???????0?1	?00???0
Qaisracetus	B???100?02	????B1121?	??0???1200	1101120???	??00?1?

[a]N = character inapplicable; A = 0 + 1, B = 1 + 2, C = 1 + 3, D = 3 + 4, E = 0 + 2, F = 2 + 3, G = 1 + 2 + 3, H = 2 + 3 + 4, I = 0 + 1 + 2.

APPENDIX 3

Anatomical Abbreviations Used in Figures

II/V	path of optic nerve and ophthalmic branch of V
VII	foramen for facial nerve
VIII	foramina for vestibulocochlear nerves
ac	alveolus for canine
ai#	alveolus for lower incisor no.
aI#	alveolus of upper incisor no.
al	alisphenoid
alf	alar foramen
ant	anterior
ap	anterior process of petrosal
aP#	alveolus of premolar no.
asp	ascending process of premaxilla
C	canine
cn	cingulum
co	condyle
cos	canal for cranio-orbital sinus
cp	coronoid process
dor	dorsal
dt	dorsal tuberosity
eam	external auditory meatus
ec	ethmoid canal
elf	endolymphatic foramen
eo	exoccipital
etc	endocranial opening of temporal canal
eut	opening for eustachian tube
fev	foramen for emissary vein
fm	fossa for the malleus
fo	foramen ovale
fp	falciform process
fr	fenestra rotunda
ft	frontal
ft/pa	frontal/parietal suture
fv	fenestra vestibuli
gl	glenoid fossa
gss	groove for superior sagittal sinus
gtt	groove for tensor tympani muscle
hf	hypoglossal foramen
hy	hypophysis
iam	internal acoustic meatus
iv	involucrum
ju	jugal
lat	lateral
lvf	lateral vertebral foramen
m#	molar no.
man	mandibular angle
max	maxilla
mf	median furrow
mfr	mandibular foramen
mfs	mandibular fossa
mg	medial groove for inferior petrosal sinus
mp	mastoid process of the petrosal
mt	medial tuberosity of the promontorium
na	nasal
nc	nuchal crest
no	external nares
nt	nuchal tubercle
of	odontoid fossa
op	odontoid process
or	orbit
pa	parietal
pdt	posterodorsal tongue of the petrosal
pf	perilymphatic foramen
pgf	postglenoid foramen
pmf	postmeatal fossa
pmx	premaxilla
pop	postorbital process
poz	postzygapophysis
pp	palatal process of premaxilla
ppt	posterior process of tympanic
pr	promontorium
prz	prezygapophysis
ptp	posttympanic process
sc	sagittal crest
scr	supracondylar ridge
sgf	sigmoid fossa
smf	suprameatal fossa
smp	suprameatal process
sn	supracondylar notch
snp	supraneural projection
so	supraoccipital
sop	supraorbital process
sp	spinous process
sq	squamosal
sqf	squamosal fossa
sqr	squamosal rise
T#	thoracic vertebra no.
tc	tympanic cavity
tiam	tube for internal acoustic meatus
tf	temporal fossa
tp	transverse process
trf	transverse foramen
vo	vomer

Complete lists of all issues of the *Novitates* and the *Bulletin* are available at World Wide Web site http://library.amnh.org/pubs. Inquire about ordering printed copies via e-mail from scipubs@amnh.org or via standard mail from: American Museum of Natural History, Library—Scientific Publications, Central Park West at 79th St., New York, NY 10024. TEL: (212) 769-5545. FAX: (212) 769-5009.

♾ This paper meets the requirements of ANSI/NISO Z39.48-1992 (Permanence of Paper).